UNIVERSITY OF CALGARY

Remote Sensing Boreal Coarse Woody Debris

by

Gustavo Lopes Queiroz

A THESIS

SUBMITTED TO THE FACULTY OF GRADUATE STUDIES

IN PARTIAL FULFILMENT OF THE REQUIREMENTS FOR THE

DEGREE OF MASTER OF SCIENCE

GRADUATE PROGRAM IN GEOGRAPHY

CALGARY, ALBERTA

SEPTEMBER, 2019

© Gustavo Lopes Queiroz 2019

Abstract

Coarse woody debris (CWD) are vital components of forested environments, affecting the physical structure and biochemistry of forests, supplying habitats, nutrients and food for many organisms. Additionally, CWD is an especially important element in boreal forest management in Alberta, Canada. Large quantities of CWD can configure a fire hazard, whereas moderate quantities of CWD in linear disturbances can aid newly planted seedlings to survive and hinder the hunting effectiveness of predators of endangered caribou herds. Forest managers and ecologists can benefit from large-scale high-accuracy quantitative mapping of CWD in complex boreal environments. This thesis represents the first high-resolution remote sensing study of CWD within the context of Alberta's boreal forest. The research conducted here tested the effectiveness of a geographical object-based image analysis (GEOBIA) workflow with random forest classification for mapping CWD logs and snags in a 4300-hectare study area in northeastern Alberta, Canada. Additionally, zero-adjusted models were selected for accurate estimation of CWD volume in the study area using Akaike's information criterion. The developed models successfully mapped (up to 93.4% completeness and 94.5% correctness) and estimated volume of CWD (0.623 R^2, 0.224 RMSE) with good accuracies. Light detection and ranging (LiDAR) data improved the distinction between logs and snags in CWD maps (~6% better distinction; significant at α 0.05), and multispectral LiDAR data improved the estimation of CWD volume occluded by superimposed vegetation (~ 0.1 higher R^2 and ~0.018 lower RMSE). Models developed in a calibration area could be applied to a verification area 4 km distant from all training data without substantial differences in accuracy (average 9% drop in mapping accuracy, no decrease in R^2 or increase in RMSE when estimating volume). Given the potential of emerging multispectral LiDAR technologies, it is likely that future improvements to sensors will make ever more accurate CWD predictions possible. Site managers, as well as ecologists and foresters interested in studying the spatiality of CWD can make use of the developed workflows to obtain accurate and extensive map products in forested areas.

Keywords: coarse woody debris, CWD, log, snag, boreal forest, remote sensing, GEOBIA, random forest, machine learning, LiDAR

Preface

This is a manuscript-based thesis prepared in accordance with the Faculty of Graduate Studies Guidelines at the University of Calgary. Chapter 2 of this thesis was published in the open-access, peer-reviewed journal Forests, and has been reproduced under copyright agreement with the publisher MDPI. Chapter 3 is at the time of writing being prepared for submission for peer-review by the same journal. I am intellectually responsible for the greater part of the works presented in this thesis, including research design, data collection, analysis, graphical preparation, and writing. Some of the original datasets used as basis for analysis in both Chapters 2 and 3 were obtained in collaboration with other Boreal Ecosystem Recovery and Assessment (BERA) project parties. The raw aerial photos and Light Detection and Ranging (LiDAR) datasets used in both chapters were provided by the Alberta Biodiversity Monitoring Institute (ABMI). Air photos and dense LiDAR datasets were mosaicked and georeferenced by Dr. Mustafizur Rahman, who wrote an original version of the description of how the mosaicking and georeferencing were performed in Chapter 2 (Subsection 2.3.2). Ground control points, previously placed in the study area by Man Fai Wu, were used by Dr. Rahman in order to georeference such datasets. Dr. Guillermo Castilla has provided highly valuable criticism which helped to refine the classification logic used to create the reference dataset discussed in Chapter 2. Dr. Greg McDermid and Dr. Julia Linke aided in refining research objectives of Chapter 2 and all coauthors of this chapter reviewed the text prior to publication. The multispectral LiDAR used in Chapter 3 was obtained and pre-processed by The Advanced Resolution Terradynamics Monitoring System Laboratory (Artemis) at University of Lethbridge. Dr. Julia Linke provided valuable suggestions and readings which were useful in choosing the model selection strategy for Chapter 3. The shape of seismic lines used in Chapter 3 was delineated by colleague Silvia Losada. At the time of writing only Dr. Greg McDermid has reviewed Chapter 3 and all other coauthors intend to review that chapter

prior to publication. The following have assisted with overall research design for the thesis and field logistics: Dr. Greg McDermid, Dr. Mustafizur Rahman and Dr. Julia Linke.

There have been few studies of Geographical Object-Based Image Analysis (GEOBIA) of coarse woody debris (CWD) in the literature. In fact, there were no studies of GEOBIA of CWD using machine learning, or within the context of boreal forests. This gap in the literature was explored by Chapter 2, which also answered a variety of research questions related to optimization and accuracy of the presented workflow. Chapter 3 expands on the findings of the previous chapter by using field data to model CWD volume in an extensive application area. The main contributions of this chapter are implementing an accurate solution for CWD volume estimation on extensive areas and assessing the value of multispectral LiDAR for CWD volume models. The coauthors of chapter 2 and the anticipated coauthors of chapter 3 have granted their permission to publish the materials of these chapters in this thesis, and copyright permissions are presented in the Appendix section of this document. The anticipated citations for the published chapters are as follows:

Chapter 2: Lopes Queiroz, G., McDermid, J. G., Castilla, G., Linke, J., & Rahman, M. M. (2019). Mapping Coarse Woody Debris with Random Forest Classification of Centimetric Aerial Imagery. *Forests*, *10*(6). https://doi.org/10.3390/f10060471

Chapter 3: Lopes Queiroz, G., McDermid, J. G., Castilla, G., Linke, J., & Rahman, M. M., Hopkinson, C., Kariyeva, J. (2019). Estimating Coarse Woody Debris Volume Using Image Analysis and Multispectral LiDAR. [Manuscript in preparation]

Acknowledgements

I would like to recognize the incredible support I have received from family, friends, university colleagues and advisors. My supervisor, Dr. Greg McDermid, had confidence in my potential as a student. He provided guidance through my masters by pointing me in the right direction while giving me the freedom to pursue what I wanted, and by helping me adapt my timeline to meet both my personal and academic needs. Another coworker from whom I have received much appreciated help was Dr. Mustafizur Rahman, who was always available to listen to daily challenges and provide support with lab tasks and field planning. Dr. Julia Linke and Dr. Guillermo Castilla also provided vital criticism to my research design which helped to refine and strengthen my knowledge and publications. Other colleagues which provided intermittent help were Jennifer Hird, Man Fai Wu and Talyor Mckeeman.

Finally, I could not put in words my appreciation for all that my fiancée Liv Waldorf has done for me in aiding my studies, providing all the emotional and intellectual support I could ever need. I deeply appreciate all the help I was given during graduate school and I thank everyone that has pushed me to achieve my goals.

For little Remy, his mom, and his grandparents.

Table of Contents

Abstract i

Preface ii

Acknowledgements iv

Table of Contents vi

List of Tables ix

List of Figures xii

List of Symbols, Abbreviations and Nomenclature xv

Epigraph xvi

Chapter One: Introduction 1

1.1. Definition and Ecology of Coarse Woody Debris 1

1.2. Remote Sensing of CWD 2

1.2.1. Image Analysis *4*

1.2.2. LiDAR *5*

1.2.3. Modelling *7*

1.3. CWD in Alberta's Boreal Forests 10

1.4. BERA Project and Study Area 12

1.5. Statement of the Problem 16

1.6. Research Objectives 16

1.7. Organization of the Thesis 17

Chapter Two: Mapping Coarse Woody Debris with Random Forest Classification of Centimetric Aerial Imagery 19

2.1. Abstract 19

2.2. Introduction 19

2.3. Materials and Methods 22

2.3.1. Study Area *24*

2.3.2. Image Acquisition and Pre-Processing *26*

2.3.3. Training the Classifier *27*

2.3.4. Classification Accuracy Analysis *30*

2.4. Results 32

2.4.1. General Accuracy and Transferability *32*

2.4.2. Significance of LiDAR-derived height variables *33*

2.4.3. Importance of Predictor Variables *34*

2.4.4. Effect of Training-Sample Size *36*

2.5. Discussion **38**

2.5.1. General Accuracy and Transferability *38*

2.5.2. Significance of LiDAR-Derived Height Variables *40*

2.5.3. Importance of Predictor Variables *40*

2.5.4. Effect of Training-Sample Size *41*

2.5.5. Sources of Error *41*

2.5.6. Application and Next Steps *42*

2.6. Conclusions **45**

2.7. Appendix A **45**

2.8. Appendix B **47**

2.9. Appendix C **50**

2.10. References **52**

Chapter Three: Estimating Coarse Woody Debris Volume Using Image Analysis and Multispectral LiDAR **55**

3.1. Abstract **55**

3.2. Introduction **55**

3.3. Methods **58**

3.3.1. Study Area *59*

3.3.2. CWD Survey *62*

3.3.3. Remote Sensing and Pre-Processing *64*

3.3.4. Geographic Object-Based Image Analysis *67*

3.3.5. Additional Layers *69*

3.3.6. Model Selection *70*

3.3.7. Map Production *73*

3.4. Results **75**

3.4.1. Accuracy of Best Models *75*
3.4.2. Map Products *77*
3.4.3. Model Selection Tables *81*
3.4.4. Accuracy of Visible-CWD Layer *82*
3.5. Discussion **83**
3.5.1. Model Selection *86*
3.5.2. Importance of Multispectral LiDAR for Infra-Canopy Predictions *87*
3.5.3. Two-Part Models Versus Simple Models *88*
3.5.4. Standardized Model Coefficients *89*
3.5.5. Issues and Limitations *91*
3.5.6. Future Work *93*
3.6. Conclusions **94**
3.7. Appendix D: Illustrated Field Sampling Strategy **95**
3.8. References **98**
Chapter Four: Conclusions **103**
4.1. Research Objectives Summary **104**
4.2. Research Contributions **107**
4.3. Recommendations for Future Research **109**
4.3.1. Future Remote Sensing of CWD Research *109*
4.3.2. Future Ecology Research Using CWD Maps *110*
4.4. Bibliography **112**
Appendix: Copyright Permissions **121**

List of Tables

Table 1.1. Forest inventory on uplands and lowlands in the study area. Area in hectares (Ha) was derived from species percentage on individual stands. Data derived from Alberta's Vegetation Inventory (AVI; Government of Alberta, 2019). 14
Table 2.1. Flight specifications for airborne remote sensing mission. Projection uses the Canadian Spatial Reference System (CSRS) in Universal Transverse Mercator (UTM) coordinates. 26
Table 2.2. Name and description of each of the classes in the reference dataset. The five first classes were used for training and testing (Y) the random forest classifier, and the last two were not used for either training or testing but for discarding some of the randomly selected objects (N). 28
Table 2.3. Accuracy metrics completeness and correctness for all CWD, only logs, and only snags. Training samples were obtained solely from the calibration area; the first application has testing samples in the calibration area and the second has testing samples in the verification area. These numbers reflect the average metrics of 100 random forests runs with a 80/20 training/testing random split of samples. 33
Table 2.A1. Detailed description and examples of the classes in the reference dataset of the verification area that were used for random forest classification, including count (N) and area. Example images provide both the visible (RGB) spectrum and a false-color image using near infrared (NIR). 46
Table 2.A2. Detailed description and examples of the classes in the reference dataset of the verification area that were not used for classification, including count (N) and area. Example images provide both the visible (RGB) spectrum and a false-color image using near infrared (NIR). Normalized difference vegetation index (NDVI) is used as one of the indicators for coarse woody debris (CWD). 47
Table 2.B1. Average accuracy of tests using different height attributes as predictor variables: spectral variables along with canopy height model (CHM) and digital surface model (DSM), only spectral and CHM, only spectral and DSM, only spectral variables (no height), and only height variables. Average completeness (Comp) and correctness (Corr) of 100 random forests for the classes: CWD union (Union), logs, and snags. 48
Table 2.B2. Accuracy standard deviation of tests using different height attributes as predictor variables: spectral variables along with canopy height model (CHM) and digital surface model (DSM), only spectral and CHM, only spectral and DSM, only spectral variables (no height), and only height variables. Standard deviation of completeness (Comp) and correctness (Corr) of 100 random forests for the classes: CWD union (Union), logs, and snags. 48
Table 2.B3. Results of t-tests comparing average accuracies of tests using different height attributes as predictor variables: spectral variables along with canopy height model (CHM) and digital surface model (DSM), only spectral and CHM, only spectral and DSM, only spectral

variables (no height), and only height variables. P-values are provided for completeness (Comp) and correctness (Corr) for the classes: CWD union (Union), logs, and snags. 49
Table 2.B4. Results of t-tests comparing average accuracies of tests using different height attributes as predictor variables: spectral variables along with canopy height model (CHM) and digital surface model (DSM), only spectral and CHM, only spectral and DSM, only spectral variables (no height), and only height variables. Provided for completeness (Comp) and correctness (Corr) for the classes: CWD union (Union), logs, and snags. 49
Table 2.C1. Image-object attributes obtained in eCognition (Trimble, 2016) used as predictor variables for creating the random forests (RF) and their importance for coarse woody debris classification according to the RF importance function. The average between log importance and snag importance was used for ranking (N) the variables. The types (T) of predictor variables are: spectral red, green, blue (RGB) and near-infrared (NIR) combined (RGBN, R), normalized difference index (NDVI, N), spatial (S), digital surface model (DSM, D) and canopy height model (CHM, C). 51
Table 3.1. Mean canopy closure on vegetated portions of the study area. Uplands are divided into forest stand types (Government of Alberta, 2019) and lowlands into wetland classes (DeLancey et al., 2019). 61
Table 3.2. Description and summary statistics of all variables used in model selection, each variable summarized with: mean, standard deviation (Std Dev), minimum (Min) and maximum (Max). The response variable was Coarse Woody Debris (CWD) volume measured in the field, and the predictor variables were derived from a variety of remote sensing products. Visible CWD (vCWD) and water (vWater) area were derived from the results of geographical object-based image analysis (GEOBIA) on aerial orthophotos obtained over the study area. A wetland probability raster was obtained from ABMI (Hird et al., 2017). Canopy closure (CC) was derived from a canopy height model (CHM). Passive normalized difference vegetation index (NDVI) was derived from the orthophotos used in GEOBIA, while active NDVI and normalized burn ratio (NBR) were derived from multispectral LiDAR datasets. 71
Table 3.3. Candidate two-part models for coarse woody debris (CWD) volume according to small sample Akaike information criterion (AICc). The rank (r), degrees of freedom (df) and delta AICc (ΔAICc) are provided for each model. The following variables were selected in all continuous models: area of detected CWD objects via image-analysis (vCWD); canopy closure (CC); and height of the tallest tree (CHM_{max}). The following were selected in some continuous models: standard deviation of the active normalized burn ratio ($aNBR_{sd}$) and range of passive NDVI ($pNDVI_r$). Finally, all logistic models included: vCWD, standard deviation of passive NDVI ($pNDVI_{sd}$), visible water area (vWater) and wetland probability (WP). 82
Table 3.4. Minimum and maximum average coarse woody debris volume (m^3/ha) over varied boreal forest types presented in other studies. Note that the present study estimated volumes in 100m^2 plots and upscaled the values for an estimate per hectare. Minimum value from

Pedlar et al. (2002) includes snags. Sturtevant et al. (1997) values are for individual stands, while all other studies present averages. 84
Table 3.5. Intercept and coefficients for binomial part of the best zero-adjusted gamma model. Values are presented for models created with the original training data and models using standardized predictor variables (mean of zero and standard deviation of one). Variables include visible coarse woody debris area (vCWD), standard deviation of passive normalized difference vegetation index ($pNDVI_{sd}$), visible water (vWater) and wetland probability (WP). 89
Table 3.6. Intercept and coefficients for continuous part of the best zero-adjusted gamma model. Values are presented for models created with the original training data and models using standardized predictor variables (mean of zero and standard deviation of one). Variables include squared area of visible coarse woody debris (vCWD), canopy closure (CC), height of tallest tree (CHM_{max}), squared height of tallest tree (CHM_{max}^2) and squared standard deviation of active normalized burn ratio ($aNBR_{sd}^2$). 89

List of Figures

Figure 1.1. Flowchart for classification of woody debris adopted in this thesis. Adapted and simplified from Yan et al. (2006). 1

Figure 1.2. Study area map showing disturbances (seismic lines in red; roads, cut-blocks, constructions and power lines in dark gray), upland forest stands and lowland classes. Seismic lines were manually delineated. Upland forest composition was derived from Alberta's Vegetation Inventory (Government of Alberta, 2019); lowlands were divided into wetland classes according to Alberta Biodiversity Monitoring Institute's wetland inventory (DeLancey et al., 2019). 13

Figure 1.3. Field photos of example lowland sites where coarse woody debris was sampled. Most sites were black spruce (*Picea mariana* (Mill.) B.S.P.) dominated fens and swamps (a and b). These were sampled on seismic lines (b) as well as on the unaffected forest (a). A few bogs and marshes were also sampled (c). 14

Figure 1.4. Field photos of example upland sites where coarse woody debris (CWD) was sampled. Coniferous (a and d), deciduous (b and e) and mixed (c and f) forest stands were sampled on seismic lines (d, e and f) as well as on the unaffected forest (a, b and c). Human-placed piles of CWD can be seen in (d) and (f). 15

Figure 2.1. Workflow chart of this study with the sub-section numbers where each step is explained in this document. Coarse woody debris (CWD) are mapped via image segmentation and random forest (RF) classification of the image objects. Multiple tests are performed to assess implications of inputs on classification accuracy. Specific tests are based solely on calibration samples. 24

Figure 2.2. Location of the training and verification areas within the 250-hectare area of study. Background image for the overall study area obtained from the ArcGIS mapping software using the following sources: Esri, DigitalGlobe, GeoEye, i-cubed, USDA FSA, USGS, AEX, Getmapping, Aerogrid, IGN, IGP, swisstopo, and the GIS User Community.2.2. Image Acquisition and Pre-Processing 25

Figure 2.3. Bar plots of completeness (left) and correctness (right) using different combinations of height attributes: both canopy height model (CHM) and digital surface model (DSM), only CHM, only DSM, and no height data. Average metrics for 100 runs with randomly selected training/testing samples on the calibration area. 34

Figure 2.4. Box and whisker plot of the random forest (RF) importance relative to the CWD classes for different predictor variable categories: normalized difference vegetation index (NDVI), canopy height model (CHM), visible and near-infrared layers (RGBN), extent and shape (spatial) attributes, and digital surface model (DSM). The number of attributes in each category is shown in parenthesis. Importance shown is the average of 500 random forests using all available attributes on the calibration area. 35

Figure 2.5. Line graph of number of attributes versus classification accuracy of CWD. Accuracy metrics shown are the average of 100 random forests for logs, snags, and the CWD union classes on the calibration area. 36
Figure 2.6. Graphs of completeness (a) and correctness (b) versus number of training samples on the calibration area..... 37
Figure 2.7. Histograms of area (pixels) of snag objects in the calibration (a) and verification (b) areas. Mean and standard deviations (sd) are indicated on each graph. 39
Figure 2.8. Application example of the developed method in a small subset of the study area without (**A**) and with (**B**) the classified CWD objects. 43
Figure 3.1. Workflow chart of this study with the sub-section numbers where each step is explained in this document. We mapped non-occluded coarse woody debris (CWD) via a geographic object-based image analysis (GEOBIA) workflow. Occluded CWD quantities were estimated using multispectral LiDAR (ML) vegetation indices from underneath the canopy. We selected potential models for CWD volume using the small sample Akaike information criterion (AICc) as an indicator for model predictive power. 59
Figure 3.2. Location of the calibration and verification areas within the 4300-hectare study area as well as the location of the field plots where CWD volume was surveyed. The background image is a false-color image using near infrared, red and green spectral bands. Upland broadleaf stands dominated by trembling aspen appear as lighter shades of red; conifer-dominated lowlands and mixed-wood uplands appear as darker tones. Roads, seismic lines (petroleum-exploration corridors), and petroleum well pads appear as lines and geometric features. 60
Figure 3.3. Scatter plots of actual versus predicted coarse woody debris (CWD) volume in m^3. The best model with multispectral LiDAR (ML) data was used to estimate CWD volume on a) the calibration area plots using keep-one-out cross-validation, and on b) the verification area plots using the calibration plots to train the model. Similarly, the best model without ML data was also applied to the c) calibration and d) verification areas. Goodness-of-fit (R^2), root mean square error (RMSE) and sample size (S) are indicated on each plot. 76
Figure 3.4. Map of coarse woody debris (CWD) volume per hectare (m^3/ha) over the study area. High quantities of CWD are displayed in red, medium quantities in yellow and low quantities in blue. Roads and water bodies are excluded from the CWD volume model and are presented as dark blue. Insets (a) and (c) showcase hotspots of CWD in false-color imagery. Insets (b) and (c) showcase the CWD volume map over (a) and (c) respectively. 78
Figure 3.5. Map of coarse woody debris (CWD) volume per hectare (m^3/ha) over seismic lines on the study area. The gray-scale background image presents volume per hectare for the entire study area, while the seismic lines are classified as high (red) medium (yellow) and low (blue) CWD quantities. (a) and (c) are false-color aerial images showing examples of high and low CWD densities respectively. (b) and (d) are field photos of (a) and (c) respectively. 79

Figure 3.6. Box and whisker diagram for coarse woody debris (CWD) volume on reference data (green, total of 108 field plots) on the CWD map for the entire application area (blue, total of 379,025 cells) and on seismic lines (red, 63,816 sampling points). All reference data (a) is divided into (b) disturbance plots (54 plots) and (c) forest plots (54 plots). Forest plots are divided into (d) lowland plots (14 plots) and (e) upland plots (40 plots). All map predictions (f) are divided into (g) lowland (38% of cells) and (h) upland (62% of cells) predictions. Seismic line predictions (i) are divided into (j) untreated lines (90% of samples) and (k) treated lines (10% of samples). Original values were in m^3/100m and were projected to m^3/ha. Box-plot outliers are presented in gray. 81
Figure 3.7. Scatter plots of actual versus predicted coarse woody debris (CWD) ground cover in m^2. Predicted ground cover presented here is the area sum of CWD objects detected via image-analysis. A weak relationship is observed when a) all field plots are used in regression, and a much stronger relationship is observed in b) plots with negative average normalized-difference vegetation index (NDVI). 83
Figure 3.8. Examples of sampling areas for the collection of training and calibration CWD data. For each study site two (belt) disturbance plots are laid out on the seismic line and two (circle) forest plots are laid out off the seismic lines centered within a buffer from 12 to 36 meters away from the line. 96
Figure 3.9. Belt plot design for disturbance sampling. The belts have 100 m^2 area and the same width as the seismic line, the first belt starts 15 meters away from the start of the line, the second belt starts 75 meters away from the end of the first belt. A real-time kinematics (RTK) base-station is located somewhere close to the site for good signal with a rover sensor which was used to collect the coordinates of the start and end points. 96
Figure 3.10. Measuring volume of fallen dead trees (logs). 97
Figure 3.11. Measuring strategy for CWD partly outside the sampling area. Only the (blue) segment within the area is measured, as if it ended at the edge of the sampling area. The dashed red lines represent tape used in (A) disturbance plots or biodegradable paint used in (B) forest plots to mark the edges of the plots. 97

List of Symbols, Abbreviations and Nomenclature

Abbreviation	Definition
ABMI	Alberta Biodiversity Monitoring Institute
AIC	Akaike Information Criterion
AICc	Small Sample AIC
aNBR	Active Normalized Burn Ratio
aNDVI	Active Normalized Difference Vegetation Index
CC	Canopy Closure
CHM	Canopy Height Model
CWD	Coarse Woody Debris
DSM	Digital Surface Model
GCP	Ground Control Point
GEOBIA	Geographical Object-Based Image Analysis
GNSS	Global Navigation Satellite System
GSD	Ground Sampling Distance
LiDAR	Light Detection and Ranging
ML	Multispectral LiDAR
NBR	Normalized Burn Ratio
NDVI	Normalized Difference Vegetation Index
NIR	Near Infrared
pNDVI	Passive Normalized Difference Vegetation Index
R	R Programming Language
R^2	Coefficient of Determination
RF	Random Forest
RGB	Red Green Blue
RGBN	Red Green Blue Near Infrared
RMSE	Root Mean Square Error
SWIR	Short Wave Infrared
UAV	Unmanned Aerial Vehicle
vCWD	Visible Coarse Woody Debris
vWater	Visible Water
WP	Wetland Probability
ZAGA	Zero-Adjusted Gamma Distribution

Epigraph

"There is geometry in the humming of the strings. There is music in the spacings of the spheres."

-Pythagoras

Chapter One: Introduction

1.1. Definition and Ecology of Coarse Woody Debris

The definition of coarse woody debris (CWD) varies in the literature but a common denominator, derived from the work of Yan et al. (2006), is that CWD is defined as dead wood, which can be either intact or in varied stages of decomposition, with at least 7 cm of diameter at the largest end and at least 1 m of length. If the CWD is standing with an inclination smaller than 45° relative to vertical, then it can be classified as a snag. If it is horizontal or leaning with an inclination greater than 45° relative to vertical, then it is classified as a log. If the dead wood has a diameter smaller than 7 cm at the largest end or a length inferior to 1 m, then it is classified as fine woody debris (FWD). A flowchart of the woody debris classification strategy adopted in this thesis is presented in Figure 1.1.

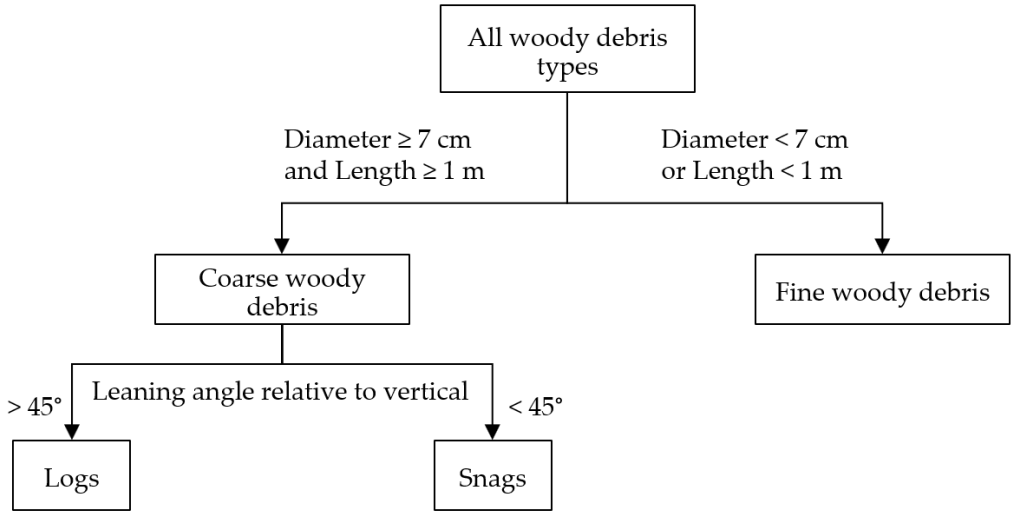

Figure 1.1. Flowchart for classification of woody debris adopted in this thesis. Adapted and simplified from Yan et al. (2006).

Woody debris occurs naturally in forest ecosystems, with highly variable input rates that can go up to 30,000 kg/ha/year; the causes of tree mortality include wind, fire, insects, diseases and suppression (i.e. competition between trees; Harmon et al., 1986). CWD decomposes naturally through physical and biological processes, slowly decaying in situ until

it is completely consumed by the environment or being removed by fire, floods, soil mass movements, or human activity; snags usually decay until their stems are no longer able to support their weight and collapse becoming logs, which therefore are usually in more decayed states on average than snags (Harmon et al., 1986).

CWD in the natural forest is vital to the success many local flora and fauna, acting as habitat, source of food, shelter and soil nutrients (McWinn et al., 1996; Hagan and Grove, 1999; Riffell et al., 2011). Additionally, CWD influence the microtopography and erosional dynamics of hillslopes, as well as sediment transportation and flow of rivers (Harmon et al., 1986). Conversely, excessive quantities of CWD on rivers can be a hazard to navigation and property during floods (Harmon et al., 1986); and excessive quantities on land can be a fire hazard, which was historically removed from boreal worksites to prevent the spread of wildfires and only recently reincorporated given its benefits to the ecosystem (Brown et al., 2003; Vinge and Pyper, 2012).

Given the important roles of CWD in forested environments and given the human impact on CWD distribution, this thesis is interested in investigating a strategy for locating and quantifying CWD distribution across extensive altered and natural forests, with special attention to human disturbances.

1.2. Remote Sensing of CWD

Since studies concerning forests commonly investigate large areas, it becomes unfeasible to rely solely on field work or on manual digitization of aerial images when mapping specific small-scale objects such as CWD. Additionally, since CWD quantities are highly variable between and within different ecosystems (Harmon et al., 1986), it becomes difficult to model CWD occurrence in unstudied areas. In order to obtain accurate maps of CWD distribution on forests several authors have studied and developed varied methods for automated extraction of these objects from remotely sensed data.

Remote sensing comprises acquisition, processing, analysis and interpretation of datasets obtained indirectly (i.e. without physical contact), most commonly aerial or satellite images of urban and natural areas (Jensen, 2015). Remote sensing has been applied extensively to the study of forests, most notably visualization, classification, mensuration, modeling and change detection of forest elements and phenomena. CWD are relatively small objects when compared to the 30-meter ground sampling distance (GSD) of traditional Landsat satellite imagery and therefore has mostly been studied in the form of large post-fire or windthrow cut blocks within the context of satellite data (Baumann et al., 2014; Rüetschi et al., 2019).

Inoue et al. (2014) demonstrated that human interpreters were able to successfully identify 85% of CWD logs on high-resolution (1 cm GSD) aerial images of a forested area in Japan, obtained with an unmanned aerial vehicle (UAV). Other studies have applied automated solutions to identify CWD objects on high-resolution images obtained with unmanned and piloted aircraft, usually grounding their automation on manually-crafted classification-trees, likelihood estimation, or supervised machine learning (Polewski et al., 2015; Richardson and Moskal, 2016; Stereńczak et al., 2017; Duan et al., 2017; Panagiotidis et al., 2019).

The main types of remote sensing data obtained for the purpose of CWD detection are optical red-green-blue (RGB) imagery, near infrared (NIR) imagery, and light detection and ranging (LiDAR) laser scanning (Marcus et al*.,* 2002; Pasher and King, 2009; Selvarajan, 2011; Blanchard et al*.,* 2011; Lindberg et al*.,* 2013; Polewski et al*.,* 2015; Richardson and Moskal, 2016; Duan et al*.,* 2017). The most common platform used for obtaining the remote sensing data in this context are manned aircrafts, although recent studies have started to adopt unmanned aerial vehicles (UAVs), as the prices for these become more accessible and their payload capacities increase. Data is usually collected by carrying the sensor in a grid pattern on constant altitude over the study area, with the aim of obtaining continuous data for the entire site.

A powerful spectral index used in remote sensing of vegetation is the normalized-difference vegetation index (NDVI), which normalizes the difference between the near-infrared (NIR) values and the visible (usually the red band) values of pixels in an image (equation 1.1). NDVI is useful because alive vegetation has a much higher normalized difference between NIR and visible light than dead vegetation, and therefore in an NDVI layer alive and dead vegetation become easy to distinguish. Another useful index is the normalized burn ratio (NBR), which measures the normalized difference between NIR and short-wave infrared (SWIR) light (equation 1.2). NBR has a similar effect to NDVI on alive and dead objects but it is more often used on a time-series of images to detect burned areas on satellite images (Escuin et al., 2008).

$$NDVI = (NIR - red)/(NIR + red) \tag{1.1}$$

$$NBR = (NIR - SWIR)/(NIR + SWIR) \tag{1.2}$$

1.2.1. Image Analysis

The two central types of image analysis used for the detection of features such as CWD are pixel-per-pixel analysis and object-based analysis. Pixel-based analysis has been the classic solution to the extraction of information from remotely sensed images since the development of such products. However, with the availability of high-resolution data, a pixel-based approach lacks the capability of identifying larger objects, composed of many pixels and identifiable by context and relationship to its surroundings (Fisher, 1997). Additionally, the individual values of pixels can be affected not only by the area they contain but also by their surroundings.

To solve the limitations of pixel-based analysis an alternative approach called object image analysis (OBIA) was created, based on the concept of image segmentation (i.e. partitioning) into image-objects containing several similar pixels. This concept applied to

remote sensing is called geographical object image analysis (GEOBIA) and represents a new paradigm in land cover classification (Blaschke et al., 2014). In GEOBIA, source images are entirely partitioned into separate image-objects, each containing relatively homogeneous pixels, usually with the aim of each object representing a real-world object or its parts. Image-objects can be analyzed not only in terms of spectral properties, but also in size, shape, and context (King, 2002). An object hierarchy can be created, with larger conceptual objects containing several smaller objects, their relationship serving as an additional tool for image analysis and classification (Burnett and Blaschke, 2003; Blaschke et al., 2014).

To classify pixels or GEOBIA image-objects as CWD or otherwise, the two most common workflows in remote sensing are: a) the development of human-derived rules and b) supervised machine learning classification. Human-derived rules are classification rules built based on the knowledge of a human expert, where each object is analyzed through a series of rules in the form of a decision tree (Jensen, 2015). Each rule is a condition related to a remote sensing variable, such as a minimum threshold for the mean value in a spectral band, or a range for mean elevation. On the other hand, supervised machine learning decision trees are built by a computer via some algorithm that analyzes a training dataset, composed of varied examples of the desired output classes, and creates the rulesets which best fit the data (Jensen, 2015).

1.2.2. LiDAR

In forested areas with closed canopy, a considerable part of the CWD present is likely to be occluded by superimposed vegetation and therefore not visible in aerial imagery. To circumvent this issue, studies have used light detection and ranging (LiDAR) point clouds to obtain more detailed information of the forest floor and understory. While traditional optical remote sensing is considered passive imaging because the sensors do not emit any light themselves, LiDAR is considered active imaging because the sensors emit laser beams that reflect on objects and return to the sensor. LiDAR is especially useful to the study of forests

because beams are not only capable of detecting the first layer of objects between the sensor and the ground but can also penetrate through canopy and return to the sensor after reaching the understory or forest floor, capturing the position of multiple forest layers with a single laser pulse. Each time a beam returns to the sensor the distance to the target object is calculated based on the speed of light and the time elapsed since emitting the beam. Typically, LiDAR surveys produce large point clouds which represent the three-dimensional positioning of all points captured in the landscape and for each point the intensity value of the returning light. According to Lim et al. (2003), commercial LiDAR sensors typically emit from 5,000 to 50,000 pulses per second of light within the near-infrared spectrum (1064 nm), on a scan angle of up to 75 degrees. After surveying a study area with a LiDAR sensor, the raw data is normally pre-processed to remove outliers and geometric effects, and the point clouds can then be used for classification and mensuration of forest elements, for example to generate a canopy height model (CHM; Lim et al., 2003) which measures the height of trees by subtracting the forest surface elevation, modeled by the canopy returns, by the forest floor elevation, modeled by the ground returns.

Studies modelling CWD and using exclusively aerial LiDAR data have struggled with obtaining accurate measurements of smaller debris. Mücke et al. (2013) obtained good accuracy on a classification workflow for woody debris larger than 30 cm at the largest end in a small application area (~ 6 ha) of Euro-Siberian steppic woods (75% completeness and 90% correctness), and Sumnall et al. (2016) obtained moderately accurate measurements on CWD larger than 10 cm at the largest end (0.51 R2, 2.74 RMSE) on a large application area (2200 ha) containing semi-natural and plantation coniferous and deciduous forests by modelling LiDAR statistics.

While point clouds obtained via traditional LiDAR contain pulse intensity information for each return, the main use of LiDAR historically has been to obtain 3D spatial information of environments. Multispectral LiDAR (ML) is an emerging technology which allows sensors to capture returns from multiple wavelengths simultaneously. With ML intensity information,

LiDAR point clouds could become much more valuable since the multiple bands allow for the creation of spectral indices and for improved separation between different objects based on their spectral signature (i.e. spectral ranges within each channel; Hopkinson et al., 2016). For example, Chasmer et al. (2017) successfully derived an active NBR index from ML data obtained with a Titan (Teledyne Optech, Toronto, ON, Canada) sensor to identify burn severity in boreal peatlands, demonstrating that even though ML intensity values do not represent actual surface reflectance (Hopkinson et al., 2016) they can be used to generate active analogues of passive vegetation indices. There have been no studies using ML data to model CWD quantities that I am aware of.

1.2.3. Modelling

According to Korzukhin et al. (1996), the two main types of models used in forest management are process and empirical models. Empirical models use statistical methods to accurately predict forest values. In contrast, process models are usually applied to study the interrelationships between forest elements (Korzukhin et al., 1996). Since in this thesis the aim is to quantify CWD and not understand the relationship between CWD and other forest components, the models presented here are empirical. A variety of empirical models can be applied to map CWD in a study area using remote-sensing datasets as input, on which the characteristics of CWD are studied based on a training set allowing the models to make predictions on new datasets. The most common types of models within this context use either classification or regression. Classification involves labeling a dataset with discrete categories that represent real-world classes, in this case perhaps binary (two labels: CWD and non-CWD) but can also include multiple classes (common land cover classes: water, soil, vegetation, shadow, CWD). Regression within this context typically involves measuring and predicting some continuous variable related to CWD such as volume (m^3, m^3/ha), mass (kg, kg/ha), ground cover (m^2, m^2/ha). Classification and regression of CWD normally require a training dataset, on which the models are trained, and a testing dataset to assess the accuracy of the

trained models. The kind of classification model that is constructed manually by a trained analyst can be denoted manual classification tree, and the kind that is automatically created by a computer following statistical procedures can be denoted either supervised or unsupervised model. Supervised classification models use a labeled training dataset as reference to tune the classification process that can be applied on unlabeled data. Unsupervised classification automatically assigns unique labels to statistically distinct groups within an unlabeled dataset and can be useful in other types of land classification studies (Jensen, 2015) but given the relative rarity of CWD on the overall landscape it is unlikely that unsupervised learning would have accurate results for classifying objects as small and rare as CWD. Some studies have also used change detection solutions to identify windthrown trees on multitemporal datasets (Rüetschi et al., 2019) however this technique would not be applicable to detect trees which have died prior to the time when the first datasets where acquired.

Classification models can be constructed by manual decision rules forming a classification tree. Classification trees are denoted as such because an input data point goes through a series of branching decision nodes, until it reaches a final branch where it is assigned a certain class label. For example, a trained analyst can create rules that separate objects based on their spectral signature on aerial images. Each node of the classification tree will use threshold values for certain input variables (for example brightness, mean red intensity or standard deviation of NDVI) in order to separate a portion of the input datasets into different bins which will be gradually filtered by additional nodes until they reach a final node. Richardson and Moskal (2016) used a manual classification tree mostly structured using LiDAR, spatial and NDVI variables to classify riparian CWD in Washington State, USA.

There are multiple solutions for automated classification models not based on manual decision rules. Automated supervised classification models use complex statistical algorithms to analyze the training data and create solutions to classify new datasets. Despite requiring training data, supervised classification does not require a trained analyst capable of creating

classification rules and, if used properly and provided a large enough training sample, is commonly capable of more-accurate and less-biased predictions than manual decision trees. This is particularly true on large multi-variate datasets containing many possible predictor variables (Jensen, 2015). Common types of supervised learning models used for CWD analysis include support vector machines (Baumann et al., 2014), maximum-likelihood (Stereńczak et al., 2017) and random forest (Duan et al., 2017). Random forest is a type of machine learning which is very popular in the recent science literature due to its ease of use and powerful predictive power (Jensen, 2015). Random forest is named as such because it uses a training dataset to create a "forest" of classification trees, each constructed with an independent randomized selection of the training data and variables, and the forest predicts class labels via a majority vote of the trees (Breiman, 2001). Duan et al. (2017) used a random forest binary classifier to identify pixels containing windthrown trees on aerial images of a rubber tree plantation in China.

Regression involves modeling the relationship between a response variable (i.e. dependent variable; e.g. CWD volume, mass or area), and one or more predictor variables (i.e. independent variables; e.g. reflectance, NDVI, shape, size, etc.). Parameters for each one of the predictor variables are calculated based on the training data. This is normally achieved through the least-squares method, which minimizes the squared sum of the residuals (i.e. distance between the actual and predicted values for the response variable). Sumnall et al. (2016) successfully achieved regression of CWD volumes on an extensive area by analyzing LiDAR point clouds.

One common method used to compare and select candidate models when there are many possible regression models using the same training dataset is to calculate Akaike's Information Criterion (AIC). AIC is based on the concept of maximum likelihood and compares the model and its parameters with the "truth", which is represented by the training sample, while accounting for overfitting by penalizing the addition of each new predictor variable

(Burnham and Anderson, 2002). AIC has not yet been used within the context of remote sensing of CWD.

1.3. CWD in Alberta's Boreal Forests

The Canadian boreal forest is a vital ecosystem to many socioeconomic and ecological processes in the country. It is central to the production of raw materials and feedstock, while also being important to the lifestyle and culture of aboriginal communities (Brandt et al., 2013). Boreal forests regulate climate, purify water and are home to many unique wildlife including the largest caribou herds in the world (Schneider and Dyer, 2006). Additionally, due to its vegetation type and climate, Canadian boreal forests are especially prone to local and regional wildfires (Macias Fauria and Johnson, 2007). Boreal forests in Alberta are located over the third largest oil reserves in the world, containing 170 billion barrels of oil recoverable with modern technology (Percy, 2012). The underground bitumen deposits are a driving force to the economy of the province. To locate these deposits, extensive networks of vegetation-free corridors, known as seismic lines, are created across the forests to facilitate mapping the underground rock layers via analysis of seismic wave reflectance (Dabros et al., 2018). In 2001, there was a conservative minimum estimate of 1.5 million km of seismic lines in Alberta alone (Timoney and Lee, 2001).

Seismic lines, as well as other resource-extraction infrastructure in the region, modify the environment by compacting soil, affecting the hydrology, temperature, carbon dynamics, solar radiation and wind regime (Dabros et al., 2018). These effects have many negative implications on native fauna and flora, the most famous of which is the habitat destruction of endangered woodland caribou (*Rangifer tarandus*; Hebblewhite, 2017). One of the key factors for the decline of caribou populations is the fragmentation of their habitat by seismic lines and other linear features such as roads and railways, which increased the porosity for other ungulate species and their predators (Dickie, 2015). More adaptable species benefit from the altered landscape and thrive while less adaptable species lose their habitat (Fisher and Burton,

2018). Therefore, apparent competition has increased predation rates for caribou and contributed to widespread population declines (Hebblewhite, 2017).

Boreal forest restoration in Alberta is a practice of managing disturbed forest sites to promote the reestablishment of native vegetation with the overarching goal of recovering caribou populations (Government of Alberta, 2017). There are many types of restoration treatments being applied on Alberta's boreal sites, including planting native seedlings and limiting the movement of humans and predators on seismic lines with coarse woody debris (CWD) as physical barriers (Government of Alberta, 2017). The main reason for limiting movement across the landscape is to prevent animals from using these human-made linear features, diminishing the advantage of predators. Boreal vegetation can take up to 60 years to grow and fully mature in this environment (Hebblewhite, 2017). Lee and Boutin (2006) studied vegetation recovery on seismic lines at least 5 meters wide in northeastern Alberta and found that even 35 years after the disturbances were established only 8.2% of upland lines recovered with more than 50% of woody vegetation cover and of none of the lowland lines significantly recovered. Therefore, if no measure is taken to boost vegetation recovery and, in the meantime, reduce predation rates, endangered caribou will have no chance of survival. Humans sometimes drive all-terrain vehicles (ATV) and trucks on seismic lines, which disturb the soil and destroy growing seedlings; further delaying re-growth. Additional benefits of CWD include creating valuable microsites for the growing seedlings, protecting them from wind and cold, providing humidity and nutrients to the soil over time, reducing erosion on soil, and promoting an overall richer and healthier local habitat for the growing vegetation and local fauna (Vinge and Pyper, 2012).

CWD in boreal forests occurs with volumes varying from 11.3 m^3/ha to 166 m^3/ha (Linder et al., 1997; Sippola et al., 1998). In the context of this study, most of the CWD present on seismic lines is man-made with the objective of fulfilling the requirements of the provincial framework for restoration of seismic lines. The most common techniques used to create CWD for the seismic lines include: rollback, where CWD is brought from nearby sites and placed

along a certain segment or the entire length of the line; tree felling, where the trees adjacent to the line are partially or completely chopped across it; and tipping, where trees are pulled over to lean towards the line, without killing the tree outright (Government of Alberta, 2017).

1.4. BERA Project and Study Area

This study exists as part of the Boreal Ecosystem Recovery and Assessment (BERA) project, which aims to use geospatial and modelling techniques to measure, monitor and predict vegetation recovery in disturbed boreal forests. One of the main motivating factors for this thesis was to generate accurate CWD maps to aid boreal restoration programs and the environmental recovery of seismic lines using CWD. Since the main objective of CWD on seismic lines is to block the movement of predators, with the added benefit of providing healthy microsites, most of the woody debris used in seismic line treatment are in the form of large intact logs (Vinge and Pyper, 2012). Therefore, in this research there is a focus on CWD as opposed to FWD. Additionally, FWD are much more difficult to detect in aerial images due to their small projected area.

The area studied in this thesis is a 4300-hectare area located in northeastern Alberta, Canada, and this area is also studied by other BERA project-related research (Figure 1.2). Located in the boreal forest natural region, central mixed wood subregion (Natural Regions Committee, 2006), the area has a gently undulating terrain formed by 57% uplands and 43% lowlands (DeLancey et al., 2019). Uplands in the study area are composed of natural forest stands: 56% coniferous, 12% broadleaf and 32% mixed forest stands (Government of Alberta, 2019; Figure 1.2). Lowlands are composed of varied types of wetlands including fens, bogs, swamps and marshes (Figure 1.2; DeLancey et al., 2019). Upland forests are mainly populated by Black spruce (32.6%; *Picea mariana* (Mill.) B.S.P.), Jack pine (39.5%; *Pinus banksiana* Lamb.) and Trembling aspen (22.2%; *Populus tremuloides* Michx.); while lowland coniferous stands are mainly populated by Black spruce (64.8%) and Tamarack (26.0%; *Larix laricina* (Du Roi) K. Koch; Table 1.1; Government of Alberta, 2019).

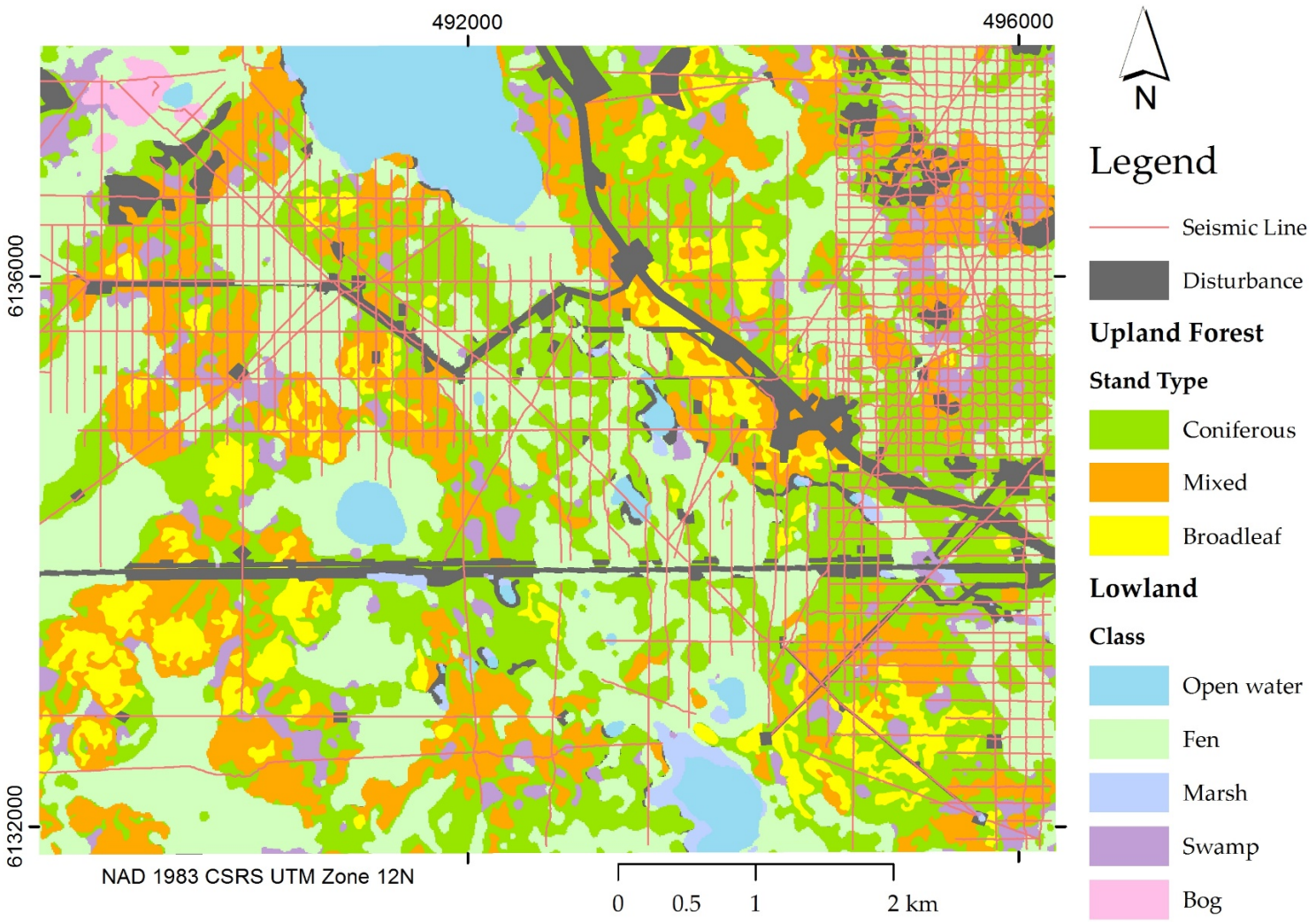

Figure 1.2. Study area map showing disturbances (seismic lines in red; roads, cut-blocks, constructions and power lines in dark gray), upland forest stands and lowland classes. Seismic lines were manually delineated. Upland forest composition was derived from Alberta's Vegetation Inventory (Government of Alberta, 2019); lowlands were divided into wetland classes according to Alberta Biodiversity Monitoring Institute's wetland inventory (DeLancey et al., 2019).

Table 1.1. Forest inventory on uplands and lowlands in the study area. Area in hectares (Ha) was derived from species percentage on individual stands. Data derived from Alberta's Vegetation Inventory (AVI; Government of Alberta, 2019).

Species			Upland		Lowland		Total	
Code	Latin Name	Common Name	Ha	%	Ha	%	Ha	%
Sb	*Picea mariana*	Black spruce	717	32.6%	950	64.8%	1668	45.5%
Pj	*Pinus banksiana*	Jack pine	868	39.5%	123	8.4%	992	27.0%
Aw	*Populus tremuloides*	Trembling aspen	489	22.2%	6	0.4%	496	13.5%
Lt	*Larix laricina*	Tamarack	55	2.5%	381	26.0%	436	11.9%
Sw	*Picea glauca*	White spruce	41	1.9%	2	0.1%	43	1.2%
Bw	*Betula papyrifera*	White birch	23	1.1%	4	0.3%	27	0.7%
Pb	*Populus balsamifera*	Balsam poplar	5	0.2%	0	0.0%	5	0.1%
Fb	*Abies balsamea*	Balsam fir	1	0.0%	0	0.0%	1	0.0%
TOTAL			2200	100.0%	1467	100.0%	3666	100.0%

The tree density of forest stands is much denser on uplands than on lowland stands (Government of Alberta, 2019), and using LiDAR-derived canopy closure (further explained on chapter 3) I measured an average canopy closure of 68.4% on uplands and 27.2% on lowlands.

(a) (b) (c)

Figure 1.3. Field photos of example lowland sites where coarse woody debris was sampled. Most sites were black spruce (*Picea mariana* (Mill.) B.S.P.) dominated fens and swamps (a and b). These were sampled on seismic lines (b) as well as on the unaffected forest (a). A few bogs and marshes were also sampled (c).

There are approximately 342 km of seismic lines (i.e. petroleum exploration corridors) within the study area and about 10% of them have received some sort of restoration treatment, including CWD treatment. CWD was sampled in disturbed and natural forests both in lowlands (Figure 1.3) and uplands (Figure 1.4).

Figure 1.4. Field photos of example upland sites where coarse woody debris (CWD) was sampled. Coniferous (a and d), deciduous (b and e) and mixed (c and f) forest stands were sampled on seismic lines (d, e and f) as well as on the unaffected forest (a, b and c). Human-placed piles of CWD can be seen in (d) and (f).

Given the structural diversity of the study area in terms of forests, terrain and disturbances, it is ideal for developing CWD remote sensing workflows capable of handling complex boreal environments. The extensive remote sensing datasets used to conduct the research in this thesis, including orthomosaics, high-density LiDAR and multispectral LiDAR point clouds, are some of the data obtained in this area for the BERA project. Additional details about the study area and remote sensing datasets are presented in the following chapters.

1.5. Statement of the Problem

CWD quantities in forested environments are highly variable and relatively unpredictable (Harmon et al., 1986). However, given its important role in the biochemistry and physical structure of forests, acting both as habitat and food for wildlife, the location and quantities of CWD are desirable information for forestry and biogeography (Riffell et al., 2011). Since field operations demand a high amount of time and resources, to accurately locate and quantify CWD in forests recent studies have used a variety of remote sensing techniques and datasets. The role of CWD in the boreal forest is even more complex, given that woody debris acts as fire fuel in an environment that is highly susceptible to wildfires (Rowe and Scotter, 1973), and that woody debris are for the most part nonexistent on the more than 1.5 million km of seismic lines in Alberta (Vinge and Pyper, 2012; Dabros et al., 2018). Most studies of remote sensing of CWD have either studied large CWD (larger than 30 cm), snags or logs exclusively, recently windthrown trees, small application areas or riparian CWD. There are no studies of remote sensing of CWD on seismic lines or within the context of the boreal forest. A more detailed review of the literature on remote sensing of CWD is presented at the introduction section of Chapter 2 of this thesis. This thesis aims to fill these gaps in the literature of remote sensing of boreal CWD.

1.6. Research Objectives

Two greater objectives are targeted by this thesis:

1. Evaluate the capability of GEOBIA via supervised classification of aerial photos and LiDAR to accurately classify both logs and snags in the boreal forest. To do so smaller objectives were pursued:
    a. Assess the accuracy and transferability of the best developed workflow in the study area.
    b. Evaluate the worth of LiDAR in addition to spectral predictor variables to increase classification accuracies.
    c. Gain insight into the minimum number of predictor variables and number of training samples required for accurate classification.
2. Select the best regression models for CWD volume estimation on the study area using image-analysis layers, multispectral LiDAR and other spectral indices. In addressing this objective two smaller goals were pursued:
    a. Test the accuracy and transferability of the best predictive model in the study area.
    b. Assess the value and impact of multispectral LiDAR data in improving the prediction of occluded CWD.

1.7. Organization of the Thesis

The research conducted to address the objectives outlined for this thesis are described in two independent articles, presented in Chapters 2 and 3. The first article, presented in chapter two, addresses research objective one and its three sub-objectives, by providing a review of the literature on remote sensing of CWD, a detailed description of the datasets and methods used for mapping logs and snags in the study area, including the steps of the GEOBIA workflow and training and testing the random forest classifier. Additionally, article one provides detailed accuracy tests concerning the LiDAR variables, the predictor variables ranked in terms of prediction importance, and the size of the training datasets. The second article, presented in chapter three, addresses research objective two and its sub-objectives

by making use of the GEOBIA layers produced through the development of the first article to develop accurate regression models of CWD volume on the study area. These models were tested with and without multispectral Lidar, and within the calibration area using cross-validation as well as in a verification area, geographically detached from all training data. This article also produces two extensive and accurate maps of CWD volume: a map of volume per hectare over all land cover types in the study area, and a map of volume per hectare over segments of seismic lines in the study area. Chapter four summarizes the conclusions reached through both articles, highlights the main contributions to the literature and the possible avenues for exploration in related future research.

Chapter Two: Mapping Coarse Woody Debris with Random Forest Classification of Centimetric Aerial Imagery

2.1. Abstract

Coarse woody debris (CWD; large parts of dead trees) is a vital element of forest ecosystems, playing an important role in nutrient cycling, carbon storage, fire fuel, microhabitats, and overall forest structure. However, there is a lack of effective tools for identifying and mapping both standing (snags) and downed (logs) CWD in complex natural settings. We applied a random forest machine learning classifier to detect CWD in centimetric aerial imagery acquired over a 270-hectare study area in the boreal forest of Alberta, Canada. We used a geographic object-based image analysis (GEOBIA) approach in the classification with spectral, spatial, and LiDAR (light detection and ranging)-derived height predictor variables. We found CWD to be detected with great accuracy (93.4 ± 4.2% completeness and 94.5 ± 3.2% correctness) when training samples were located within the application area, and with very good accuracy (84.2 ± 5.2% completeness and 92.2 ± 3.2% correctness) when training samples were located outside the application area. The addition of LiDAR-derived variables did not increase the accuracy of CWD detection overall (<2%) but aided significantly ($p < 0.001$) in the distinction between logs and snags. Foresters and researchers interested in CWD can take advantage of these novel methods to produce accurate maps of logs and snags, which will contribute to the understanding and management of forest ecosystems.

2.2. Introduction

Woody debris—dead trees and branches—is a key element of forest ecosystems, providing nutrient cycling, carbon storage, microhabitats, and overall forest structure, and can feature prominently in studies of wildlife habitat (Jonsson and Kruys, 2001), forest fuel load (Ucitel et al., 2003), bioenergy (Kirkland, 2015), and forest disturbances (Pedlar et al.,

2002). Coarse woody debris (CWD) can be distinguished from fine woody debris on the basis of length (at least 1 m) and diameter (at least 10 cm at the largest end) (Yan et al., 2006). The two most common classes of CWD are snags and logs. If the CWD is standing with an inclination relative to vertical smaller than 45° then it can be classified as a *snag*. If it is positioned horizontally or is leaning with an inclination greater than 45° relative to vertical then it is classified as a log (Yan et al., 2006).

In the boreal forest of Alberta, Canada, extensive human disturbances, mostly side products of resource development such as roads, mineral exploration corridors, and well-sites, have been shown to increase predation rates on woodland caribou (*Rangifer tarandus*), especially by wolves (*Canis lupus*) (Hebblewhite, 2017). This is one of the reasons why caribou populations in Alberta have declined significantly in the last two decades and consequently the species has been listed as threatened by the federal and provincial governments (Environment Canada, 2012). Within this context, CWD is especially important, since it is widely applied to linear-disturbance features to obstruct the movement of predators and humans, while creating valuable microsites for improved growth and protection of newly planted seedlings (Vinge and Pyper, 2012).

Traditional methods for detecting and measuring CWD rely on manual field operations—an activity that is labor intensive and difficult to scale. Therefore, a variety of studies have applied remote sensing solutions to detect CWD. For example, Inoue et al. (2014) used nadir-looking air photos of ground sampling distance (GSD) around 1 cm obtained with an unmanned aerial vehicle (UAV) to visually detect logs under leaf-off conditions in a temperate deciduous forest, achieving about 85% completeness on CWD detection. The authors concluded that this kind of approach is promising for lowering costs of ground surveys, but the study area was small (200 × 300 m), focused only on logs, and involved identification through visual detection—a strategy that would be inappropriate over large areas.

Some studies have used satellite data to delineate CWD. For example, Baumann et al. (2014) applied support vector machine classification on multi-temporal Landsat data to detect

windthrown areas with good accuracy (about 95% completeness and 67% correctness). Similarly, Rüetschi et al. (2019) detected windthrown areas through multi-temporal analysis of Sentinel-1 C-band datasets, obtaining reliable results (88% completeness and 85% correctness). However these approaches are generally only suitable for detecting large windthrow disturbances.

Light detection and ranging (LiDAR) has been used in many studies of forest structure, including some aimed at the detection of CWD. For example, Sumnall et al. (2016) applied regression of LiDAR statistics on study plots, obtaining a strong relationship with snag volume (R^2 = 0.91) but weaker for log volume (R^2 = 0.51). Their strategy did not involve the explicit detection of CWD objects, but rather relied on implicit relationships between field measurements and LiDAR-derived metrics. It is unclear how well such relationships would extend beyond their study site in southern England.

There have been few studies presenting accurate methods for detecting individual CWD objects in forested environments. Polewski et al. (2015) detected logs in a forested area via multiple classification steps over a LiDAR point cloud (30 points/m^2), obtaining good results (~80% completeness and correctness). Richardson and Moskal (2016) detected logs in riparian areas via a rule-based geographical object image analysis (GEOBIA) workflow applied to LiDAR (8 points/m^2) and four-band imagery (15 cm GSD), reporting a good relationship between measured and predicted CWD area (R^2 = 0.65). Stereńczak et al. (2017) detected snags via maximum likelihood classification of LiDAR (6 points/m^2) and four-band data (<50 cm GSD), achieving high-accuracy products (93.65% completeness and 99.95% correctness of testing points). Duan et al. (2017) classified wind-thrown logs on visible band (RGB) UAV images (20 cm GSD) through random forest classification of image pixels. The authors then used a Hough-transform algorithm to delineate each log object, reporting good results (75.7% completeness and 92.5% correctness). A study by Panagiotidis et al. (2019) also detected wind-thrown logs in a forest environment by processing UAV-obtained aerial images (3 cm

GSD) via a series of edge-detection filters and then applying the Hough transform to delineate individual logs, with good results (84.6% completeness and 94.9% correctness).

None of the studies listed above has attempted to identify both logs and snags through a single classification method, none has used object-based classification in conjunction with area-based verification, and none has been applied to the boreal ecosystem. Additionally, except for Richardson and Moskal (2016) and Stereńczak et al. (2017), all previous studies used very small application areas and focused only on recently downed trees (wind-throws). Thus, additional studies are required aimed at larger, more complex study areas in a broad variety of settings.

The aim of this study was to develop and test a GEOBIA-based workflow for classifying logs and snags in the boreal forest using random-forest classification of multispectral and LiDAR data acquired from an aerial platform. In pursuing this work, we addressed two main objectives. First, we assessed the accuracy and transferability of our workflow by conducting validation exercises in both a calibration area, where the classifier was trained, and a separate verification area located in another portion of the study area. Second, we evaluated the need for supplementary LiDAR metrics in this classification task. Additional analyses were performed to gain insight into the number of predictor variables required to map CWD effectively with random forest, and the effect of training-dataset size on classification accuracy.

2.3. Materials and Methods

This paper presents a novel approach to CWD detection in centimetric (i.e., dimensioned in the order of centimeters) aerial imagery using a geographic object-based image analysis (GEOBIA) workflow, where the image-objects are classified by a random forest (RF) using spectral and LiDAR data as predictor variables. In this demonstration, we identify logs and snags in a boreal forest study site located in northern Alberta, Canada.

GEOBIA consists in partitioning images into a set of mutually exclusive and collectively exhaustive groups of connected pixels (a.k.a. image-objects) that are relatively homogeneous internally, and then analyzing such objects based on their spectral and spatial features (Hay and Castilla, 2008). Random forest is a machine-learning algorithm that creates (trains) an ensemble of classification trees, each with a distinct random selection of the input features, then classifies objects through a voting system for all created trees (Breiman, 2001). The approach has been previously demonstrated to be efficient in classifying log objects (Duan et al., 2017).

To assess accuracy, we conducted a number of experiments. The main one assessed the accuracy of our approach for classifying CWD in both the calibration (where the classifier was trained and tested) and the verification (a separate portion only used for testing) parts of the study area. A second set of experiments involved removing certain predictor variables from the training process and assessing their effect on accuracy. Finally, a training-dataset-size test was performed by gradually reducing the number of training samples and assessing the trade-offs in classification accuracy.

A graphical summary of our workflow and the tests performed in this study is shown in Figure 2.1; details are provided in the following subsections. Image segmentation and image-object attribution with spatial and spectral features were performed in eCognition (Version 9.4; Trimble, 2018). All other procedures, including training random forest and assessing the accuracy of classifiers, were performed in R (Version 3.5.1; R Core Team, 2018) using the "*randomforest*" package (Liaw and Wiener, 2018).

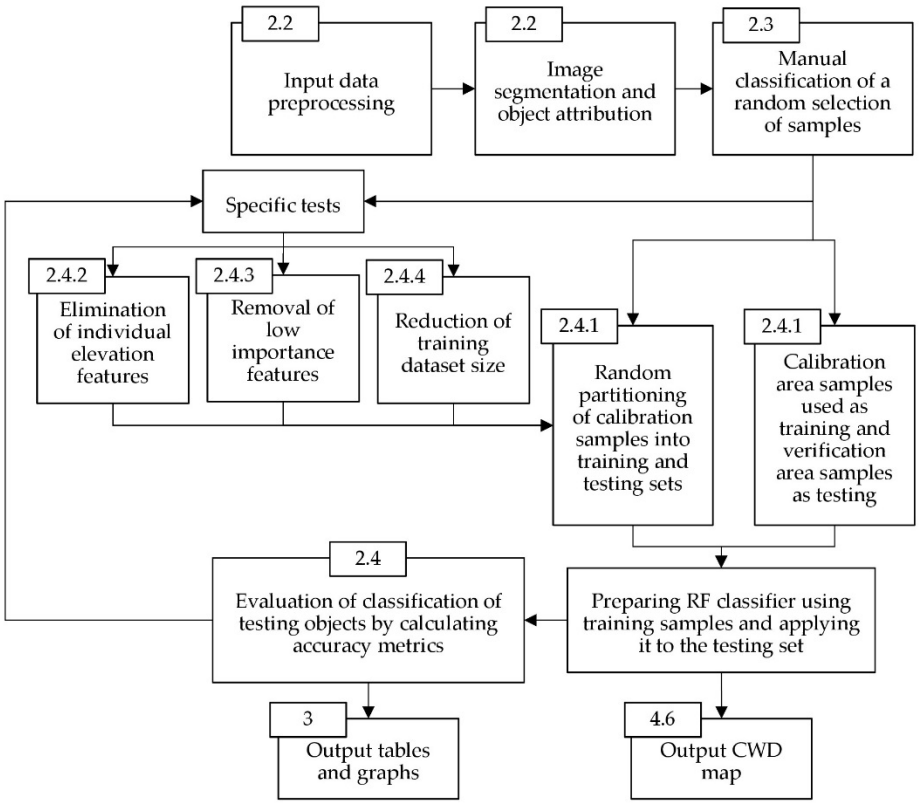

Figure 2.1. Workflow chart of this study with the sub-section numbers where each step is explained in this document. Coarse woody debris (CWD) are mapped via image segmentation and random forest (RF) classification of the image objects. Multiple tests are performed to assess implications of inputs on classification accuracy. Specific tests are based solely on calibration samples.

2.3.1. Study Area

The study area (Figure 2.2) is located in the boreal forest natural region near Conklin, Alberta, in the central mixed-wood subregion (Natural Regions Committee, 2006). The gently rolling terrain, which can be divided into uplands and wetlands, is mainly populated by jack pine (*Pinus banksiana* Lamb.), black spruce (*Picea mariana* (Mill.) B.S.P.), and trembling aspen (*Populus tremuloides* Michx.) trees (Natural Regions Committee, 2006). The region contains a dense network of reclaimed and un-reclaimed seismic lines (petroleum exploration corridors 5–10 m wide) and well sites. CWD can be found dispersed in the undisturbed forest, as well as concentrated in piles on seismic lines. The study area was selected for being

representative of its natural subregion, as well as containing a good variety of disturbances and restoration strategies on seismic lines. A 250-hectare calibration area was selected to develop and fine-tune the CWD classification method. A smaller 20-hectare verification area, about 4 km SE of the calibration area, was used to assess the accuracy of the classifier developed in the calibration area when applied "as is" to a similar area with no further training or tuning.

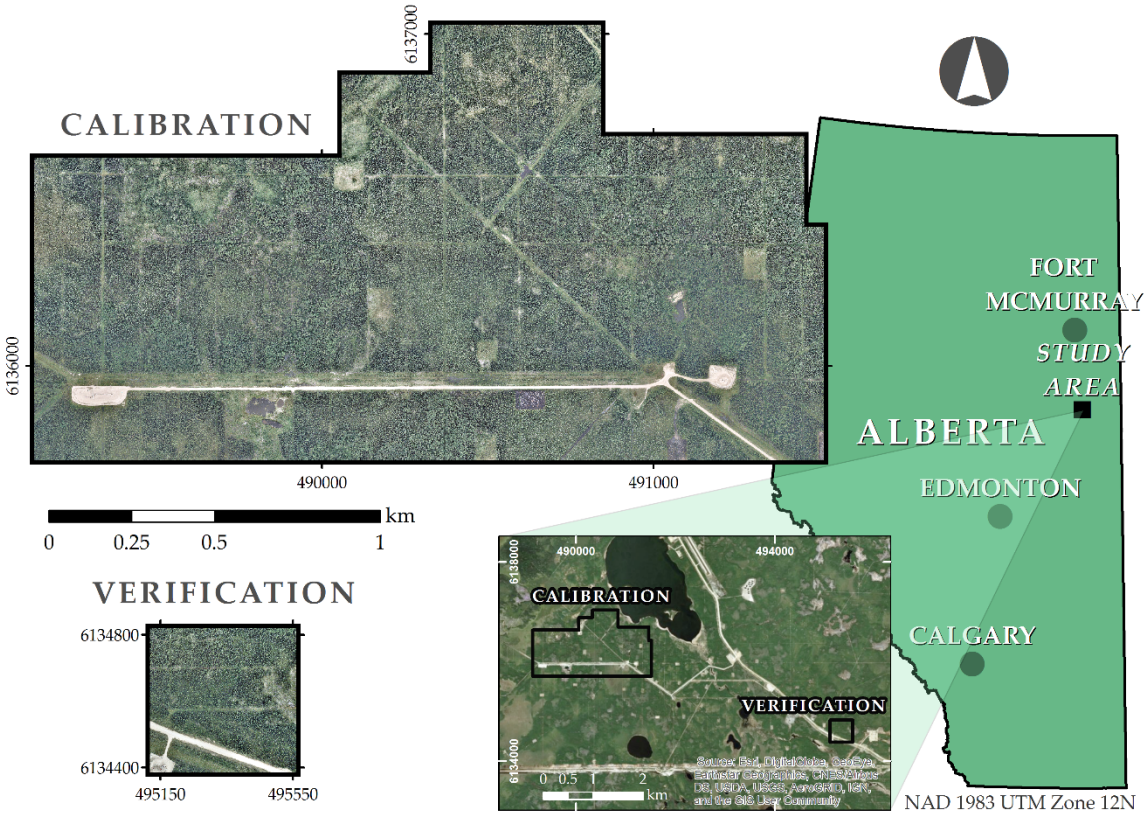

Figure 2.2. Location of the training and verification areas within the 250-hectare area of study. Background image for the overall study area obtained from the ArcGIS mapping software using the following sources: Esri, DigitalGlobe, GeoEye, i-cubed, USDA FSA, USGS, AEX, Getmapping, Aerogrid, IGN, IGP, swisstopo, and the GIS User Community.2.2. Image Acquisition and Pre-Processing

2.3.2. Image Acquisition and Pre-Processing

Remote sensing data for this project were obtained via a piloted aircraft (Cessna 210T) mission executed by OGL Engineering of Calgary on August 2 and 4, 2017. The aircraft was equipped with a LiDAR sensor (Leica ALS70, Leica Geosystems AG, Heerbrugg, Switzerland), an optical sensor (Leica RCD30, Leica Geosystems AG, Heerbrugg, Switzerland), a global navigation satellite system (GNSS) unit, and an inertial measurement unit. The flight detail for this mission is provided in Table 2.1. Prior to the flight mission, 250 visible ground control points (GCPs, 60 cm squares with a bullseye marking) were deployed across the study area and their coordinates measured using a real-time kinematic GNSS (Trimble R8 – 8 mm horizontal and 15 mm vertical precision - Trimble, Sunnyvale, United States). Out of the 250 GCPs, 100 were used for georeferencing, and the remaining 150 were used for accuracy assessment. The X, Y, and Z accuracy (root-mean-square error) of the final products were 5, 10, and 11 cm, respectively.

Table 2.1. Flight specifications for airborne remote sensing mission. Projection uses the Canadian Spatial Reference System (CSRS) in Universal Transverse Mercator (UTM) coordinates.

Projection/Datum	NAD83 (CSRS) UTM Zone 12N, CGVD2013
Flying Height	850 m Above Ground Level
Flying speed	130 knots, 67 m/s
Overlap	80% forward and 60% side
Ground Resolution (RGB)	5.5 cm or less
Sensor calibration	Yes, Leica Geosystems

The average raw LiDAR point density was ~40 pts/m^2. OGL Engineering (Orthoshop Geomatics Ltd.) Calgary performed noise removal from the raw points, then classified them into ground and non-ground points, using Bentley Microstation with Terrasolid software to accomplish this task. We then rasterized (25 cm pixel) the ground points into a digital terrain model (DTM) and the first-return points into a digital surface model (DSM) in ESRI

(Environmental Systems Research Institute) ArcMAP (Version 10.6.1; ESRI, 2017). Finally, a canopy height model (CHM) was obtained by subtracting the DTM from the DSM.

We used a structure-from-motion (Westoby et al., 2012) workflow in Agisoft Photoscan (Version 1.2.4.2399; Agisoft, 2016) to generate a photogrammetric point cloud and an orthomosaic from the raw photos (~2200). However, only the orthomosaic was used for this project. First, the photo quality was assessed using Agisoft Photoscan photo-quality assessment tool. All the photos were found to be above the minimum quality threshold. Then, the photos were aligned and a sparse point cloud was generated using the camera positions estimated by the onboard GPS. The camera position and orientation, and the X, Y, and Z locations of the sparse point cloud were further adjusted with the georeferenced GCPs. The sparse point cloud was next used to generate a dense point cloud and DSM. Finally an orthomosaic was generated at 5 cm GSD using the true DSM. A normalized difference vegetation index (NDVI) for the area of study was also generated from the Red and the Near-infrared (NIR) bands of the orthomosaic.

The LiDAR DSM and CHM, the orthorectified Red, Green, Blue, and NIR bands, and NDVI were stacked together and used as input image bands in Trimble eCognition (Version 9.4). Only the Red, Green, Blue, NIR, and NDVI bands were used for image segmentation (i.e., creation of image-objects), since the LiDAR layers had a less dense GSD (25 cm) and were too smooth to provide information about the edge of objects, while all the input bands were used to attribute the generated image-objects. After some initial testing to find a reasonable balance between under- and over-segmentation, the segmentation parameters were set to scale 10, shape 0.6, and compactness 0.4. The resulting image-objects and their attributes were used for further analysis.

2.3.3. Training the Classifier

A reference dataset in the calibration area was created by manually classifying 5000 randomly selected image-objects (hereafter called just "objects" for short). To account for

the lower frequency in the orthomosaic of objects with a NDVI similar to that of CWD (<−0.1 in the NDVI image), a stratified random sample with two strata (with −0.1 separating "high" vs. "low" NDVI) was extracted. Out of the 5000 objects, 1000 came from the "high" NDVI stratum and 4000 and 1000 from the "low" NDVI objects. Similarly, a second randomly selected reference dataset was created in the verification area, with 300 "high"-NDVI objects and 1200 "low"-NDVI objects. Objects in these datasets were classified by an experienced human analyst. The analyst viewed the reference-object polygons and the spectral and height layers in a GIS environment, then labeled the 6500 calibration-verification objects with one of the classes in Table 2.2.

Table 2.2. Name and description of each of the classes in the reference dataset. The five first classes were used for training and testing (Y) the random forest classifier, and the last two were not used for either training or testing but for discarding some of the randomly selected objects (N).

Name	Description	Train/Test
Log	Downed CWD. Horizontal or leaning with an angle ≥45°	Y
Snag	Standing CWD. Vertical or leaning with an angle < 45°	Y
Water	Puddles and ponds	Y
Dirt	Road, mud and exposed soil	Y
Other	Shrubs, moss, alive trees, shadowed areas	Y
Man-made	Ground control points, buildings, power lines	N
Unidentified	Unclassifiable object due to practical issues or limitations	N

The five object classes used for random forest classification were as follows: logs, snags, water, dirt, and other (Table 2.2). This class composition was deemed to be optimal for the present study after preliminary accuracy tests were performed with different combinations of training classes. Using just the classes of interest (log and snag plus "other") decreased the number of false positives, but also increased the number of false negatives. By adding water and dirt as formal classes, which correspond to low-NDVI objects often confused with CWD, we obtained a better trade-off between false positives and false negatives.

Objects that the human analyst was unable to unambiguously identify were labeled as unidentified and discarded from the reference dataset. Common unidentified objects included miniscule features composed of few pixels, heavily shaded objects that are distinct from their surroundings but too dark to identify, and blurry objects positioned in areas where the ortho-mosaicking produced artifacts.

The reference dataset for the calibration area had 3710 objects, of which 364 were logs and 537 were snags. The remaining objects in the calibration area of the original 5000 were discarded for being unidentified and not beneficial for training. The reference dataset for the verification area had 1500 objects, of which 40 were logs, 51 were snags, and 192 were unidentified objects. More detail and descriptions about each class can be found in Appendix A.

The manually classified image-objects had spatial, spectral, and height attributes that were exported from eCognition for use as predictor variables in R. The spectral attributes for each band and height layer included the following: mean, standard deviation, difference from neighbors, band ratio, border contrast, mean inner border, mean outer border, minimum, maximum, and skewness. The spatial attributes included density, asymmetry, length by width, border length by length, shape index, compactness, polygon width, pixel area, border index, main line width, pixel length, rectangular fit, perimeter, roundness, elliptic fit, and curvature by length. Full attribute definitions can be found in the eCognition Reference Book (Trimble, 2016).

Before running the random forest classification in the calibration area, a stratified-random selection of the reference dataset was performed. In each run, we used 80% of the reference objects for training and 20% for testing, while maintaining the original proportion of object classes. No training was performed in the verification area. Out of the 1500 reference objects in it, 1388 were used for testing, and the remaining 192 unidentified objects were discarded.

2.3.4. Classification Accuracy Analysis

Random forest classifiers, specific for each individual test (explained in the following subsections), were trained using their respective training datasets and then tested against reference data. In this manner, we created confusion matrices and derived two accuracy metrics: *completeness* and *correctness*. Completeness indicates the areal proportion (i.e., proportion by total area, not by number of objects) of all the target-class objects in the test data which were correctly assigned the target class. Correctness is the areal proportion of all objects in the target class that actually belong to this class in the reference data. These metrics are calculated as:

$$\text{Completeness} = \frac{\text{TP}}{\text{TP} + \text{FN}} = 1 - \text{Omission} \tag{2.1}$$

$$Correctness = \frac{TP}{TP + FP} = 1 - Comission \tag{2.2}$$

where *TP* is the total area of true positives: actual target class objects correctly classified as such; *FN* is the total area of false negatives: actual target class objects incorrectly classified with a different class; and *FP* total area of false positives: non-target objects incorrectly classified as the target class. In this study, we defined target classes at two hierarchical levels: (i) logs and snags at the lower level; and (ii) a "CWD union" class at the upper level, which represents all CWD objects together.

Since there can be variability in the results due to the training and testing selection, as well as in the way the RF algorithm constructs the classification trees, the accuracy metrics in this study were obtained by running 100 independent instances of random forests for each test (i.e., for each instance, an independent 80/20 training/testing stratified random split was drawn from the reference dataset of the calibration area). Results are reported as averages (arithmetic mean) and standard deviations.

2.3.4.1. General Accuracy and Transferability

In order to test the reliability of our workflow for CWD identification, we applied it first to the calibration area and then to the verification area. In the calibration area, a random selection of 80% of the reference samples were used to train the classifier. The remaining 20% were used for testing (i.e., for assessing the performance of the classifier). We repeated this process 100 times and averaged the results. In order to test the transferability of the classifier to a spatially segregated area, we performed a second test using the reference objects in the verification area. This test was also repeated 100 times (once per each classifier instance) and the results were averaged.

2.3.4.2. Value of LiDAR-Derived Height Variables

Two types of height data were tested in this study: a digital surface model (DSM) and a canopy height model (CHM), both derived from LiDAR. We tested their effect on RF classifier accuracy using four combinations of predictors: (i) all spectral and height attributes; (ii) all spectral data plus CHM data; (iii) all spectral data plus DSM data; and (iv) only spectral attributes. Each of these combinations were used in 100 RF runs, and their results were averaged. We used a series of pairwise difference-of-means t-tests to look for statistically significant differences on completeness and correctness accuracies in each of the three CWD classes: CWD union, logs, and snags. The null hypothesis was that there is no difference in the mean accuracy of any given CWD class between one combination of predictor variables and another. The significance level for these t-tests was 0.05.

2.3.4.3. Importance of Predictor Variables

The Random Forest R package provides a built-in "*importance*" function, which measures the impact of each predictor variable on classification error by calculating the difference between the error before and after randomizing each variable (Liaw and Wiener, 2018). More important variables have a greater effect on classification accuracy, and therefore receive a

higher importance score. For example, a variable with an importance score of 20 means that randomly permuting the values of that variable leads to a 20% decrease in accuracy. These values are discriminated for each of the output classes. The importance values of 100 RF for the two CWD classes (logs and snags) were averaged and then the predictor variables were ranked from most important to least important in terms of CWD detection accuracy. In order to test the effect of the number of predictor variables on CWD classification accuracy, the least-important variables were gradually removed one by one. We performed classification-accuracy tests for each iteration, based on 100 random forests, until no more variables could be removed.

2.3.4.4. Effect of Training-Sample Size

We tested the effect of training-sample size on classification accuracy by systematically reducing the number of training samples—from 2374 (64% of the calibration reference) down to 32—while maintaining a constant number of testing samples (592 samples, 16% of the reference). For each iteration the classification accuracy average and standard deviation of 100 RF runs was calculated, where every forest had samples selected through stratified-random sampling.

2.4. Results

2.4.1. General Accuracy and Transferability

The random-forest classification GEOBIA workflow resulted in highly complete (93.4%) and correct (94.5%) detections for overall CWD in the calibration area (Table 2.3). The correctness for the individual log and snag classes were also very high (87.0% and 91.7%, respectively), which was also the case for completeness of the snag detections (95.5%). Completeness for logs was slightly lower (76.9%, Table 2.3).

When applied to the verification area without any further training, the workflow still produced good overall CWD completeness (80.6%) and very high overall CWD correctness

(92.3%) results (Table 2.3). The correctness for the log and snag classes were good, but slightly lower (75.8% and 88.8%, respectively) than observed in the calibration area (87.0% and 91.7%, respectively). The completeness was higher for logs (81.5%) and considerably lower for snags (65.7%) in the verification area, relative to the calibration area (76.9% and 95.5%, respectively; Table 2.3). The standard deviations for completeness and correctness for the CWD union class is about half that noted in the other classes. The standard deviation of completeness and correctness was higher for logs than snags in the calibration area. The opposite was observed in the verification area.

Table 2.3. Accuracy metrics completeness and correctness for all CWD, only logs, and only snags. Training samples were obtained solely from the calibration area; the first application has testing samples in the calibration area and the second has testing samples in the verification area. These numbers reflect the average metrics of 100 random forests runs with a 80/20 training/testing random split of samples.

		Completeness			Correctness		
Application	Statistic	CWD union	Log	Snag	CWD union	Log	Snag
Calibration	Average	93.4%	76.9%	95.5%	94.5%	87.0%	91.7%
	Standard Deviation	2.1%	5.4%	2.2%	1.6%	4.5%	2.7%
Verification	Average	80.6%	81.5%	65.7%	92.3%	75.8%	88.8%
	Standard Deviation	3.0%	5.4%	4.8%	2.9%	4.9%	4.7%

2.4.2. Significance of LiDAR-derived height variables

Accuracy statistics for the RF test using CHM and DSM variables together were not significantly different than those produced using CHM variables alone (Figure 2.3). Models using CHM variables had higher snag completeness and log correctness than those using only a DSM.

Models using any sort of height variables performed significantly better than those using spectral variables alone. However, the difference was more noticeable in the log and snag classes, and less-so in the CWD union class.

Statistical significance was tested for all of the results reported above using difference-of-means t-tests, and are provided in Appendix B.

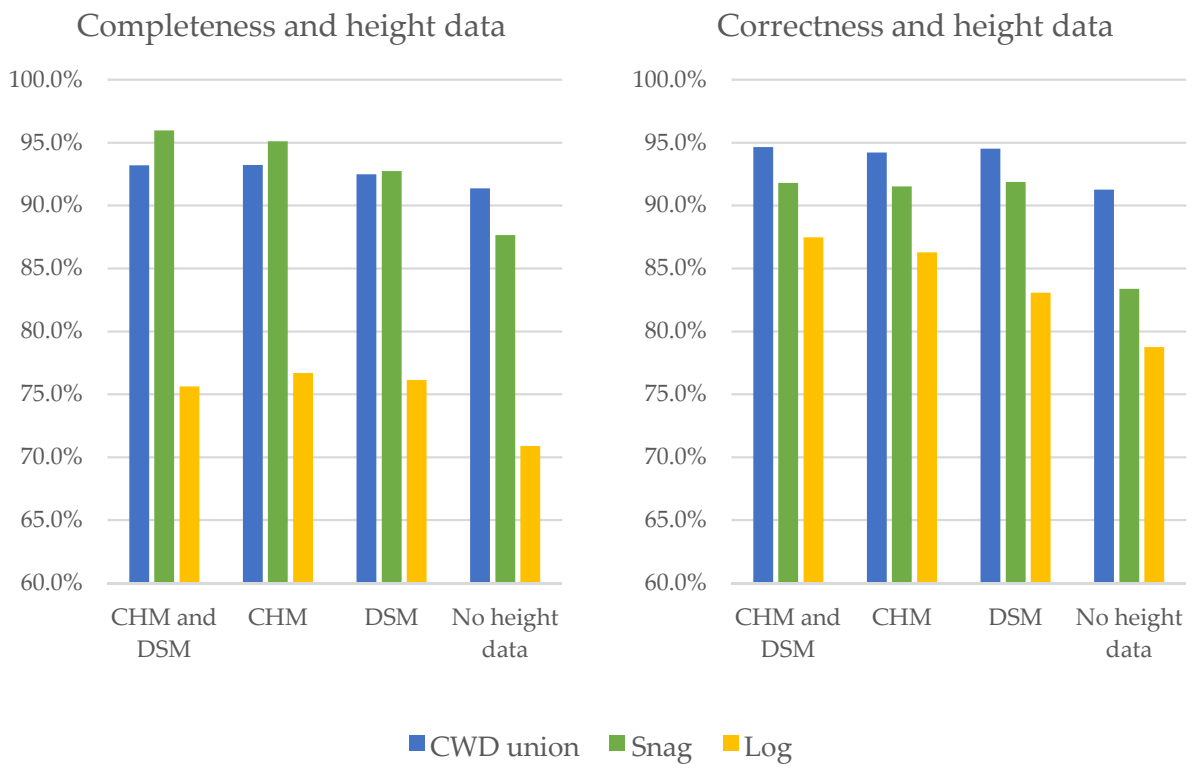

Figure 2.3. Bar plots of completeness (left) and correctness (right) using different combinations of height attributes: both canopy height model (CHM) and digital surface model (DSM), only CHM, only DSM, and no height data. Average metrics for 100 runs with randomly selected training/testing samples on the calibration area.

2.4.3. Importance of Predictor Variables

The *importance* scores of predictor variables in the 100 RF runs for the log and snag classes is summarized in Figure 2.4. The NDVI predictor variables received the highest minimum, maximum, median, first-quartile, and third-quartile importance amongst all types of predictor variables. CHM received the second highest third-quartile and median importance amongst all categories, ranking much higher on average than most DSM variables. The visible and near-infrared layers category (RGBN) received the second highest maximum and first-quartile importance. Most spatial variables received low importance values, with a few

exceptions. Almost all DSM variables ranked very low on importance, except DSM standard deviation, which scored a 4.9 average CWD importance value (displayed as an outlier in Figure 2.4).

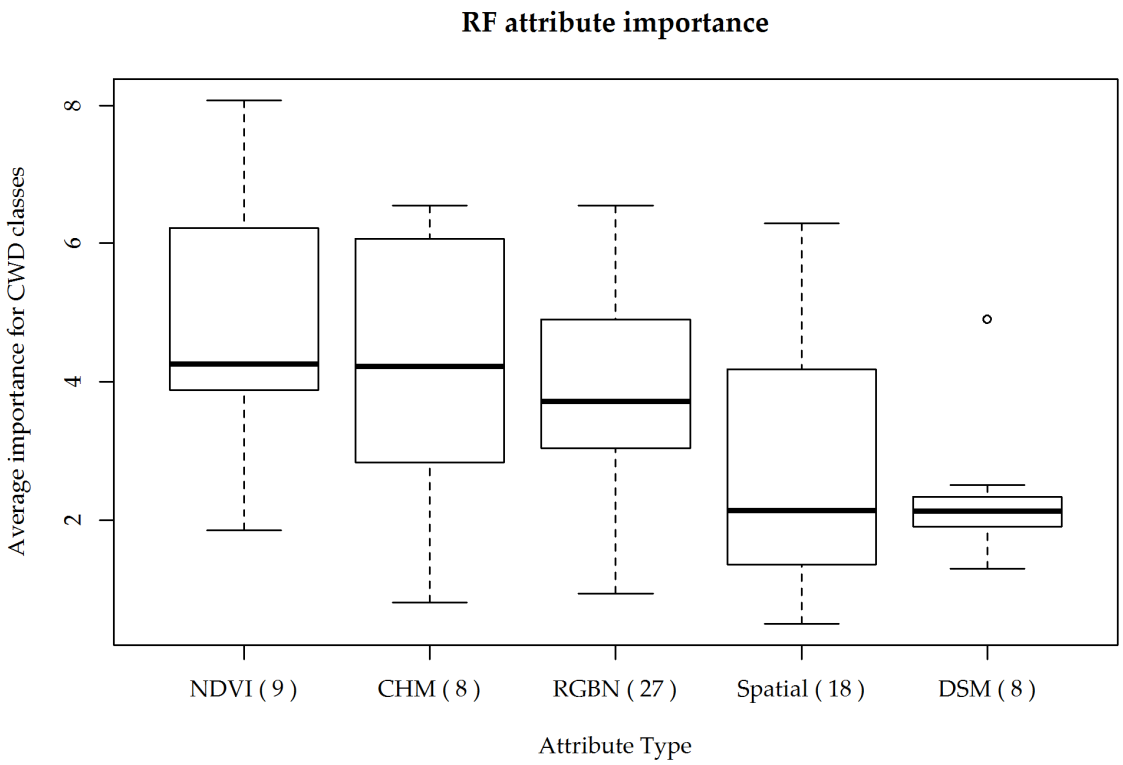

Figure 2.4. Box and whisker plot of the random forest (RF) importance relative to the CWD classes for different predictor variable categories: normalized difference vegetation index (NDVI), canopy height model (CHM), visible and near-infrared layers (RGBN), extent and shape (spatial) attributes, and digital surface model (DSM). The number of attributes in each category is shown in parenthesis. Importance shown is the average of 500 random forests using all available attributes on the calibration area.

The top 15 most important variables for CWD classification in decreasing order of importance were as follows: mean NDVI, mean inner border NDVI, green/RGB, mean CHM, density, mean inner border CHM, minimum NDVI, asymmetry, polygon length by width, mean outer border CHM, border length by length, blue/RGB, red border contrast, red difference

from neighbors, green border contrast. A list with the importance of all predictor variables is presented in Appendix C.

The minimum number of attributes required to obtain reliable average CWD accuracy above 90% completeness and 87% correctness was 15, below which the accuracy metrics decreased drastically (Figure 2.5). Completeness seemed to slightly rise indefinitely as new attributes were added, whereas correctness seemed to stabilize at about 88.5% after 45 attributes were included as predictor variables.

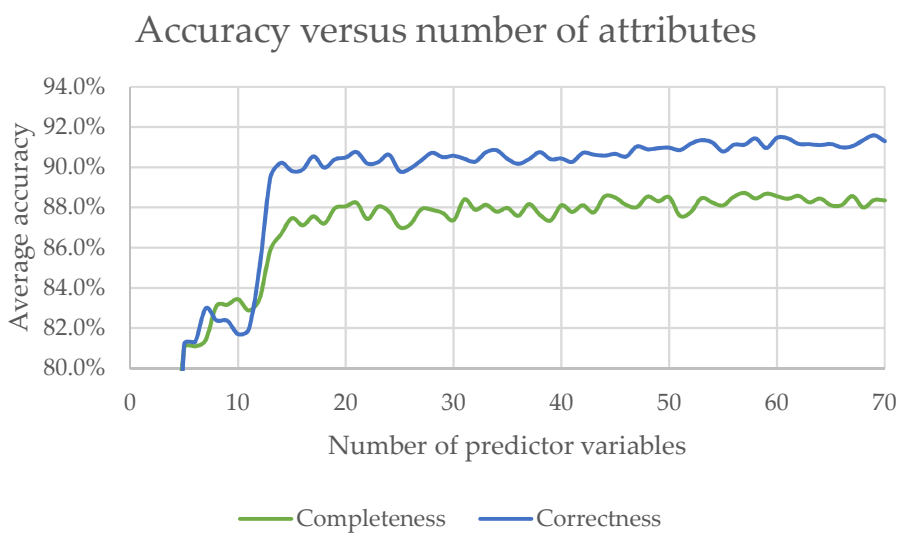

Figure 2.5. Line graph of number of attributes versus classification accuracy of CWD. Accuracy metrics shown are the average of 100 random forests for logs, snags, and the CWD union classes on the calibration area.

2.4.4. Effect of Training-Sample Size

Both completeness and correctness continually decreased as the number of training samples decreased, but completeness was found to decrease more drastically when there were less than 40 samples (Figure 2.6). Correctness never crossed the 65% threshold, whereas completeness was lower than 40% for logs when there are less than 35 training samples. Levels of 90% average completeness for the CWD union class could be achieved with as few as 512 training samples. Levels of 90% average correctness could be achieved

with as few as 64 samples. Standard deviation smaller than 4% could be achieved with as few as 256 samples for completeness and 100 samples for correctness.

Figure 2.6. Graphs of completeness (a) and correctness (b) versus number of training samples on the calibration area.

2.5. Discussion

2.5.1. General Accuracy and Transferability

The proposed method was able to map CWD in the study area with great accuracy on the calibration area and good accuracy in the verification area. This means that models trained in one location can be applied in distant locations, as long as the imagery and ground conditions remain similar. The measured log accuracy metrics completeness and correctness for the calibration area were 76.9% and 87.0%, respectively, and for the verification test were 81.5% and 75.8%, respectively. Even though these numbers fluctuated between the two areas they are still within the same range given their respective standard deviations. Therefore, the method was considered to achieve the same accuracy for logs on the two areas.

Other studies mapping logs on aerial images were able to detect logs with comparable accuracy, such as Baumann et al. (2014) with about 68% and 95%, Duan et al. (2017) with 75.7% and 92.5%, Rüetschi et al. (2019) with 88% and 85%, and Panagiotidis et al. (2019) with 84.6% and 94.9% completeness and correctness, respectively. However, the accuracies in the present study reflect more challenging conditions involving CWD in diverse settings—natural and disturbed forest—at varying stages of decomposition and over a large application area.

The present study mapped individual CWD pieces, analogous to the results of Richardson and Moskal (2016) and Duan et al. (2017), but was also able to map snags obtaining 95.5% completeness and 91.6% correctness in the calibration area and 65.7% completeness and 88.8% correctness in the verification area. These are comparable to the results of Bütler and Schlaepfer (2004) and Stereńczak et al. (2017). The accuracy metrics presented in this study are unique in that they are based on the area of individual objects, whereas the other studies use count-based measures of the detected objects or summary of the area of multiple objects.

The considerable decrease in snag completeness between the calibration and verification tests in this study is likely due to the fact that most snags identified in the verification area

were small coniferous trees, whereas most snags identified in the calibration area corresponded to medium to large sized conifers or large deciduous trees, as can be seen in the histograms of the area of snag objects (Figure 2.7). This highlights that the method is most effective when applied to an area with similar species compositions to the training area, or when ensured that the full range of composition is included in the training part.

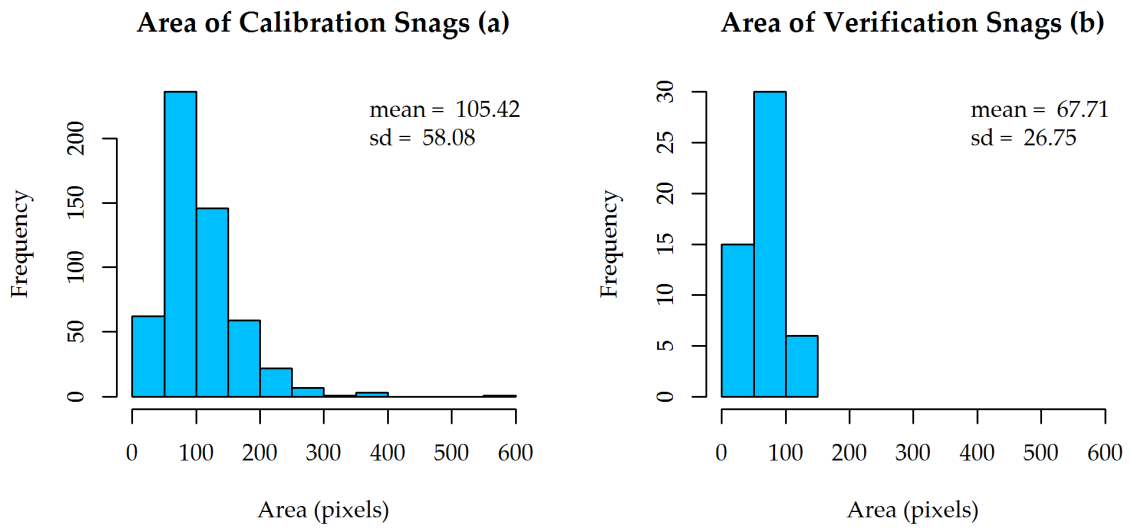

Figure 2.7. Histograms of area (pixels) of snag objects in the calibration (a) and verification (b) areas. Mean and standard deviations (sd) are indicated on each graph.

The developed method was most accurate when mapping CWD regardless of the log/snag distinction, obtaining completeness and correctness for the CWD union class of 80.6% and 92.3%, respectively, in the verification area, and 93.4% and 94.5%, respectively, in the calibration area. These results support the observation that the workflow yields highly accurate detection of overall CWD given the complex and extensive nature of the study area. Since the accuracy metrics for the log and snag classes is significantly lower than for the CWD union class, it is evident that there is some confusion between log and snag objects. This suggests that there is room for improvement in the automated distinction between the CWD classes, which could be addressed in future studies.

2.5.2. Significance of LiDAR-Derived Height Variables

Experiments using both, either, and none of the two types of height data—DSM and CHM—significantly increased the distinction between logs and snags, though the classification accuracy of the undistinguished CWD union improved by just 2%. We found the CHM to be significantly better than the DSM for the purpose of distinguishing logs from snags, particularly with respect to completeness. Although they theoretically present the same information, this difference might be due the fact that the dynamic data range in the CHM is larger (compared to the DSM), which is able to account for smaller variability of objects (heights).

There were no significant benefits of using both a DSM and a CHM. Since the CHM was derived from the DSM and a digital terrain model, the addition of DSM variables could be considered redundant in this case. The handling of redundant variables by the random forest algorithm is further discussed in the following subsection. We suggest that the most parsimonious selection of attributes concerning height data is the CHM, in addition to the spectral and shape attributes.

Future studies using similar methods that are not concerned with the distinction between logs and snags might choose to not use height data as predictor variables for CWD, since neither the CHM nor DSM significantly increased CWD union accuracy. Conversely, studies targeting snags or logs specifically, or concerned with the distinction between the two classes, will benefit from adding height data as predictor variables.

2.5.3. Importance of Predictor Variables

The NDVI was the most important predictor variable type overall, which was expected since CWD exhibits a very low NDVI signal overall. The top 15 attributes in the importance test included a mix of NDVI, spectral, spatial, and CHM variables, with DSM being the only variable type not included. This can be explained as random forest prioritizing CHM variables as better predictors than DSM for the target classes. However, one DSM-related variable was

an outlier. DSM standard deviation ranked 18th place, while CHM standard deviation ranked 31st. It is possible that some of the local variability of the DSM was lost when subtracting a terrain model to generate the CHM, which could explain why RF ranks higher this one instance of DSM vs. CHM variables.

We found that accurate CWD detection could be achieved with as few as 15 predictor variables. As more attributes are added completeness seems to rise indefinitely, while correctness peaks around 45 attributes, after which it stabilizes around 88.5%. This effect suggests that RF is highly effective in boosting the effect of more important variables in its classification trees, minimizing the influence of redundant or ineffective variables.

2.5.4. Effect of Training-Sample Size

Larger training-sample sizes yielded higher accuracy results, as expected. However, this effect seemed to be more drastic for the log class than the snag or CWD union classes. Since there were more snag samples (537) than log samples (364) in the calibration area, and since the number of samples in this experiment was decreased while maintaining the original proportion of samples for each class, it is logical to expect that the class with less samples will be more strongly affected when reducing the sample size. Completeness and correctness above 90% could be achieved in the CWD union class with as few as 512 samples. Good distinction between logs and snags, with accuracy metrics higher than 70%, could be achieved with about 1000 training samples.

2.5.5. Sources of Error

One important limitation to note is that the proposed method is only as reliable as the quality of the remote sensing data used, since blurriness, shadows, and occlusions can interfere with the identification of CWD. The accuracy tests performed in this study were based on what the human interpreter was capable to identify on the segmented orthomosaic, therefore human mistakes, as well as unidentifiable objects caused by small size,

segmentation problems, and image processing artifacts, could not be fully accounted for in the accuracy assessments. These factors add a certain degree of uncertainty to our reported results. However, we consider the error sources related to pre-processing and segmentation to be minor relative to the number of meaningful identifiable objects in the images, as explained in Appendix A.

Some initial tests comparing leaf-on (summer) and leaf-off (spring) data of the study area suggested that there are trade-offs in accuracy when using either. Leaf-on has the advantage of much stronger NDVI contrast between live and dead vegetation, increasing the correctness of CWD detection. Leaf-off enables a more complete view of logs, since the occlusion caused by canopy is lessened, increasing the completeness of CWD detection. In this study, we prioritized correctness and used leaf-on data; future studies may compare and combine data obtained at different times for an assessment of the best configuration of input images for CWD classification.

Given the variability built into the selection process of the training and testing samples, as well as the creation of the random forest classifier, we suggest that the accuracy metrics be considered alongside their respective standard deviations. For example, given the results of Table 2.3 and given the normal distribution of completeness and correctness for CWD union in the calibration area, test metrics could be expressed as 93.4 ± 4.2% and 94.5 ± 3.2%, respectively, 19 out of 20 times.

2.5.6. Application and Next Steps

The developed method could be promptly applied to studies interested in CWD detection under any environmental context, be it forestry, biogeography, or disaster management. All that is required is for the user to possess aerial data of equivalent resolution to this study and produce a modest number (~100) of training samples. A sample CWD map, derived from a small subset of the study area, is shown in Figure 2.8.

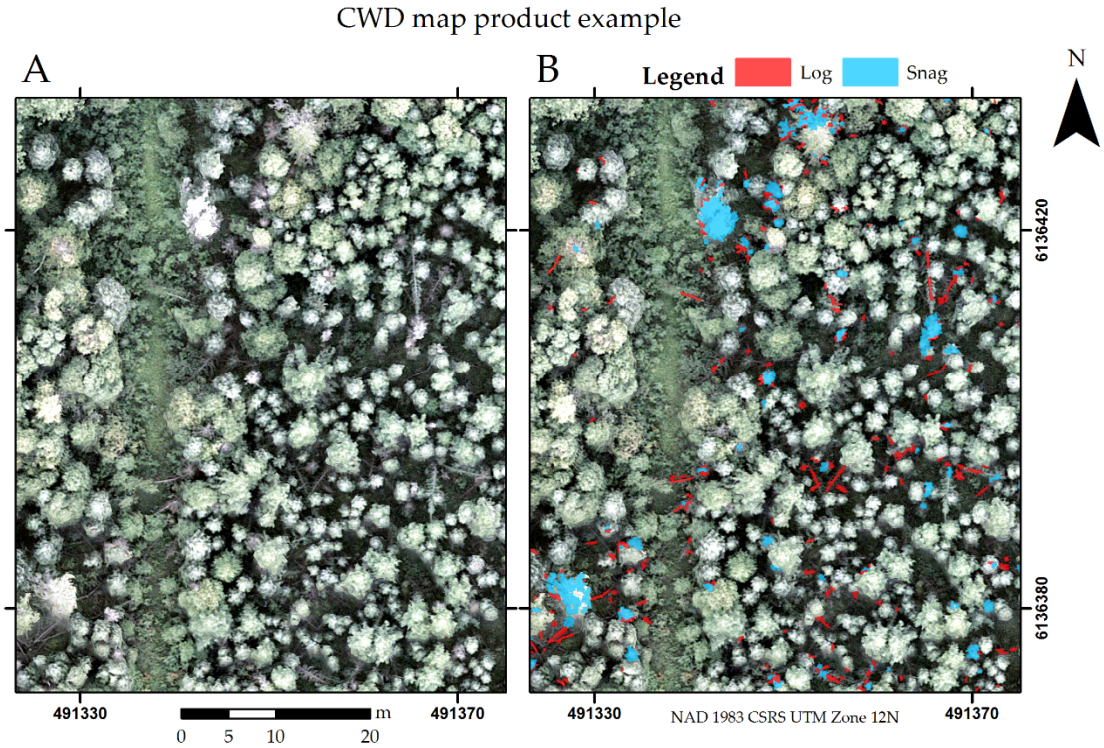

Figure 2.8. Application example of the developed method in a small subset of the study area without (**A**) and with (**B**) the classified CWD objects.

Assuming that a hypothetical application area has similar variability in terms of CWD distribution and image-object attributes to the areas in this study, reliable accuracy could be expected by using the top 35 predictor variables listed in Appendix C. If an end user was not concerned with the distinction between logs and snags, then our experience suggest that a minimum of 100 training samples, assuming a NDVI-based random stratified sampling strategy, should suffice. If the distinction between logs and snags was important, then our results suggests that 1000 training samples would be required.

When applying this method to a different area, differences in CWD spatial distribution, species composition, class distribution, and climate will affect the accuracy of this method and importance of its predictor variables. The verification area test demonstrated that it is possible to apply a model developed in a different area of the same natural sub-region and overall structure without additional training and obtain reliable results. Studies outside of the boreal

forest context or containing different unique features, such as an urban environment, should utilize their own training samples as explained above and expect similar results given an appropriate number of training samples. The more different the ecosystem of an application area is from the boreal context, the larger the anticipated difference between the results of this hypothetical application area and the results of this study in terms of accuracy, significance, and importance of predictor variables. However, given the robustness of random forests in prioritizing important variables based on the reference data, a new round of training on a hypothetical area should produce a random forest classifier well prepared for the specific features of this area. Additionally, the relative effect of transferability on classification accuracy, as observed in the verification area test, should be similar in different ecosystems when using a unique training set, assuming that these environments have similar within-ecosystem variability to the study area presented here.

This study achieved accurate detection of logs and snags in high-resolution (centimetric) images of an extensive and complex application area, located in the boreal forest of Alberta. We note the results in this paper are relative to what is visible in the input images. Occlusion caused by superimposed vegetation and visual ambiguities, such as similarities between live and recently dead trees or any other factor that may hinder manual visual identification of CWD objects, should also be expected to affect CWD detection based on supervised classification. For example, Inoue et al. (2014) evaluated manually identified remotely-sensed CWD relative to ground-truth and achieved about 85% completeness in a broadleaf forest of Japan. Further research could involve validating this method according to field-measured CWD and modelling the volume of the detected CWD objects, similar to Davis (2017), but concerning both logs and snags in both forested and disturbed areas within the boreal application context.

2.6. Conclusions

We applied random-forest classification within a GEOBIA workflow to identify logs and snags in aerial four-band centimetric images (5.5 cm GSD) and LiDAR data (20 cm pixel CHM and DSM derived from 20 points/m^2 ALS) of the boreal forest. Great accuracy results—93.4 ± 4.2% completeness and 94.5 ± 3.2% correctness—were documented when training samples were present in the application area. Good accuracy results—80.6 ± 6.0% completeness and 92.3 ± 5.8% correctness—were found when training samples were detached from the application area. Experiments with CHM and DSM height variables as predictor variables revealed that even though height data did not increase overall CWD classification accuracy by more than 2% overall, it significantly improved the distinction between logs and snags. The CHM was significantly better than the DSM for this purpose. An attribute-importance test revealed that the most important predictor variables were a mix of NDVI, spectral, spatial, and CHM variables, and that a minimum of 15 attributes was required to obtain accurate classification. Adding more than 45 variables did not increase overall correctness. A test of training-dataset size showed that accurate results for the CWD union class could be achieved with as few as 512 training samples, but about 1000 samples were required to distinguish between logs and snags. Our results suggest that researchers, foresters, biogeographers, and government agencies can reliably make use of the developed workflow for mapping CWD on complex environments, such as the boreal forest of Alberta, and generate accurate products of strong ecological value.

2.7. Appendix A

Since the reference objects used for training or testing were randomly selected in this study, there were many instances where the objects were imperfect or unidentifiable. The meaningful classes used in random forest classification are described in Table 2.A1.

Table 2.A1. Detailed description and examples of the classes in the reference dataset of the verification area that were used for random forest classification, including count (N) and area. Example images provide both the visible (RGB) spectrum and a false-color image using near infrared (NIR).

	Name	N	Area (m^2)	Area (%)	RGB	NIR	Description
	Log	40	5.18	1.4%		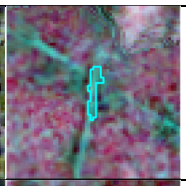	Part of downed coarse woody debris. Horizontal or leaning with an angle > 45°.
	Snag	51	8.63	2.3%		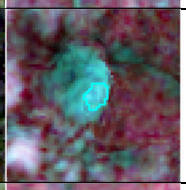	Part of standing coarse woody debris. Vertical or leaning with an angle < 45°.
	Water	7	1.42	0.4%	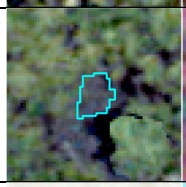	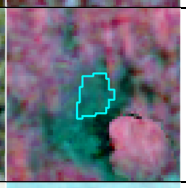	Portions of puddles, ponds and lakes.
	Dirt	253	100.27	26.6%			Segment of road, soil and mud.
Other	Low vegetation	325	90.50	24.0%	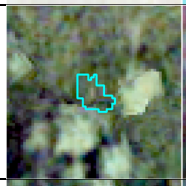	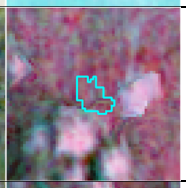	Segment of grass, shrub and moss.
Other	Tree	315	43.13	11.4%			Part of alive tree. Deciduous or coniferous canopy.
Other	Shadow	315	91.47	24.3%	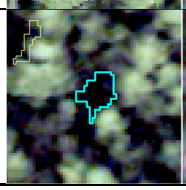	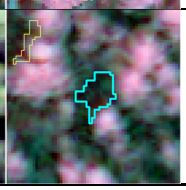	Object located in extremely shadowed area with irregular or round shape.

Artificial objects, such as ground control points, buildings, and power lines, were tagged as man-made. In cases where the human analyst was unable to discern if the object belonged

to any specific class, it was tagged as unidentified. These two classes were not used for training or testing, and are described in Table A2.

Table 2.A2. Detailed description and examples of the classes in the reference dataset of the verification area that were not used for classification, including count (N) and area. Example images provide both the visible (RGB) spectrum and a false-color image using near infrared (NIR). Normalized difference vegetation index (NDVI) is used as one of the indicators for coarse woody debris (CWD).

Name	N	Area (m^2)	Area (%)	RGB	NIR	Description
Man-made	2	0.56	0.1%			Part of human-made feature: ground control, building, power line.
Unidentified object	192	35.97	9.5%	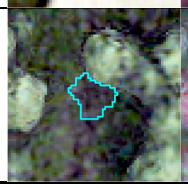	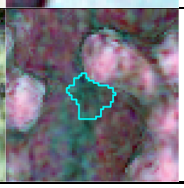	Usually small, round and dark object. Unclear if shaded coarse woody debris, dirt or water.

Given the inability of assigning unidentified objects as any of the classes used in training and their small total area (9.5% of testing objects), unidentified objects are not considered to significantly affect the accuracy of the method and were not used for either training or testing purposes. However, their existence makes it evident that even though the ground sampling distance was quite dense in this study (5cm pixel-size), some objects would require an even denser sampling distance for better identification.

2.8. Appendix B

The tables used for the pairwise difference-of-means t-test, performed on random forests using different combinations of height predictor variables, are provided in Tables 2.B1, 2.B2, 2.B3, and 2.B4.

Table 2.B1. Average accuracy of tests using different height attributes as predictor variables: spectral variables along with canopy height model (CHM) and digital surface model (DSM), only spectral and CHM, only spectral and DSM, only spectral variables (no height), and only height variables. Average completeness (Comp) and correctness (Corr) of 100 random forests for the classes: CWD union (Union), logs, and snags.

	Average completeness and correctness					
Attributes	**Comp Union**	**Corr Union**	**Comp Log**	**Corr Log**	**Comp Snag**	**Corr Snag**
CHMandDSM	93.2%	94.6%	75.6%	87.5%	95.9%	91.8%
CHM	93.2%	94.2%	76.7%	86.3%	95.1%	91.5%
DSM	92.5%	94.5%	76.1%	83.1%	92.7%	91.9%
No height	91.3%	91.3%	70.9%	78.7%	87.6%	83.4%
Only height	10.8%	36.0%	11.7%	24.6%	9.4%	45.9%

Table 2.B2. Accuracy standard deviation of tests using different height attributes as predictor variables: spectral variables along with canopy height model (CHM) and digital surface model (DSM), only spectral and CHM, only spectral and DSM, only spectral variables (no height), and only height variables. Standard deviation of completeness (Comp) and correctness (Corr) of 100 random forests for the classes: CWD union (Union), logs, and snags.

	Standard Deviation					
Attributes	**Comp Union**	**Corr Union**	**Comp Log**	**Corr Log**	**Comp Snag**	**Corr Snag**
CHMandDSM	2.3%	1.8%	6.3%	4.7%	1.9%	2.4%
CHM	2.3%	1.7%	6.3%	4.4%	2.1%	2.4%
DSM	2.4%	1.7%	6.5%	4.7%	3.0%	2.3%
No height	2.3%	2.6%	6.6%	5.6%	3.6%	3.5%
Only height	2.3%	7.7%	3.6%	9.1%	2.7%	11.8%

Table 2.B3. Results of t-tests comparing average accuracies of tests using different height attributes as predictor variables: spectral variables along with canopy height model (CHM) and digital surface model (DSM), only spectral and CHM, only spectral and DSM, only spectral variables (no height), and only height variables. P-values are provided for completeness (Comp) and correctness (Corr) for the classes: CWD union (Union), logs, and snags.

Two-sample difference of means:				H0: $x1 = x2$		HA: $x1 \neq x2$	
		P values					
Reference	**Comparison**	**Comp Union**	**Corr Union**	**Comp Log**	**Corr Log**	**Comp Snag**	**Corr Snag**
CHMandDSM	**CHM**	0.950	0.080	0.229	0.071	0.003	0.427
CHM	**DSM**	0.034	0.190	0.532	<0.001	<0.001	0.296
DSM	**No height**	<0.001	<0.001	<0.001	<0.001	<0.001	<0.001
No height	**Only height**	<0.001	<0.001	<0.001	<0.001	<0.001	<0.001

Table 2.B4. Results of t-tests comparing average accuracies of tests using different height attributes as predictor variables: spectral variables along with canopy height model (CHM) and digital surface model (DSM), only spectral and CHM, only spectral and DSM, only spectral variables (no height), and only height variables. Provided for completeness (Comp) and correctness (Corr) for the classes: CWD union (Union), logs, and snags.

Significance (α):		0.05					
		FAIL or PASS to reject null hypothesis					
Reference	**Comparison**	**Comp Union**	**Corr Union**	**Comp Log**	**Corr Log**	**Comp Snag**	**Corr Snag**
CHMandDSM	**CHM**	FAIL	FAIL	FAIL	FAIL	PASS	FAIL
CHM	**DSM**	PASS	FAIL	FAIL	PASS	PASS	FAIL
DSM	**No height**	PASS	PASS	PASS	PASS	PASS	PASS
No height	**Only height**	PASS	PASS	PASS	PASS	PASS	PASS

If at least one of the classes in a test of Table 2.B4 displayed significant improvement from one group to the next, then the group with the higher results was considered to be significantly superior for CWD prediction than the competitor. In this case, using both CHM and DSM was not significantly better than only using CHM, which was significantly better than using only DSM (specifically for log correctness and snag completeness), which in turn was

better than not using any height data. Using only height data was significantly worse than any other scenario. In conclusion, the simplest, best model used CHM predictor variables in conjunction with spectral variables.

2.9. Appendix C

Table 2.C1 summarizes the predictor variable importance for the log and snag classes, as obtained from the built in RF importance function, as well as the average CWD importance and the resulting rank from highest to lowest importance.

Table 2.C1. Image-object attributes obtained in eCognition (Trimble, 2016) used as predictor variables for creating the random forests (RF) and their importance for coarse woody debris classification according to the RF importance function. The average between log importance and snag importance was used for ranking (N) the variables. The types (T) of predictor variables are: spectral red, green, blue (RGB) and near-infrared (NIR) combined (RGBN, R), normalized difference index (NDVI, N), spatial (S), digital surface model (DSM, D) and canopy height model (CHM, C).

N	Attribute	T	Avg.	Log	Snag	N	Attribute	T	Avg.	Log	Snag
1	Mean NDVI	N	8.08	6.70	9.46	36	Brightness RGBN	R	3.58	2.94	4.23
2	Mean inner border NDVI	N	7.11	5.48	8.74	37	Polygon Width	S	3.58	4.74	2.42
3	Green/RGB	R	6.56	7.01	6.12	38	Mean green	R	3.54	2.76	4.31
4	Mean CHM	C	6.56	5.42	7.69	39	Green/RGBN	R	3.43	2.54	4.31
5	Density	S	6.30	7.51	5.08	40	Standard deviation green	R	3.08	3.22	2.93
6	Mean inner border CHM	C	6.23	5.30	7.16	41	Minimum CHM	C	3.07	3.28	2.85
7	Minimum NDVI	N	6.23	5.97	6.48	42	Standard deviation red	R	3.01	3.30	2.72
8	Asymmetry	S	5.93	6.91	4.95	43	Standard deviation NDVI	N	2.84	2.28	3.40
9	Polygon length by width	S	5.90	6.59	5.22	44	Mean Standard deviation	R	2.81	3.23	2.38
10	Mean outer border CHM	C	5.89	5.20	6.59	45	Standard deviation NIR	R	2.72	1.67	3.78
11	Border length by length	S	5.30	5.98	4.62	46	CHM skewness	C	2.62	1.89	3.34
12	Blue/RGB	R	5.15	5.97	4.34	47	DSM skewness	D	2.52	0.64	4.39
13	Red border contrast	R	5.10	7.02	3.19	48	Standard deviation Blue	R	2.36	2.94	1.77
14	Red difference from neighbors	R	5.03	6.10	3.96	49	Area in pixels	S	2.24	2.96	1.52
15	Green border contrast	R	5.00	6.75	3.25	50	Number of pixels	S	2.19	2.96	1.42
16	Mean NIR	R	4.98	5.08	4.87	51	Mean outer border DSM	D	2.18	1.73	2.63
17	Blue/RGBN	R	4.92	3.44	6.39	52	Mean DSM	D	2.15	1.87	2.42
18	Standard deviation DSM	D	4.90	4.35	5.44	53	Mean inner border DSM	D	2.13	1.75	2.51
19	Blue difference from neighbors	R	4.89	5.89	3.88	54	Border Index	S	2.11	1.18	3.04
20	Mean outer border NDVI	N	4.78	2.64	6.93	55	Maximum DSM	D	2.04	1.40	2.67
21	Green difference from neighbors	R	4.63	5.45	3.81	56	Main line width	S	2.02	1.94	2.09
22	Maximum CHM	C	4.61	3.57	5.65	57	Main line length by width	S	1.98	1.26	2.70
23	Blue border contrast	R	4.36	6.06	2.65	58	NDVI skewness	N	1.85	0.91	2.80
24	Maximum NDVI	N	4.26	3.27	5.26	59	Minimum DSM	D	1.76	1.74	1.77
25	Mean blue	R	4.24	2.96	5.52	60	Length in pixels	S	1.54	1.11	1.98
26	NDVI difference from neighbors	N	4.20	4.96	3.45	61	Rectangular fit	S	1.36	0.63	2.09
27	Shape index	S	4.18	4.32	4.05	62	DSM border contrast	D	1.30	2.08	0.52
28	Red/RGBN	R	3.94	3.11	4.77	63	Red skewness	R	1.27	0.59	1.96
29	Red/RGB	R	3.94	4.47	3.40	64	Perimeter	S	1.20	0.60	1.80
30	NDVI border contrast	N	3.88	5.40	2.35	65	Roundness	S	1.18	0.21	2.15
31	Standard deviation CHM	C	3.85	3.23	4.47	66	Green skewness	R	1.11	0.67	1.56
32	Compactness	S	3.80	3.78	3.82	67	Elliptic fit	S	1.11	0.32	1.90
33	Brightness RGB	R	3.72	2.77	4.68	68	Blue skewness	R	0.94	0.92	0.95
34	Mean red	R	3.70	2.91	4.48	69	CHM border contrast	C	0.81	1.87	-0.25
35	NIR difference from neighbors	R	3.63	2.92	4.33	70	Curvature by length	S	0.50	0.17	0.83

2.10. References

Agisoft. (2016). AgiSoft PhotoScan (Version 1.2.4.2399). St. Petersburg, Russia: Agisoft LLC.

Baumann, M., Ozdogan, M., Wolter, P. T., Krylov, A., Vladimirova, N., & Radeloff, V. C. (2014). Landsat remote sensing of forest windfall disturbance. *Remote Sensing of Environment*, *143*, 171–179. https://doi.org/10.1016/j.rse.2013.12.020

Breiman, L. (2001). Random Forests. *Machine Learning*, *45*(1), 5–32. https://doi.org/10.1023/A:1010933404324

Bütler, R., & Schlaepfer, R. (2004). Spruce snag quantification by coupling colour infrared aerial photos and a GIS. *Forest Ecology and Management*, *195*(3), 325–339. https://doi.org/10.1016/j.foreco.2004.02.042

Davis, B. (2017). *Refinement of a Drone-Based Method for Estimating Coarse Woody Debris and Biomass Residue Following Forest Harvest* (Master of Science). University of Georgia, Athens, Georgia.

Duan, F., Wan, Y., & Deng, L. (2017). A Novel Approach for Coarse-to-Fine Windthrown Tree Extraction Based on Unmanned Aerial Vehicle Images. *Remote Sensing*, *9*(4). https://doi.org/10.3390/rs9040306

Environment Canada. (2012). *Recovery strategy for the woodland caribou (Rangifer tarandus caribou), Boreal population, in Canada* (No. 9; p. 138). Ottawa, Canada: Environment Canada.

ESRI. (2017). ArcGIS Desktop (Version 10.6.1). Redlands, California.

Hay, G. J., & Castilla, G. (2008). Geographic Object-Based Image Analysis (GEOBIA): A new name for a new discipline. In T. Blaschke, S. Lang, & G. J. Hay (Eds.), *Object-Based Image Analysis: Spatial Concepts for Knowledge-Driven Remote Sensing Applications* (pp. 75–89). https://doi.org/10.1007/978-3-540-77058-9_4

Hebblewhite, M. (2017). Billion dollar boreal woodland caribou and the biodiversity impacts of the global oil and gas industry. *Biological Conservation*, *206*, 102–111. https://doi.org/10.1016/j.biocon.2016.12.014

Inoue, T., Nagai, S., Yamashita, S., Fadaei, H., Ishii, R., Okabe, K., … Suzuki, R. (2014). Unmanned Aerial Survey of Fallen Trees in a Deciduous Broadleaved Forest in Eastern Japan. *PLOS ONE*, *9*(10), e109881. https://doi.org/10.1371/journal.pone.0109881

Jonsson, B. G., & Kruys, N. (2001). Ecology of Coarse Woody Debris in Boreal Forests: Future Research Directions. *Ecological Bulletins*, (49), 279–281. Retrieved from JSTOR.

Kirkland, J. (2015, June). Bioenergy From Forests: The Power Potential of Woody Biomass. *Science Findings*, (174), 5.

Liaw, A., & Wiener, M. (2018). Breiman and Cutler's Random Forests for Classification and Regression (Version 4.6-14) [R]. Retrieved from https://cran.r-project.org/web/packages/randomForest/randomForest.pdf

Natural Regions Committee. (2006). Natural regions and subregions of Alberta. *Compiled by DJ Downing and WW Pettapiece. Government of Alberta. Pub*.

Panagiotidis, D., Abdollahnejad, A., & Surový, P. (2019). Detection of fallen logs from high-resolution UAV Images. *New Zealand Journal of Forestry Science*, *49*.

Pedlar, J. H., Pearce, J. L., Venier, L. A., & McKenney, D. W. (2002). Coarse woody debris in relation to disturbance and forest type in boreal Canada. *Forest Ecology and Management*, *158*(1), 189–194. https://doi.org/10.1016/S0378-1127(00)00711-8

Polewski, P., Yao, W., Heurich, M., Krzystek, P., & Stilla, U. (2015). Detection of fallen trees in ALS point clouds using a Normalized Cut approach trained by simulation. *ISPRS Journal of Photogrammetry and Remote Sensing*, *105*, 252–271. https://doi.org/10.1016/j.isprsjprs.2015.01.010

R Core Team. (2018). *R: A language and environment for statistical computing*. Retrieved from https://www.R-project.org/

Richardson, J. J., & Moskal, M. L. (2016). An Integrated Approach for Monitoring Contemporary and Recruitable Large Woody Debris. *Remote Sensing*, *8*(9). https://doi.org/10.3390/rs8090778

Rüetschi, M., Small, D., & Waser, T. L. (2019). Rapid Detection of Windthrows Using Sentinel-1 C-Band SAR Data. *Remote Sensing*, *11*(2). https://doi.org/10.3390/rs11020115

Stereńczak, K., Kraszewski, B., Mielcarek, M., & Piasecka, Ż. (2017). Inventory of standing dead trees in the surroundings of communication routes – The contribution of remote sensing to potential risk assessments. *Forest Ecology and Management*, *402*, 76–91. https://doi.org/10.1016/j.foreco.2017.07.018

Sumnall, M. J., Hill, R. A., & Hinsley, S. A. (2016). Comparison of small-footprint discrete return and full waveform airborne lidar data for estimating multiple forest variables. *Remote Sensing of Environment*, *173*, 214–223. https://doi.org/10.1016/j.rse.2015.07.027

Trimble. (2016, July 27). *ECognition Developer 9.2 Reference Book*. Retrieved from http://www.ecognition.com/free-trial

Trimble. (2018). ECognition Developer (Version 9.4) [Windows]. Munich, Germany: Trimble Germany GmbH.

Ucitel, D., Christian, D. P., & Graham, J. M. (2003). Vole Use of Coarse Woody Debris and Implications for Habitat and Fuel Management. *The Journal of Wildlife Management*, *67*(1), 65–72. https://doi.org/10.2307/3803062

Vinge, T., & Pyper, M. (2012). *Managing woody materials on industrial sites: Meeting economic, ecological, and forest health goals through a collaborative approach*. Department of Renewable Resources, University of Alberta, Edmonton, Alberta.

Westoby, M. J., Brasington, J., Glasser, N. F., Hambrey, M. J., & Reynolds, J. M. (2012). 'Structure-from-Motion' photogrammetry: A low-cost, effective tool for geoscience applications. *Geomorphology*, *179*, 300–314. https://doi.org/10.1016/j.geomorph.2012.08.021

Yan, E., Wang, X., & Huang, J. (2006). Concept and Classification of Coarse Woody Debris in Forest Ecosystems. *Frontiers of Biology in China*, *1*(1), 76–84.

Chapter Three: Estimating Coarse Woody Debris Volume Using Image Analysis and Multispectral LiDAR

3.1. Abstract

Coarse woody debris (CWD, large parts of dead trees) is an important factor in forest management, given its roles in promoting local biodiversity and unique microhabitats, as well as providing carbon storage and fire fuel. However, parties interested in monitoring CWD density lack precise methods to measure CWD accurately and extensively. Here, we demonstrate a novel strategy for mapping CWD volume (m3) across a 4300-hectare study area in the boreal forest of Alberta, Canada using optical imagery and an infra-canopy vegetation-index layer derived from multispectral aerial LiDAR. Our models predicted CWD volume with a coefficient of determination (R^2) value of 0.62 compared to field data, and a root-mean square error (RMSE) of 0.224 $m^3/100m^2$. Models using multispectral LiDAR data in addition to image-analysis data performed with up to 12% lower RMSE than models using exclusively image-analysis layers. Site managers and researchers requiring reliable and comprehensive maps of CWD volume may benefit from the presented workflow, which aims to streamline the process of CWD measurement. As multispectral LiDAR sensors become more powerful and ground intensity readings more reliable, we expect CWD detection underneath canopy cover to become even more accurate.

3.2. Introduction

Woody debris is a vital component in forested environments, affecting the biochemistry and physical structure of an ecosystem (Harmon et al., 1986). Coarse woody debris (CWD) is defined here as dead wood, intact or partially decomposed, with diameter at the largest end of at least 7 cm and length of at least 1m, lying horizontally or leaning with an angle less than 45 degrees relative to the horizon. In the literature, CWD following this definition is commonly

referred to as “logs”, and standing dead trees are commonly referred to as “snags” (Yan et al., 2006). The survival and success of many types of organisms, including plants, fungi, insects, birds, reptiles, amphibians and mammals, is directly or indirectly dependent on the presence and quality of CWD (McWinn et al., 1996; Hagan and Grove, 1999; Riffell et al., 2011). Conversely, CWD logs in excessive quantities configure a fire hazard which historically has been removed from forest worksites to prevent wildfires and only recently reincorporated in forest restoration programs to promote biodiversity and soil productivity (Brown et al., 2003; Vinge and Pyper, 2012).

Extensive and accurate estimates of CWD quantities over large forested areas are difficult to achieve due to its high variability within and between regions (Harmon et al., 1986). Traditional methods to study CWD rely solely on field data collection, which is an expensive and time-consuming endeavor usually highly constrained by accessibility to the sampling sites. Since the advent of high-speed, large-data computing a variety of automated remote-sensing solutions have been implemented to identify and measure forest structure and components through the analysis of imagery collected with aircraft and satellites. Remote sensing of CWD has been achieved with variable degrees of success on satellite data (Baumann et al., 2014; Ruetschi et al., 2019) and high-resolution piloted and unpiloted aircraft imagery (Richardson and Moskal, 2016; Duan et al., 2017, Lopes Queiroz et al., 2019). These studies commonly use pixel-based or geographical object-based image analysis (GEOBIA) solutions to process aerial images using linear models, classification trees, and machine learning to extract information regarding CWD objects. However, aside from studies on post-fire forests where the canopy is reduced, canopy cover as well as superimposed vegetation present in the understory and forest floor occlude low-lying CWD and therefore represent an important limiting factor to remote sensing studies using optical data. Inoue et al. (2014) detected from 80% to 90% of CWD larger than 30 cm in diameter or 10 m in length on 1cm ground sampling distance (GSD) aerial photos of a deciduous forest in Japan during the fall (i.e. leaf-off conditions) by manually identifying and delineating objects. If human interpreters could

identify at most 90% of relatively large CWD on leaf-off, which represents good visibility conditions, one would expect automated detection to perform worse on more difficult conditions or smaller CWD. Some of the most successful recent studies of automated detection of CWD on forests such as Duan et al. (2017), Stereńczak et al. (2017) and Lopes Queiroz et al. (2019) have developed sophisticated methods for the detection of visible CWD on aerial images but have based their accuracy metrics on what is visible in aerial photos and not on field data, and therefore their efficacy based on ground truth remains unknown.

Light detection and ranging (LiDAR) technologies have been widely used for forest measurement, especially for canopy height, forest structure, and volume measurements (Lim et al., 2003). LiDAR is valuable for CWD studies since it provides information from the forest floor and understory. Terrestrial LiDAR can provide detailed point clouds of the understory and ground surface, but aerial LiDAR sensors, carried by surveying aircraft, are more commonly used for modeling extensive study areas. Mücke et al. (2013) detected CWD with diameter larger than 30cm with good accuracy, 75% completeness and 90% correctness) by analyzing dense LiDAR point clouds (29.4 returns/m^2) on a small study area (~6 ha) in Hungary. Sumnall et al. (2016) estimated various forest variables on plots located in a 2200 ha study area in southern England, containing semi-natural and plantation forests, by modelling LiDAR variables and considered their CWD (larger than 10cm at largest end) volume results moderately accurate (0.51 R^2, 2.74 RMSE). These studies have proved the potential of LiDAR in aiding CWD estimates but have acknowledged that further studies are required to improve their results and have not been tested in boreal forests.

Multispectral LiDAR (ML) is an emerging technology which uses LiDAR sensors capable of capturing returns from multiple wavelengths on the same platform, as opposed to traditional LiDAR sensors which only capture returns from a single near-infrared wavelength. ML has been applied to classify forests (Hopkinson et al., 2016; Budei et al., 2018) as well as measure vegetation indices (Chasmer et al., 2017), but has not yet been used to predict CWD quantities occluded by canopy. Chasmer et al. (2017) successfully derived an active

normalized burn ratio on boreal peatlands and suggested that ML data could be used to quantify understory and lower canopy features. We anticipated that infra-canopy vegetation indices derived from ML data could improve predictive models of CWD volume.

There have been few studies attempting to estimate CWD volumes, including debris as small as 7cm, accurately and extensively in both visible and occluded areas. The present study aims to address this gap in the literature by developing models which use both GEOBIA-layers and ML information to extract accurate CWD volumes and can be applied to an extensive study area in a boreal forest of northeastern Alberta, Canada. We expected this approach to be able to accurately quantify CWD volume based on field data and we believed that ML data would be beneficial to predictions on occluded areas. Variables we predicted would have a relationship with occurrence and quantities of CWD include: height of trees, active and passive vegetation indices, canopy cover, presence of visible CWD, shadows, water and wetlands. We tested our models both in a calibration area, where the models were developed, and in a verification area 4 km distant from the calibration area, and compared the best models using ML variables with the best models without ML variables to assess the impact of infra-canopy information on volume estimation accuracy. We then generated a series of CWD-volume maps designed to illustrate the utility of our approach to aid forest restoration efforts and fire-hazard assessments.

3.3. Methods

We used 5-cm ground sampling distance (GSD) aerial photos in a geographic object-based image analysis (GEOBIA) workflow to produce a visible CWD layer, and then processed multispectral LiDAR (ML) point clouds to produce ground-level vegetation-indices layers that allowed for better estimates of occluded CWD quantities. By joining the GEOBIA-derived and ML-derived datasets together, we achieved CWD-volume models with better predictive power than what was possible with GEOBIA alone. Our workflow is summarized in Figure 3.1 and detailed in the following subsections.

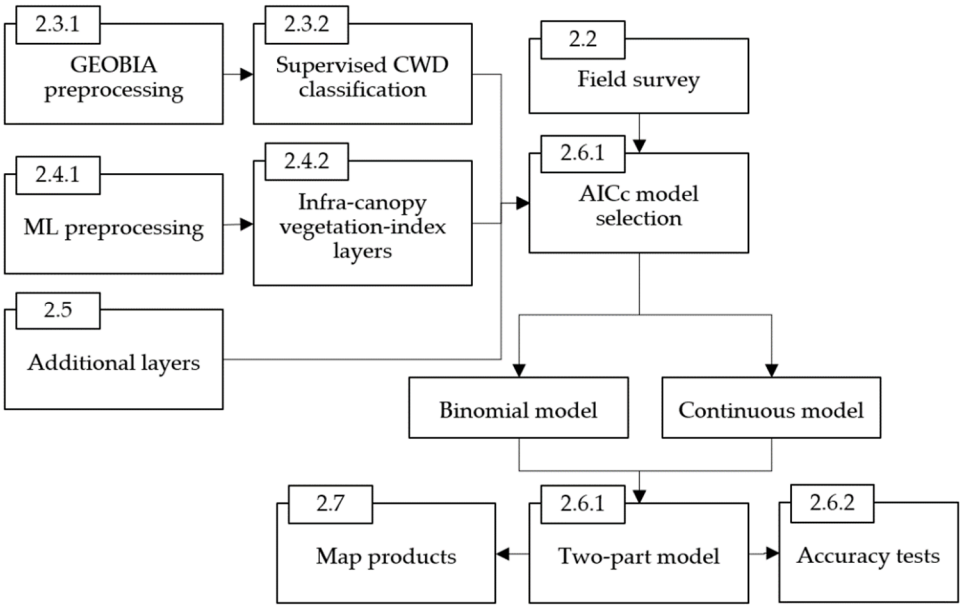

Figure 3.1. Workflow chart of this study with the sub-section numbers where each step is explained in this document. We mapped non-occluded coarse woody debris (CWD) via a geographic object-based image analysis (GEOBIA) workflow. Occluded CWD quantities were estimated using multispectral LiDAR (ML) vegetation indices from underneath the canopy. We selected potential models for CWD volume using the small sample Akaike information criterion (AICc) as an indicator for model predictive power.

3.3.1. Study Area

The 4300-hectare study area (Figure 3.2) is located in the mixed-wood natural subregion of the boreal forest (Alberta Parks, 2015) in northeastern Alberta, Canada. The rolling terrain can be divided into two distinct environments: uplands and lowlands (i.e. wetlands). The tree population in the upland areas is mostly composed of jack pine (39.5%; *Pinus banksiana* Lamb.), black spruce (32.6%; *Picea mariana* (Mill.) B.S.P.), and trembling aspen (22.2%; *Populus tremuloides* Michx.) trees. Uplands are composed of 56% coniferous, 12% broadleaf and 32% mixed forest stands (Government of Alberta, 2019) while lowlands are mostly composed of fens (83%), but also include swamps (12%) bogs (2%) and marshes (2%; DeLancey et al., 2019). Wetlands are dominated by black spruce (64.8%) and tamarack

(26.0%; Larix laricina (Du Roi) K. Koch; Government of Alberta, 2019) but can also be mostly composed of shrubs, grasses and moss (Downing and Pettapiece, 2006). There are approximately 342 km of seismic lines (i.e. petroleum exploration corridors) within this area, most of which are visible from aerial images as seen in Figure 3.2. There are a few (less than 2% of the study area) deactivated timber-harvest sites in the area from the last two decades. Some water bodies and human-made features such as power-lines, constructions and roads also exist within the study area.

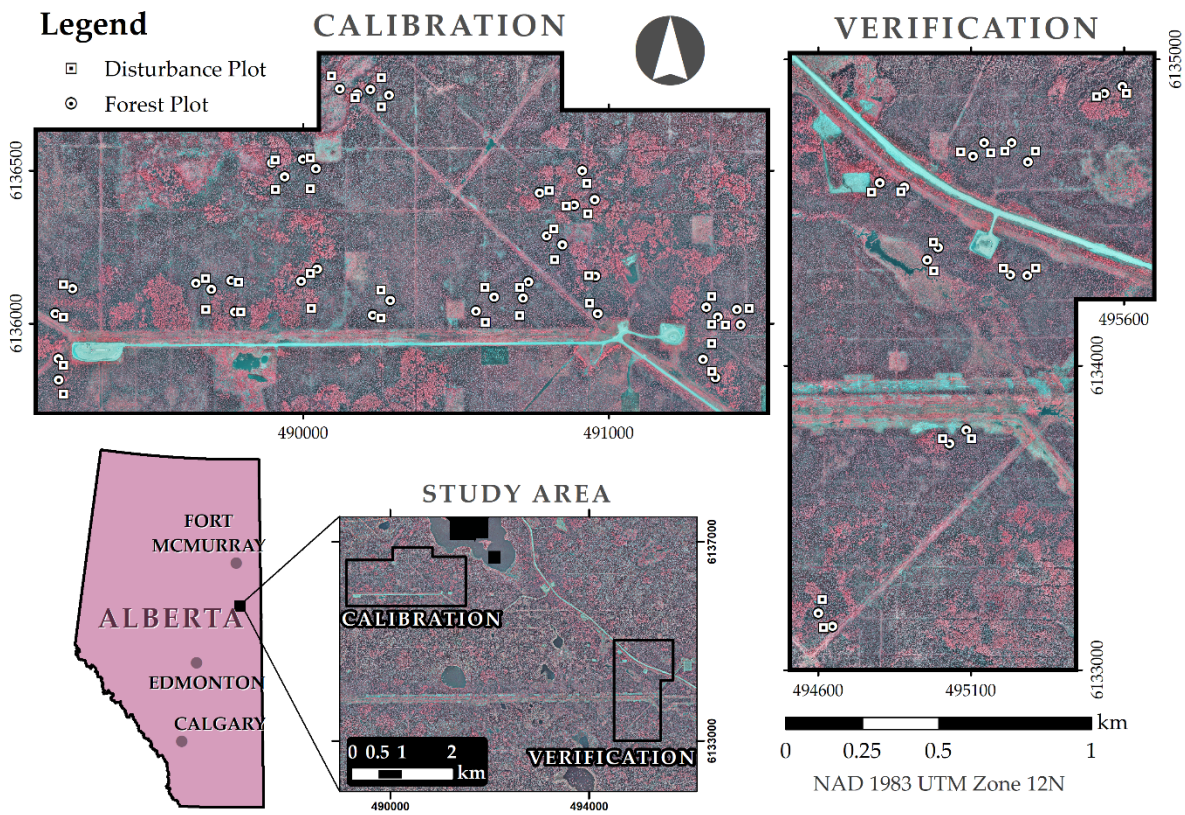

Figure 3.2. Location of the calibration and verification areas within the 4300-hectare study area as well as the location of the field plots where CWD volume was surveyed. The background image is a false-color image using near infrared, red and green spectral bands. Upland broadleaf stands dominated by trembling aspen appear as lighter shades of red; conifer-dominated lowlands and mixed-wood uplands appear as darker tones. Roads, seismic lines (petroleum-exploration corridors), and petroleum well pads appear as lines and geometric features.

An estimate of canopy closure on the study area, obtained using a LiDAR-derived CHM and further explained in subsection 3.3.5, revealed that forest stands are much denser on uplands (68.4% average canopy closure) than lowlands (27.2% average canopy closure), as seen on Table 3.1.

Table 3.1. Mean canopy closure on vegetated portions of the study area. Uplands are divided into forest stand types (Government of Alberta, 2019) and lowlands into wetland classes (DeLancey et al., 2019).

	Type	Area %	Mean Canopy Closure
Upland Forest	Broadleaf	7%	87%
	Mixed	19%	74%
	Coniferous	33%	61%
Lowland Wetland	Swamp	5%	38%
	Fen	35%	27%
	Bog	1%	11%
	Marsh	1%	1%

CWD is present in variable quantities on the undisturbed forest and are usually absent on seismic lines. This is the case because historically seismic lines have been constructed by tractors as vegetation-free corridors and all CWD were removed in order to prevent wildfires, only recently CWD have been reincorporated to seismic line management due to their ecological value (Vinge and Pyper, 2012; Dabros et al., 2018). Many of the seismic lines in the region have not received any restoration treatment, and consequently have low quantities of CWD or no CWD at all. Some seismic lines have been subjected to CWD treatment designed to limit the movement of humans and predators of Threatened woodland caribou (*Rangifer tarandus caribou*) across the landscape (Vinge and Pyper, 2012), which usually can be encountered with isolated piles of CWD and occasionally with entire sections covered by CWD (i.e. complete rollback). This area of study was selected for being a representative portion of its natural subregion, with a variety of coniferous, deciduous and mixed forest stands, as well as lowlands containing fens and bogs (DeLancey et al., 2019).

We selected two smaller areas for sampling within the 4300-hectare study area, which we denominated *calibration* and *verification* areas, respectively (Figure 3.2). The selection process was mainly based on accessibility and on a representative sample of the forest composition of the overall study area. The calibration area is a 246-hectare area designed to provide training data for our CWD volume models. The verification area is a 209-hectare area designed to provide independent testing data to assess the extensibility of models developed with calibration area data.

3.3.2. CWD Survey

During the summer of 2018, a field survey was performed within the study area to acquire precise CWD volume information on both the calibration and verification areas. Given the interest in quantifying CWD in a disturbed environment, with and without restoration efforts, as well as in the unaffected forest, we selected study sites based on the location of seismic lines. Based on this strategy sampling plots could be located within the disturbed line and in the adjacent forest. To collect a representative sample of CWD in the study area under various natural and artificial conditions, we adopted a stratified-random sampling strategy to select study sites based on the following variables: seismic-line treatment type, surrounding forest tree composition according to Alberta's vegetation inventory (Government of Alberta, 2019), and crown closure. The authors note that despite efforts to achieve a representative sample, given the difficulty in accessing remote portions of the study area and limited time and resources, the site-selection process was constrained by accessibility. The following paragraphs describe overall sampling design and strategy; for more details and figures see Appendix D.

We expected to collect about 100 samples, 4 on each site, but included more potential sites (35 total) in case there was spare time to collect additional samples or if there were any problems with the visited sites. For each site, we selected four 100 m^2 plots for sampling CWD volume. To obtain data in both natural and altered sites, while avoiding transitions between

either, two plots were located on the seismic line and two plots were located in the surrounding forest. We call the plots in the seismic line "disturbance plots", and they were designed to be rectangular areas limited by the footprint of the disturbance, with width equal to the seismic line's width and variable length to obtain a 100 m^2 area. The plots in the surrounding natural environment were denominated "forest plots", and they were circular areas with a radius of 5.64 meters. We positioned the disturbance plots systematically, one of them starting 15 meters away from the beginning of the line, and the other positioned starting 75 meters away from the end of the former disturbance plot. Finally, the forest plots were positioned randomly, with their center point located within a minimum distance of 12 meters and a maximum distance of 36 meters away from the center of the seismic line. By the end of the field season, we had sampled a total of 108 plots: 76 plots (19 sites) in the calibration area and 32 plots (8 sites) in the verification area.

Each plot was located and positioned using a real-time kinematic (RTK) global navigation satellite system (GNSS, Trimble R8 - Trimble, Sunnyvale, United States) with average horizontal precision of 4.57 cm, then every piece of CWD present within the plot was examined and measured for volume. In each plot, the volume measurements were restricted by the extent of the plot boundaries, and any CWD crossing a boundary was considered as if it ended at the edge of the plot. CWD was defined as dead wood, either intact or partially decomposed, with at least 7 cm of diameter at the largest end and at least 1 meter of length. The 7 cm diameter threshold was chosen for being a common choice in the literature and given the majority of woody debris, especially those encountered in the lowland portions of the study area, did not surpass 10 cm in diameter. Any CWD positioned horizontally or leaning with an angle larger than 45° relative to vertical was classified as a log and was measured as part of the total CWD volume per plot presented in this study. Any CWD positioned vertically or leaning with an angle smaller than 45° was classified as a snag and was also measured but is not considered for the CWD volume per plot presented in this study, since the map products

presented here mainly target seismic line restoration and fire-hazard assessment studies, which usually show little interest for snags.

Log volume was derived from three diameter measurements, one obtained at each end and one obtained in the center of the extent of the log, as well as the total stem length in meters. Volume was calculated using Newton's formula, which accounts for the tapering shape of the log (Husch et al., 2002):

$$V = \frac{L}{6}\left(\pi\left(\frac{d_L}{2}\right)^2 + 4\pi\left(\frac{d_M}{2}\right)^2 + \pi\left(\frac{d_S}{2}\right)^2\right) \tag{3.1}$$

Where V is the volume of the main stem, dL is the diameter measured at the largest end, dM is the diameter at the middle, dS is the diameter at the smallest end and L is the length of the stem.

Once data was collected in the study area, the volume per plot was calculated by summing up the total volumes of all pieces measured within. Every plot was integrated into a geodatabase, according to its size, position and orientation obtained in the field with RTK measurements, and its respective total CWD volume. We had to remove three plots from the verification area from analysis since one of them could not be positioned properly with the RTK and two of them changed significantly since the remote sensing data was captured: one was a forest in aerial images and became a clear-cut when was sampled and the other contained a recently felled large tree not captured in the remote sensing data.

3.3.3. Remote Sensing and Pre-Processing

Two different data collection missions were performed to obtain the remote sensing data over the study area: one during the summer of 2017, which captured high resolution (5cm pixel-size) visible and near-infrared spectrum images as well as a dense LiDAR point cloud (40 pts/m^2), and another during the summer of 2018, which captured multispectral LiDAR (ML) data with lower point density (raw 9 pts/m^2). The data collected during the 2017 mission was used in a geographic object-based image analysis (GEOBIA) workflow to locate visible

CWD objects (vCWD), and the 2018 ML data was used to generate infra-canopy vegetation indices useful as indicators for occluded CWD quantity. GEOBIA consists of subdividing georeferenced input images into segments denominated "image-objects": relatively internally homogenous segments of the image usually defined by contrasts around their edges, which are intended to represent distinct parts of real-world objects (Hay and Castilla, 2008). We acknowledge the temporal disconnect between the dates of the field work and first LiDAR mission (2017) and second LiDAR mission. It is our assumption that any changes in CWD volume within that time period were minor and had no significant impact on our study.

3.3.3.1. Orthomosaics and Dense LiDAR Point Cloud

The remote-sensing datasets used in the GEOBIA portion of this study were obtained prior to field data collection via a piloted aircraft mission performed by OGL Engineering of Calgary between August 2 and 4, 2017. The Cessna 210T aircraft used in this mission, flying at 67 m/s 850m above ground, carried an optical sensor, a LiDAR sensor, a GNSS, and an inertial measurement unit. The flight path obtained 5.5cm ground sampling distance (GSD) images with 80% forward overlap and 60% side overlap. We deployed 250 visible ground control points (GCP, 60 cm squares with a bullseye marking) prior to the flight and measured their locations with an RTK GNSS (8 mm horizontal and 15mm vertical precision). We used 100 of these targets for georeferencing purposes and the remaining 150 for accuracy assessment. The final products had X, Y and Z accuracies of 5, 10 and 11 cm, respectively.

A third party (Orthoshop Geomatics Ltd. Calgary) treated the raw LiDAR point cloud, with point density of approximately 40 pts/m^2, for noise removal and ground-point classification using Terrasolid software. Using ArcMAP (version 10.6.1; ESRI, 2017), we gridded the elevation of the ground points into a 25cm GSD digital terrain model (DTM), and of the first return points into a 25 cm GSD digital surface model (DSM). A canopy height model (CHM) was obtained by subtracting the DSM by the DTM. We generated a 5 cm GSD orthomosaic of the study area by processing the air photos in Pix4Dmapper (Pix4D SA, 2019), using standard

procedures for photo alignment, georeferencing and adjustments using a photogrammetric point cloud. A normalized difference vegetation index (NDVI) raster layer was generating using the near-infrared (NIR) and red bands of the orthomosaic.

3.3.3.2. Multispectral LiDAR Acquisition and Processing

Since the study area is densely vegetated, much of the CWD measured in field plots was not visible on aerial images. For this reason, Multispectral LiDAR (ML) data was used to obtain intensity information of locations under the canopy, which were then used to derive sub-canopy vegetation indices. ML-derived vegetation indices have been shown to approximate passive imagery vegetation indices such as NDVI and normalized burn ratio (NBR) (Chasmer et al., 2017). In the following sections, LiDAR-derived vegetation indices will be referred to as active vegetation indices.

ML data was collected over the study area by the University of Lethbridge ARTEMiS lab (Advanced Resolution Terradynamics Monitoring System Laboratory), during a piloted flight mission performed on July 23th of 2018, concurrently to the field data collection. The ML sensor used was a Titan (Teledyne Optech, Toronto, ON, Canada) unit, which simultaneously captures three wavelengths: 1550 nm, 1064nm and 532 nm, hereby referenced as short-wave infrared (SWIR), near infrared (NIR), and green channels, respectively. The Piper Navajo aircraft used in this mission flew at 65 m/s, 1000m above ground, with a planned side overlap of 50%, and planned pulse density of 3 pts/m2 per channel. The raw LiDAR data was calibrated in LiDAR Mapping Suite (Teledyne Optech, 2019) by the ARTEMiS lab, who reported 12cm horizontal and 5cm vertical RMSE point accuracy. The ML datasets for all three channels was supplied in 54 separate tiles of the study area.

The following procedures were performed with LAStools (Isenburg, 2019) and ArcMap (ESRI, 2017) software. Overall point density and number of points per return of the ML datasets on the study area were calculated using the lasinfo tool: 1.51 pts/m^2, 4.49 pts /m^2 and 5.00 pts/m^2 for the Green, NIR and SWIR channels respectively. The percentage of single

returns was of 99.7%, 33.5% and 27.5% respectively for these channels. Rain previous to the flight and wet ground likely caused attenuation losses on the green channel observed in these numbers. Ground points were classified on each channel with lasground (wilderness setting), which is a tool based on Axelsson's (2000) triangular irregular network filtering algorithm. Then, to avoid outliers, the maximum intensity of the ground points was set to three standard deviations plus the mean, according to the intensity distribution of each channel. These points were exported in "shapefile" (SHP) format using las2shp. The point intensity of each SHP file was gridded into raster images using the inverse distance weighted (IDW) tool in ArcMap, with a cell-size of 50 cm and a fixed search radius of 1 meter. Cells with less than 2 points within a 1m radius were set as null. IDW was used to reduce some of the bias of gridding and cell spatial attribution and was selected over simpler averaging methods because it preserved some of the variance of the raw datasets. IDW also was useful in reducing the effect of noise and banding, which was especially observed in the NIR channel, where the intensity distribution was noticeably different on each scanline due to calibration issues with the sensor.

Using the intensity raster images for each ML channel, active NDVI (aNDVI) and active NBR (aNBR) layers were calculated using the raster calculator tool in ArcMap. The green channel was used for aNDVI as a visible-spectrum substitute for the traditionally used red channel on passive NDVI calculations. Both aNDVI and aNBR layers were later used to derive vegetation-indices metrics per 100m2 plots, which were included in CWD volume models as predictor variables.

3.3.4. Geographic Object-Based Image Analysis

We created a visible-CWD (vCWD) raster image over the study area by processing aerial images as well as LiDAR data via a geographic object-based image analysis (GEOBIA) workflow, involving machine-learning "random forest" supervised classification. This process was described in detail by Lopes Queiroz et al. (2019; Chapter 2). All spectral bands from the

orthomosaic and the NDVI layer, generated with the 2017 mission data, were used to segment the study area into image-objects using eCognition (version 9.4; Trimble, 2018). We used the following parameters: scale 10, shape 0.6, and compactness 0.4. All layers used to segment the study area, as well as the CHM layer, were used to train a Random Forest (RF) machine-learning classifier.

Random Forest supervised classification involves providing a set of training samples, in this case CWD image-objects as well as other broad types of features present in the landscape, to a RF classifier which uses the training data as reference to create a set (forest) of classification trees, each tree with randomly selected input variables (Breiman, 2001). A trained RF was applied to classify all image-objects in the study area and identify the CWD objects visible on aerial images.

3.3.4.1. Classifier Training and Application

To create a reference dataset for RF classification, 5000 randomly selected image-objects over the calibration area were manually classified into five distinct classes: log, snag, water, dirt and other. The selection of the reference objects was stratified around NDVI: 20% of samples from objects with NDVI greater than -0.1 in the NDVI image and 80% of samples from objects with NDVI smaller than -0.1. This strategy was adopted given that the clear majority of identified CWD objects had an NDVI lower than that threshold and that CWD are very infrequent when compared to the other object classes. A portion of these reference objects could not be classified due to being indistinct.

The reference dataset on the calibration area had a total of 3710 classified objects, of which 364 were logs. The spatial, spectral and height attributes of these objects were used as predictor variables to train a RF classifier, which was applied to the whole study area in three processing chunks that were later merged together. More details of the reference dataset, as well as about the process used to test and apply the classifier can be found in Lopes Queiroz et al. (2019; Chapter 2), who reported completeness between 76.9% and

81.5% and correctness between 75.8% and 87.0% for logs in the study area. Completeness is defined as percentage of true positives relative to all positives in reference data and correctness is defined as percentage of true positives relative to all positives in testing data.

After the RF classifier was applied to the whole study area, a planimetric map layer of visible CWD was generated by marking all 5cm raster cells within image-objects classified as log. Some ground-cover features not included in training the classifier but present in the larger study area, such as water bodies, construction, and parking lots, were manually removed from the final product. This layer was later used to derive visible CWD area per 100m2 plots, which was included in CWD volume models as a predictor variable.

3.3.5. Additional Layers

Aside from the vCWD layer generated from GEOBIA, and the aNDVI and aNBR layers generated from ML, we produced additional layers for consideration as predictor variables in CWD volume models.

The main factors we associated to occlusions of CWD on aerial images were canopy cover, tall grass, and heavy shadow. In an attempt to account for these factors, we generated canopy cover (CC), passive NDVI (pNDVI), and brightness layers, respectively. The CHM used in GEOBIA was classified into canopy and non-canopy pixels by selecting all cells with heights greater than 2m above the ground. This layer was later used as a proxy for canopy cover in the CWD volume models. The pNDVI layer used in GEOBIA was considered as a candidate predictor variable in the CWD volume models. A brightness layer was generated by averaging the visible-spectrum (RGB) intensities of the orthomosaic used in GEOBIA.

Factors we associated to broad-scale CWD volume variance and distribution on the study area were: the spatial distribution of wetlands and uplands, and of the height of the alive trees. A visible-water area (vWater) layer was generated by selecting the image-objects classified as water by the RF classifier. Another proxy for wetland distribution we used was a

wetland probability (WP) layer obtained from ABMI (Hird et al., 2017). Finally, the CHM used in GEOBIA was selected to extract metrics of tree height per 100m2 plots.

3.3.6. Model Selection

Each of the 108 field-plot polygons were attributed with variables from the following layers: vCWD, aNBR, aNDVI, CC, pNDVI, Brightness, vWater, WP and CHM. Using the zonal statistics tool from ArcMap the following statistics were extracted for each layer on each plot: minimum, maximum, range, mean, standard deviation and sum. Given that there were many potential predictor variables, six metrics for each one of eight layers, a model selection strategy was adopted using Akaike's Information criterion (AIC), while discarding highly correlated variables ($R > 0.6$). Summary statistics of all remaining variables, after the correlated variables were discarded, is presented in Table 3.. All procedures for model selection and validation we performed in R (version 3.5.1; R Core Team, 2018).

Table 3.2. Description and summary statistics of all variables used in model selection, each variable summarized with: mean, standard deviation (Std Dev), minimum (Min) and maximum (Max). The response variable was Coarse Woody Debris (CWD) volume measured in the field, and the predictor variables were derived from a variety of remote sensing products. Visible CWD (vCWD) and water (vWater) area were derived from the results of geographical object-based image analysis (GEOBIA) on aerial orthophotos obtained over the study area. A wetland probability raster was obtained from ABMI (Hird et al., 2017). Canopy closure (CC) was derived from a canopy height model (CHM). Passive normalized difference vegetation index (NDVI) was derived from the orthophotos used in GEOBIA, while active NDVI and normalized burn ratio (NBR) were derived from multispectral LiDAR datasets.

Variable	Definition	Mean	Std Dev	Min	Max
Response	*Response variable: total ground-truth CWD volume (m^3).*	0.25	0.34	0.00	1.50
vCWD	*Total visible CWD area (m^2) on orthophotos, obtained with GEOBIA.*	1.50	2.63	0.00	11.89
vWater	*Total visible water area (m^2) on orthophotos obtained with GEOBIA.*	1.31	3.00	0.00	14.40
Brightness	*Average visible-spectrum reflectance on orthophotos. Scaled 0-255.*	99.06	10.24	75.33	122.11
WP	*Average wetland probability, scaled from 0 to 1.*	0.28	0.30	0.02	0.92
CC	*Canopy closure, obtained as proportion of cells with CHM > 2m.*	0.45	0.31	0.01	0.96
CHM_{max}	*Maximum CHM value within plot (i.e. height of tallest tree).*	14.97	5.47	2.72	30.82
$pNDVI_r$	*Passive NDVI range within plot.*	0.99	0.17	0.57	1.37
$pNDVI_{sd}$	*Passive NDVI standard deviation within plot.*	0.14	0.04	0.06	0.27
$aNDVI_r$	*Active NDVI range within plot.*	0.95	0.24	0.00	1.72
$aNBR_r$	*Active NBR range within plot.*	1.49	0.18	0.51	1.82
$aNBR_{sd}$	*Active NDVI standard deviation within plot.*	0.26	0.07	0.09	0.43

3.3.6.1. CWD Volume Modelling

CWD quantities are known to be positively skewed and not normally distributed (Harmon et al., 1986). Since we found CWD volume distribution on 100m^2 plots to follow this pattern, as well as zero-inflated, CWD volume was modeled in two parts: a binomial distribution for the presence/absence of CWD, and a continuous distribution for volume on the plots where

CWD was present. A binary response variable was created for the binomial models by treating all plots where CWD was absent as zero and all plots where CWD was present as one. The continuous model was trained on plots where CWD was present and used CWD volume as response variable. Candidate models were selected separately for the binomial and continuous parts, then combined into two-part CWD volume models. The final predicted CWD volume according to two-part models equals the predicted binomial component times the predicted continuous value. Given that the distribution of CWD volume in our study plots was positively skewed as well as zero-inflated, zero-adjusted gamma (ZAGA) distribution models were used to incorporate the best continuous and binomial models. We used the Generalized Additive Models for Location, Scale and Shape (GAMLSS) library in R to generate and test our ZAGA models (Stasinopoulos and Rigby, 2007). Generalized additive models (GAMs) allow for the response variable to be modelled with gaussian as well as numerous non-gaussian distributions, as opposed to traditional linear modelling, and allow for link functions to model the relationship between the response variable and the predictors (Guisan et al., 2002). Additionally, GAMs are well suited for modeling non-linear relationships between the response and predictor variables because they are built based on the structure of the reference datasets instead of assuming a previously selected linear distribution (Yee and Mitchell, 1991). The main assumptions of GAMs are that the samples are statistically independent, the variance and link functions are selected correctly, and that there are no outliers influencing the fit (Breslow, 1996). The stratified-random sampling strategy adopted in this study, as well as statistical tests and investigation performed with the raw data in R ensured the selected ZAGA models follow these assumptions.

Small-sample AIC (AICc) is a useful indicator for model selection when dealing with multiple potential models created with a small sample-size (Burnham and Anderson, 2002). Model selection tables were generated for CWD volume two-part linear models using the candidate variables as predictor variables. Models were candidates only if their delta AICc (ΔAICc, calculated as AICc difference from the model with the smallest AICc) was smaller

than 2, which is commonly used as a threshold for model selection in the literature (Burnham and Anderson, 2002). Many of the predictor variables were highly correlated, with Pearson's R greater than 0.6. In these cases, only the variable that was most often present in candidate models was maintained, and other correlated variables were discarded. Candidate models were selected with and without ML variables for comparison. All possible combinations of candidate binomial and candidate continuous models were tested as ZAGA models, of which only the models with ΔAICc smaller than 2 were considered as our final candidate models for CWD volume.

3.3.6.2. Keep-One-Out Cross-Validation and Verification Tests

To test the accuracy and extensibility of the candidate models, the predicted CWD volume according to the two-part model was regressed against the actual CWD volume measured in the field plots to calculate R2 and RMSE values. A keep-one-out cross validation test was performed in the calibration area by training the models once for every plot in the area using all the calibration data except for each plot where a CWD volume prediction was generated. Another test was executed by training the models using the calibration area data and applying them to predict CWD volume on the verification area plots. Finally, we tested the accuracy of predicted CWD ground cover (m^2) derived from the vCWD layer versus CWD measured ground cover per plot, without any additional modelling, to assess the potential and limitations of GEOBIA of CWD.

3.3.7. Map Production

Among all candidate models for CWD volume, we selected a two-part model with the greatest predictive power as a preferred model. The preferred model included both image analysis- and multispectral LiDAR- (ML-) derived variables and is described in the following sections of this document. Given that the ML layers contained a few void cells, the preferred model was only applied on $100m^2$ cells containing at least 50% coverage of the aNBR layer,

which accounts for 99.3% of the study area (excluding water bodies and human-made features). On cells with less than 50% coverage on the aNBR layer (0.7% of the study area) we used the best model not containing ML variables.

Given the best models selected for CWD volume estimation according to the tests and specifications previously discussed, we generated two map products of CWD volume per hectare (m3/ha) on the entire 4300-hectare study area: one map dedicated to comprehensive CWD volume across all land cover types, and another dedicated to seismic line CWD density. Since the ML layers contained many gaps due to lower ground return density on closed canopy areas, the best-performing model using ML layers was used as a preferred model to generate these maps, and the best performing model without ML layers was used as a fallback model.

3.3.7.1. Overall CWD Volume Layer

The 4300-hectare study area was gridded into 10m x 10m cells using the fishnet tool in ArcMap, and each cell was attributed with values from all relevant predictor layers using the zonal statistics tool. Water bodies and human-made features accounted for 7.5% of the study area. These were removed from further analysis, given that these land-cover types were not accounted for when training the models. The attribute table containing predictor variables for all cells, as well as their individual latitude and longitude, was extracted as a comma-separated values (CSV) file and imported into R. The ZAGA models trained with the calibration data were applied to all cells generating CWD volume predictions for the entire study area. These predictions were multiplied by 100 to obtain an estimate of volume per hectare as opposed to volume per 100m^2. Given that there were a few (less than 0.05% of the data) overpredictions well above the range of CWD volume observed in field plots, the maximum prediction value was set to the mean plus four standard deviations of the field sample distribution (~160 m^3/ha). Predictions, along with their geo-locations, were imported into ArcMap as points and rasterized using the "point to raster" tool.

3.3.7.2. Seismic Line CWD Volume Layer

Using the CWD volume layer created for the entire 4300-hectare study area described above, segments of seismic lines of the study area were attributed with their mean CWD m^3/ha. A vector layer of all seismic lines on the study area was obtained via a seismic line mapper tool (Losada et al., 2018), which uses a least-cost path solution on a CHM to trace linear features on forested environments. The "generate points along lines" tool in ArcMap was used to both generate dense sampling points as well as sparse split points to segment each seismic line. Sampling points were attributed using the "extract values to points" tool, extracting values from the raster of overall volume. Lines were split into segments using the "split line at point" tool. Finally, segments were attributed with their mean CWD volume using the "spatial join" tool to link values of sampling points with each line segment.

3.4. Results

3.4.1. Accuracy of Best Models

The accuracies of the best model using ML data and of the best model without ML data were tested both on the calibration area using keep-one-out cross-validation (0.623 R^2, 0.224 RMSE using ML data; 0.514 R^2, 0.254 RMSE without ML) and on the verification area while training only on calibration area samples (0.721 R^2, 0.198 RMSE using ML data; 0.628 R^2, 0.203 RMSE without ML). Goodness of fit (R^2) and root mean square error (RMSE) were comparable between cross-validation tests in the calibration area and tests in the verification area. Furthermore, these metrics were better in models including ML variables in relation to models without ML variables. The regression line of all models approximates the 1:1 relationship with a slightly gentler slope. The variance of CWD volume was greater in disturbance plots than in forest plots, and the former also displayed stronger zero-inflation in the calibration area plots (Figure 3.3).

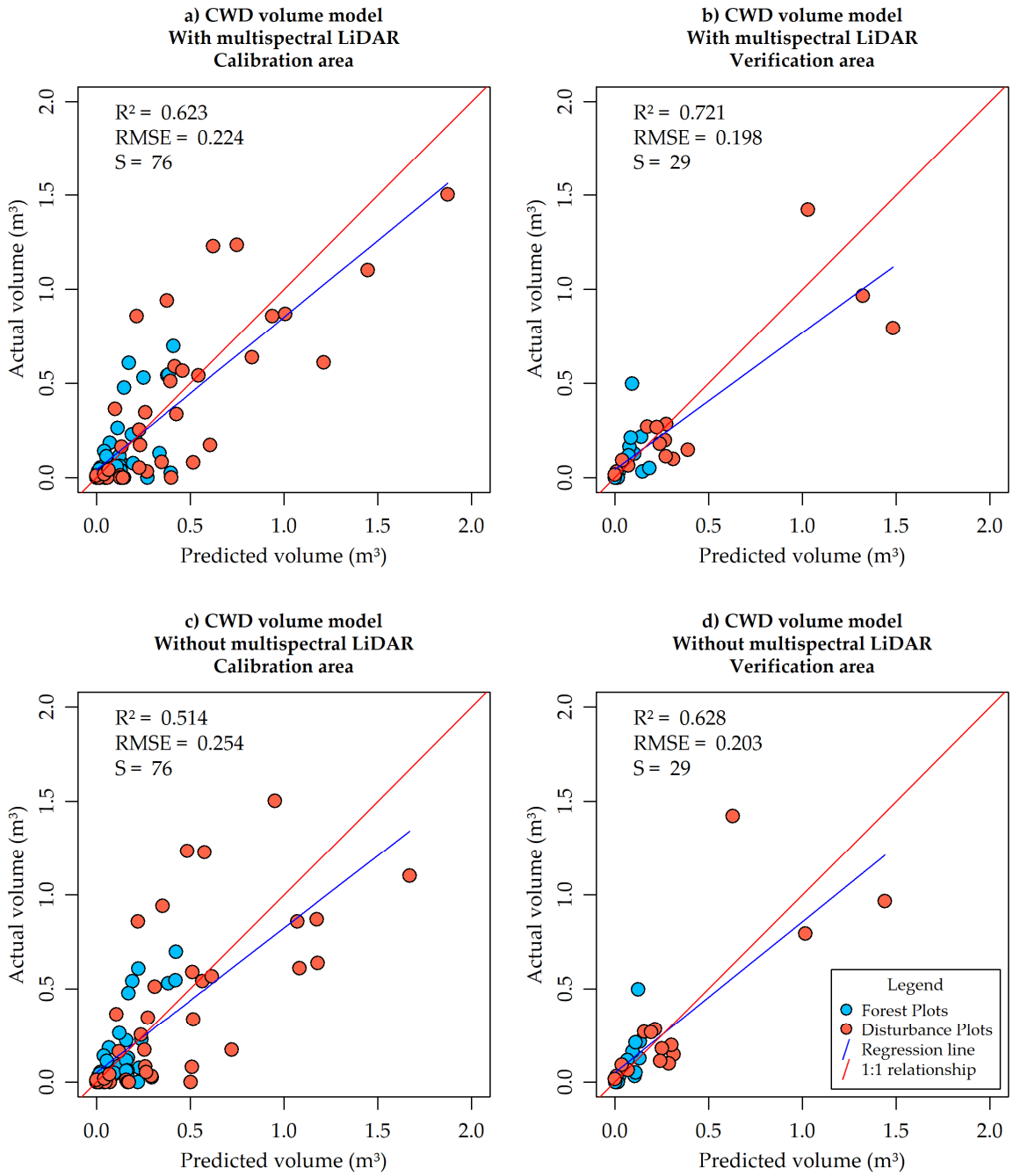

Figure 3.3. Scatter plots of actual versus predicted coarse woody debris (CWD) volume in m^3. The best model with multispectral LiDAR (ML) data was used to estimate CWD volume on a) the calibration area plots using keep-one-out cross-validation, and on b) the verification area plots using the calibration plots to train the model. Similarly, the best model without ML data was also applied to the c) calibration

and d) verification areas. Goodness-of-fit (R^2), root mean square error (RMSE) and sample size (S) are indicated on each plot.

3.4.2. Map Products

To showcase the application of the selected models, CWD volume per hectare (m^3/ha) was mapped over the 4300-hectare study area to generate two map products: A comprehensive map over all ground-cover types with 100m^2 raster cell-size (Figure 3.4), and a map of seismic line 100m segments classified according to their average CWD density (Figure 3.5). High density CWD clusters were detected at the edges of previously harvested areas (Figure 3.4a) and in the southwestern portions of the study area in the form of partial windthrows (Figure 3.4c). Seismic lines with (Figure 3.5a) and without (Figure 3.5c) CWD treatment were identified in the maps. In Figure 3.4b very low CWD quantities are observed in the interior of the harvested area (northwestern portion of Figure 3.4a), moderate CWD quantities in the natural forest (southeastern portion of Figure 3.4a) and very high CWD quantities in the transition between the two.

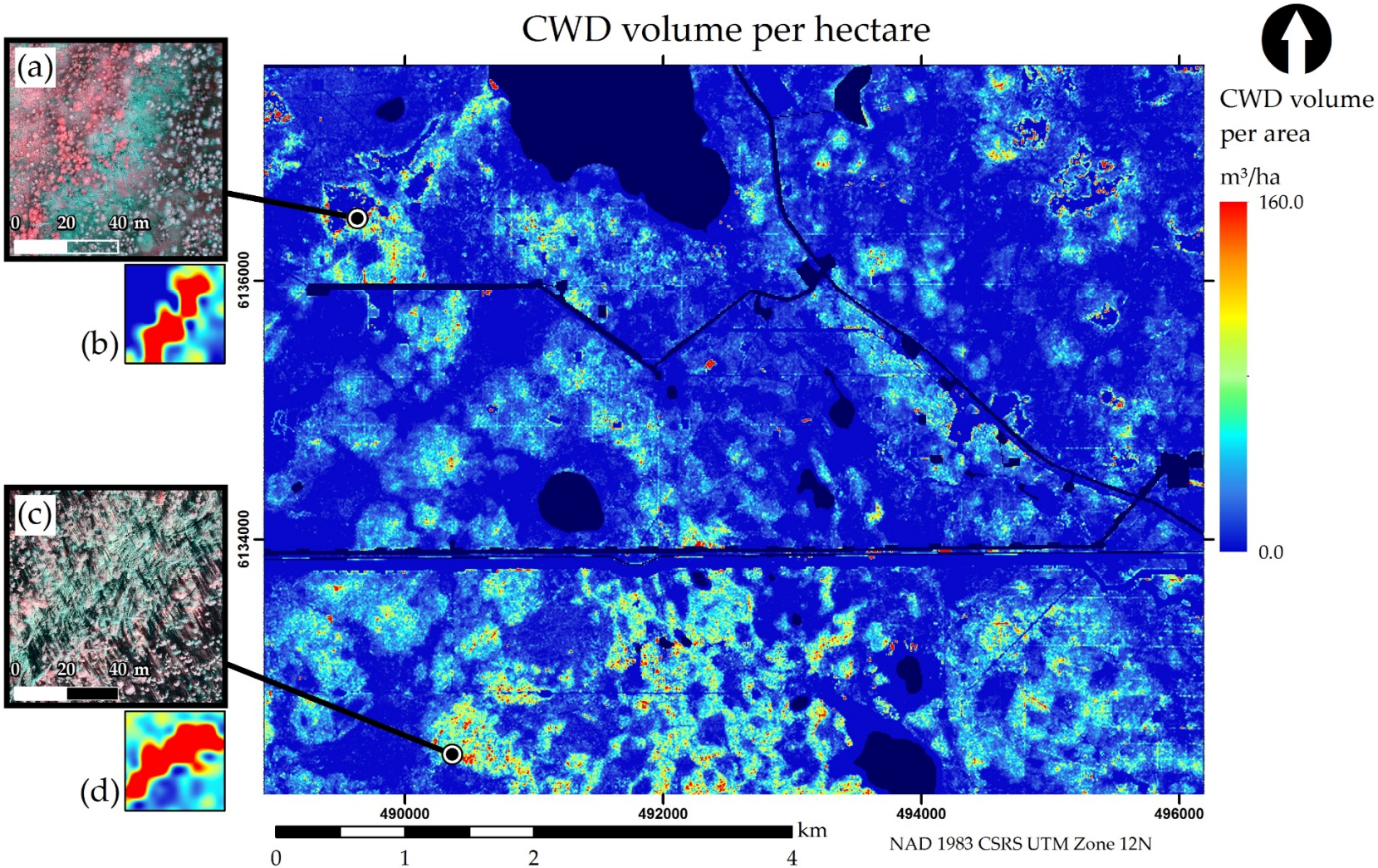

Figure 3.4. Map of coarse woody debris (CWD) volume per hectare (m^3/ha) over the study area. High quantities of CWD are displayed in red, medium quantities in yellow and low quantities in blue. Roads and water bodies are excluded from the CWD volume model and are presented as dark blue. Insets (a) and (c) showcase hotspots of CWD in false-color imagery. Insets (b) and (c) showcase the CWD volume map over (a) and (c) respectively.

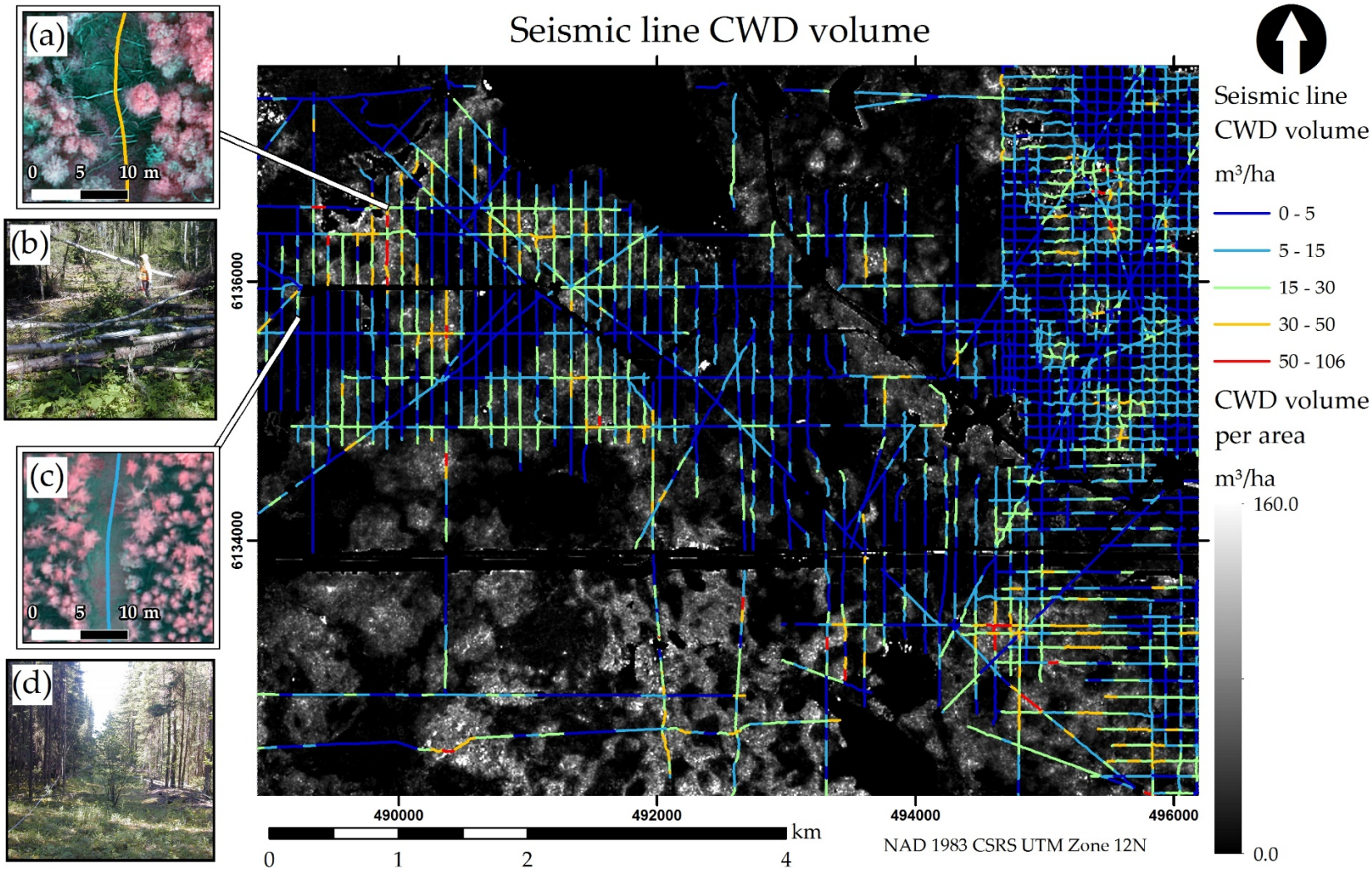

Figure 3.5. Map of coarse woody debris (CWD) volume per hectare (m^3/ha) over seismic lines on the study area. The gray-scale background image presents volume per hectare for the entire study area, while the seismic lines are classified as high (red) medium (yellow) and low (blue) CWD quantities. (a) and (c) are false-color aerial images showing examples of high and low CWD densities respectively. (b) and (d) are field photos of (a) and (c) respectively.

CWD volume in the reference data was compared to the volume in the map products (Figure 3.4 and Figure 3.5), which were divided into upland and lowland according to ABMI's wetland classification layer (DeLancey et al., 2019). These datasets are presented as box-and-whisker plots below (Figure 3.6). Distribution of CWD volume on the final maps was very similar to the distribution on forest plots, even when separating the area into lowland and upland. The average volume in upland was 13.7 m^3/ha and in lowland was 3.4 m^3/ha. Disturbance plots, most of which were located on treated seismic lines, had much higher volumes than the rest of the study area. This was expected given the practice of creating CWD piles as part of restoration treatments (Vinge and Pyper, 2012). The population of seismic lines on the map products had slightly lower volumes than the rest of the upland areas, but treated lines had much higher volumes than untreated lines. Average volume on treated and untreated seismic lines was 18.2 m^3/ha and 9.4 m^3/ha respectively.

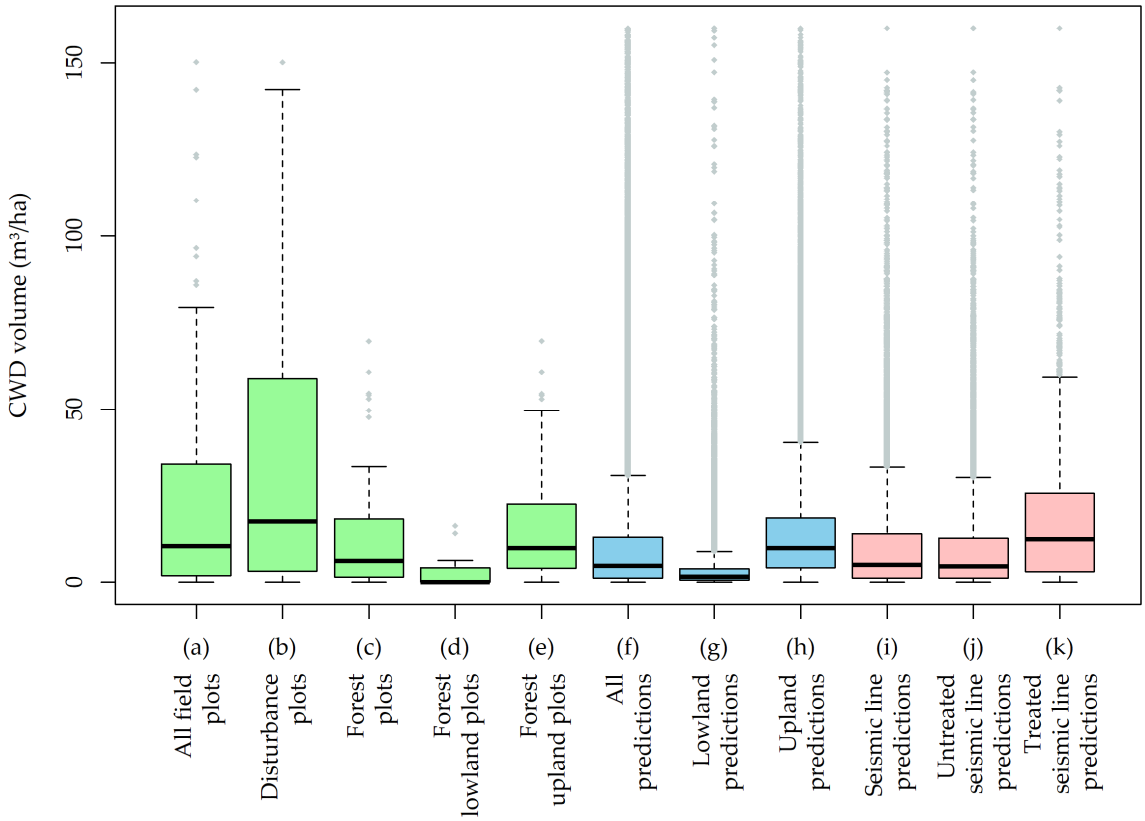

Figure 3.6. Box and whisker diagram for coarse woody debris (CWD) volume on reference data (green, total of 108 field plots) on the CWD map for the entire application area (blue, total of 379,025 cells) and on seismic lines (red, 63,816 sampling points). All reference data (a) is divided into (b) disturbance plots (54 plots) and (c) forest plots (54 plots). Forest plots are divided into (d) lowland plots (14 plots) and (e) upland plots (40 plots). All map predictions (f) are divided into (g) lowland (38% of cells) and (h) upland (62% of cells) predictions. Seismic line predictions (i) are divided into (j) untreated lines (90% of samples) and (k) treated lines (10% of samples). Original values were in m^3/100m and were projected to m^3/ha. Box-plot outliers are presented in gray.

3.4.3. Model Selection Tables

The model-selection table for the candidate ZAGA CWD volume models (Table 3.) is presented below. It is noteworthy that all candidate models shared the same logistic component: a model containing vCWD, pNDVI, vWater and WP variables. The two models with the smallest AICc were models including aNBR, while the two other models did not include

any ML variables. All continuous models shared CC, CHM and vCWD variables, and some models included either aNBR or pNDVI. No candidate models selected Brightness or aNDVI variables.

Table 3.3. Candidate two-part models for coarse woody debris (CWD) volume according to small sample Akaike information criterion (AICc). The rank (r), degrees of freedom (df) and delta AICc (ΔAICc) are provided for each model. The following variables were selected in all continuous models: area of detected CWD objects via image-analysis (vCWD); canopy closure (CC); and height of the tallest tree (CHM_{max}). The following were selected in some continuous models: standard deviation of the active normalized burn ratio ($aNBR_{sd}$) and range of passive NDVI ($pNDVI_r$). Finally, all logistic models included: vCWD, standard deviation of passive NDVI ($pNDVI_{sd}$), visible water area (vWater) and wetland probability (WP).

r	Continuous model	Logistic model	df	AICc	ΔAICc
1	$vCWD^2 + CC + CHM_{max} + CHM_{max}^2 + aNBR_{sd}^2$	$vCWD + pNDVI_{sd} + vWater + WP$	12	-2.08	0.00
2	$vCWD^2 + CC + CHM_{max} + CHM_{max}^2 + aNBR_{sd}^2 + pNDVI_r$	$vCWD + pNDVI_{sd} + vWater + WP$	13	-1.98	0.09
3	$vCWD^2 + CC + CHM_{max} + CHM_{max}^2 + pNDVI_r$	$vCWD + pNDVI_{sd} + vWater + WP$	12	-1.43	0.64
4	$vCWD^2 + CC + CHM_{max} + CHM_{max}^2$	$vCWD + pNDVI_{sd} + vWater + WP$	11	-0.43	1.65

Given the results presented in Table 3., model ranked 1 was selected as the best simplest predictive model including ML variables and model ranked 4 was selected as best simplest model excluding ML variables. Models ranked 2 and 3 are variations of these selected models adding pNDVI as a variable, and given all candidate models were "tied" with ΔAICc lower than 2, only the simplest models were chosen for application in the study area.

3.4.4. Accuracy of Visible-CWD Layer

Figure 3.7 contains graphs comparing ground cover of vCWD image-objects with measured CWD ground cover in field plots, for all calibration area plots as well as for only the plots with negative average pNDVI. Disturbance plots exhibited greater zero-inflation in the

response variable than forest plots and both types of plots had zero-inflated predictions. Goodness of fit (R^2), RMSE, and slope of regression in plots with negative NDVI were all much superior than these metrics in all field plots.

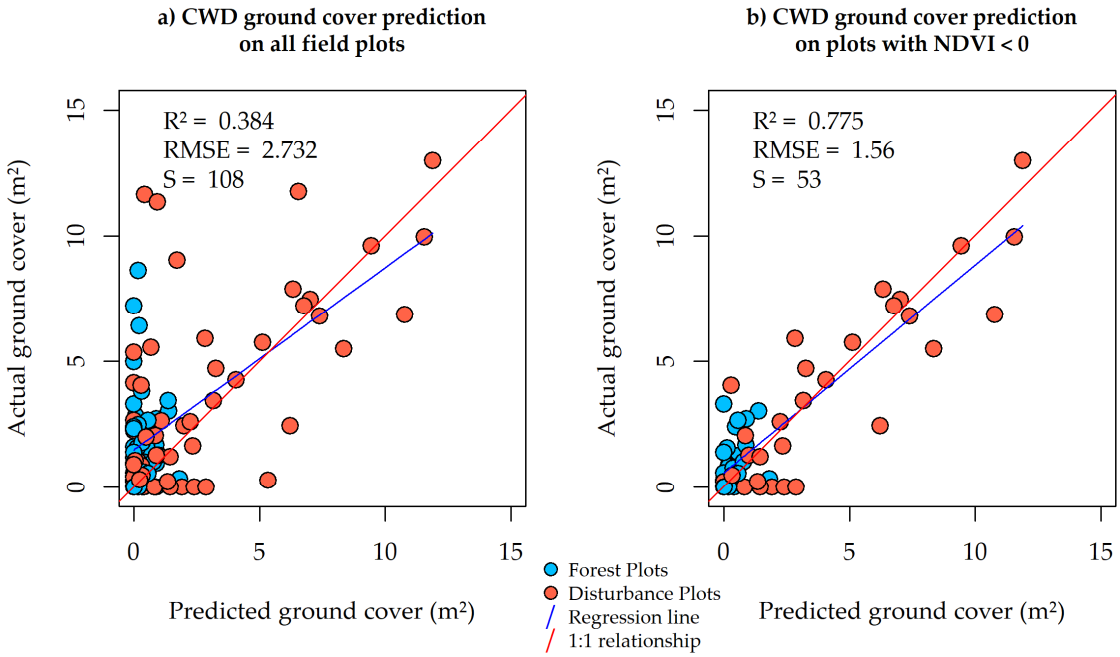

Figure 3.7. Scatter plots of actual versus predicted coarse woody debris (CWD) ground cover in m^2. Predicted ground cover presented here is the area sum of CWD objects detected via image-analysis. A weak relationship is observed when a) all field plots are used in regression, and a much stronger relationship is observed in b) plots with negative average normalized-difference vegetation index (NDVI).

3.5. Discussion

Once a model was selected, the production of map products over the entire area of study was achievable using common map algebra operations in a GIS environment. The selected models achieved good predictive accuracy (0.623 R^2, 0.224 RMSE in cross-validation; 0.721 R^2, 0.198 RMSE in the verification area) but required a sophisticated set of inputs, involving high-resolution aerial images, high density LiDAR point clouds as well as ML point clouds. The results presented in Figure 3.3 indicate that even where ML data is not available CWD volume

can still be modeled with good predictive accuracy (0.514 R^2, 0.254 RMSE in cross-validation; 0.628 R^2, 0.203 RMSE in the verification area), with a mean decrease of 0.101 in R^2 and a mean increase of 0.0125 in RMSE in relation to ML-inclusive models. The final maps of CWD volume in the study area (Figure 3.4 and Figure 3.5) reveal that even though CWD distribution is largely controlled by the occurrence of wetlands, artificial piles of CWD on seismic lines and clear-cuts are exceptions which can cause CWD anomalies. Overall average CWD volume in the study area (9.78 m^3/ha for the entire study area, 17.73 m^3/ha for uplands and 3.14 m^3/ha for lowlands) was small when compared to what Lee et al. (1997) measured in aspen-dominated stands in Alberta (108.8 to 124.3 m^3/ha), but upland volumes in the present study are comparable to several other studies in boreal forests as presented in Table 3.. It is not surprising that lowlands had a very low volume of CWD (3.14 m^3/ha) since the lowland trees observed in the field were small (commonly close to 7cm diameter at largest end) and since not all wetlands were densely populated by trees, especially bogs and marshes which were mostly shrubby. Additionally, the CWD distribution on the produced maps was very similar to the distribution in the reference data (Figure 3.6), with mean values from uplands and lowlands in the reference data (17.7 and 3.1 m^3/ha respectively) close to the mean of uplands and lowlands in the final maps (13.7 and 3.4 m^3/ha respectively).

Table 3.4. Minimum and maximum average coarse woody debris volume (m^3/ha) over varied boreal forest types presented in other studies. Note that the present study estimated volumes in 100m^2 plots and upscaled the values for an estimate per hectare. Minimum value from Pedlar et al. (2002) includes snags. Sturtevant et al. (1997) values are for individual stands, while all other studies present averages.

Citation	Forest types (Min / Max)	Location	Min	Max
Lee et al., 1997	20-30 yr. aspen stands/ 120+ yr. aspen stands	AB, Canada	108.8	124.3
Linder et al., 1997	Natural pine, spruce and deciduous stands	Sweden	62	-
Sturtevant et al., 1997	58 yr. fir stand / 80 yr. fir stand	NL, Canada	15.2	78.1
Sippola et al., 1998	Managed 15 yr. spruce stands/ Natural mixed stands	Finland	6.6	47.2
Pedlar et al., 2002	Spruce stands / mixed stands	ON, Canada	<17.8	131.5
Present study	Black spruce dominated wetlands / Upland coniferous, deciduous and mixed forests	AB, Canada	3.14	17.73

CWD amounts are known to be highly variable between and within ecosystems, being influenced by the action of fire, insects and diseases (Harmon et al., 1986; Brown et al., 2003), and to be strongly correlated with the biomass of the living trees in the area (Sippola et al., 1998; Pedlar et al., 2002). In this study most of the black spruce trees on wetland sites had a diameter close to or smaller than 7 cm at the largest end, most of which would not be classified as CWD if dead. This observation supports the results presented for CWD volumes on wetlands. It is worth noting that the CWD volume distribution for treated lines in the seismic line map (Figure 3.5; mean 18.19 m^3/ha) is smaller than the distribution in the disturbance field plots (Figure 3.6; mean 36.2 m^3/ha) which is likely due to the fact that field plots were constrained by the limits of disturbances. Artificial CWD piles are confined, while map cells were not. It is also possible that overrepresentation of plots with large quantities of CWD in the reference data samples may be inflating this difference.

It is worth noting that the calibration and verification plots were quite similar in terms of forest structure, seismic-line distribution, and fire history, and this is likely a key factor for the success in applying models trained in the calibration area on to the verification area. Water bodies and man-made structures such as buildings and parking lots were some of the ground-cover types present in the study area but not included in the training of the models or the final maps. In this case such ground cover features were removed manually since they were of no interest for this study, but it is worth noting that the model would be less capable of predicting CWD volume on ground cover types it was not trained on.

We expect the model trained in this study area to perform with lower accuracy when applied to different forests unless new reference data is introduced. We believe wetland probability was an important variable selected by the candidate models because the terrain and forest structure of our study area is highly controlled by the presence and absence of wetlands, and therefore would advise against using wetland probability when applying CWD volume estimation models on areas not affected by wetlands. Similarly, the height of the tallest tree (CHM_{max}) was an important variable to model CWD volume in our study area likely

due to the presence of deciduous, coniferous and mixed forest stands with great variance in tree size, and the fact that differently-sized trees yield different volumes of CWD. Therefore, on homogenous forest stands it is likely that CHM_{max} will not perform as well as a controlling factor for CWD volume. Finally, we predict that canopy cover and ML variables should be valuable indicators of occluded CWD volume in a variety of forest types, but their influence on model predictive power should decrease on areas with less canopy cover, such as forests recently affected by fires.

3.5.1. Model Selection

The two simplest models with and without ML variables were "tied" as candidates with a ΔAICc lower than 2 (Table 3.). However, in our case, model ranked 4 was close enough to an ΔAICc of 2 and performed worse in Figure 3.3 such that we deemed model 1 to be the best option when ML variables are available. We note that the four variables common to all candidate binomial models were directly linked to factors we predicted would control CWD occlusion and distribution: presence of canopy cover and tall vegetation being represented by pNDVI and distribution of wetlands being represented by visible water area and wetland probability. Additionally, as we expected ML variables were selected by top models as good predictor variables for CWD volume models.

Only variance-related variables (i.e.: standard deviation and range) were present in candidate models concerning vegetation indices, both active and passive. This result suggests that the mean of vegetation indices does not capture volume variance whereas the variance of vegetation indices does.

We note that one possible path for exploration in the future to circumvent some of the bias of model selection is to use ensemble models, which combine many different models to provide one "average" model that may increase the estimation accuracy. However, in this case since all candidate models were quite similar to each other and therefore not entirely independent, it is unlikely that an ensemble approach using these models would expressively

increase the predictive power of the final model. Additionally, supervised learning models would likely require a much larger number of samples.

3.5.2. Importance of Multispectral LiDAR for Infra-Canopy Predictions

Models including aNBR placed higher than models without ML data as seen in Table 3., and the best ML-inclusive model yielded more accurate results than the best model without ML variables, with lower RMSE and higher R2 as seen in Figure 3.3. It is also visible between Figure 3.3a and Figure 3.3c that the plots that benefited the most from the inclusion of ML variables were the plots with large amounts of CWD above the regression line; in other words, plots with underpredicted CWD volume. When analyzing our orthophotos and field photos of these plots we noticed that most of them were also affected by either closed canopy (off the seismic lines) or tall grass (on the seismic lines). Furthermore, as seen on Figure 3.7, the vCWD layer produced via GEOBIA is only a good estimator of CWD quantities on plots where CWD is not being occluded by closed canopy or tall grass (Figure 3.7b), and produces a zero-inflated independent variable on Figure 3.7a. These results suggest that ML variables can be valuable for CWD volume estimation, likely acting as indicators of occluded CWD quantity and consequently reducing the error on plots with occluded CWD. However, given that models without ML variables were also selected as candidates, we must conclude that there was not enough evidence to make the claim that ML substantially improved our CWD volume models.

NDVI is a much more common indicator for coarse woody debris than NBR in the literature. However, in this case aNBR was selected over aNDVI within candidate models, most likely because of the reduced ground-point frequency observed in the green ML channel, which increases the relative variance of the aNDVI values obtained at each plot. The low point density and high percentage of single returns of the Green ML channel is attributed to atmospheric attenuation losses and wet ground due to rain previous to the flight mission which collected the ML data. We expect that data collected on a clear day would yield a dataset with comparable ground return density for all ML channels. In that case aNDVI would likely

be a more appropriate indicator for spectral separation on CWD than aNBR, and it is possible that aNBR would not even be present in candidate models for such a dataset.

3.5.3. Two-Part Models Versus Simple Models

We considered that separating the CWD volume model into a binomial and a continuous part was beneficial due to the nature of the zero-inflated response variable. Tests comparing two-part models against simple linear models revealed that two-part models primarily reduce the overprediction of plots in the lower-left corner of actual-versus-predicted CWD volume scatter-plots such as the ones seen in Figure 3.3. Consequently, two-part models consistently reduced RMSE and increased R^2 values in relation to simple linear models when using either cross-validation or the verification area tests. Furthermore, AICc tests would place simple models well above the ΔAICc threshold of 2 and would only select two-part models as candidates.

In our study area, the spatial distribution of wetlands seems to control much of the forest structure and consequently CWD volume. It is noteworthy that wetland-related variables were selected by all binomial models but not by any of the continuous models in Table 3.. This result suggests that the presence or absence of wetlands is highly related to the presence or absence of CWD, and therefore the zero-inflation effect on our response variables. Furthermore, the presence or absence of wetlands is not a strong factor for CWD volume on plots where CWD is present, which is supported by the fact that most plots with large amounts of CWD were located on uplands. This pattern is expected on seismic line treatment efforts as well, since usually operators will be instructed to apply a larger amount of CWD on upland sites than they would on wetland sites (Vinge and Pyper, 2012). Tests comparing single linear models to two-part linear models indicated that the former consistently overpredicted CWD quantities on wetland plots with water.

3.5.4. Standardized Model Coefficients

To better understand the composition of the best ZAGA model, standardized coefficients for the predictors, including multispectral LiDAR, were obtained by modelling scaled predictor variables with a mean of zero and standard deviation of one (Table 3.5 and Table 3.6). This enabled us to study the relative contribution of each explanatory variable to the final model, in terms of strength and direction.

Table 3.5. Intercept and coefficients for binomial part of the best zero-adjusted gamma model. Values are presented for models created with the original training data and models using standardized predictor variables (mean of zero and standard deviation of one). Variables include visible coarse woody debris area (vCWD), standard deviation of passive normalized difference vegetation index ($pNDVI_{sd}$), visible water (vWater) and wetland probability (WP).

	Intercept	vCWD	$pNDVI_{sd}$	vWater	WP
Original	-0.137	-1.823	-17.701	0.559	4.687
Standardized	-3.674	-5.059	-0.819	1.874	1.333

Table 3.6. Intercept and coefficients for continuous part of the best zero-adjusted gamma model. Values are presented for models created with the original training data and models using standardized predictor variables (mean of zero and standard deviation of one). Variables include squared area of visible coarse woody debris (vCWD), canopy closure (CC), height of tallest tree (CHM_{max}), squared height of tallest tree (CHM_{max}^2) and squared standard deviation of active normalized burn ratio ($aNBR_{sd}^2$).

	Intercept	$vCWD^2$	CC	CHM_{max}	CHM_{max}^2	$aNBR_{sd}^2$
Original	-6.956	0.012	-3.070	0.581	-0.012	11.284
Standardized	-1.547	0.133	-0.662	1.161	-0.369	0.061

The standardized coefficients of the binomial model (Table 3.5) reveal that all variables substantially contribute to the prediction of this model, with vCWD being the strongest predictor. The response variable for the binomial model can be understood as the likelihood

of absence of CWD. Therefore, a strong negative coefficient for vCWD is to be expected and signifies that the larger the quantities of detected CWD area, the smaller the likelihood that CWD is absent. Positive coefficients for vWater and WP show that high wetness and presence of wetlands increase likelihood of absence of CWD, as would be expected given the smaller stature of the forests in these areas. A negative coefficient for standard deviation of passive NDVI leads us to believe that NDVI-homogeneous areas are less likely to contain CWD in relation to areas with high NDVI variability, which is plausible given that during leaf-on conditions (summer) ground vegetation is widespread in the study area and sites without CWD will generally have either very high NDVI in the case of vegetated areas and very low NDVI in the case of roads and open water without much variability. Conversely, sites with CWD will have the presence of low NDVI pixels on CWD and high NDVI pixels in the surrounding ground vegetation, causing a greater variance for NDVI.

Standardized coefficients of the continuous model (Table 3.6) reveal that aNBR was the least important predictor. This effect is not surprising considering models without ML predictor variables were tied in terms of ΔAICc with the ML-inclusive models (Table 3.3). Given aNBR was selected in some candidate models we assume that, to some extent, it must contain valuable information regarding the variance of CWD volume. However, its small standardized coefficient and its absence in other candidate models suggest that it does not contain substantial information to conclude it is on the same level of importance as the other variables. We believe that the information being supplied by $aNBR_{sd}$ is similar to the information being supplied by $pNDVI_{sd}$ in the binomial model, namely that vegetated areas without CWD will have high aNBR without much variance, and that areas with CWD will have low aNBR pixels on CWD and high aNBR pixels on the surrounding vegetation, causing greater variance. In other words, the positive nature of the $aNBR_{sd}$ coefficient shows that an increase of CWD quantities can cause higher variance in aNBR captured with ML LiDAR. Finally, we believe that aNBR is not supplying substantial information about the variance of the response variable due to noise in the intensity values given that the intensity information available in

LiDAR returns of the ground surface is very likely to have been affected by environmental factors such as target roughness, reflectance and wetness, as well as attenuation due to pulses being split into multiple returns (Kashani et al., 2015).

A positive coefficient for squared vCWD in the continuous model shows there is a positive relationship between predicted area of CWD according to our GEOBIA and actual CWD volume. Given a negative coefficient for CC we interpreted that gaps in the canopy may indicate larger quantities of fallen trees, whereas tightly packed canopies are unlikely to have large quantities of sound logs. We recognize that this assumption may indicate the model is less capable for heavily decayed CWD. The standardized coefficients for CHM_{max} at Table 3.6 indicate that an increase on tree size has a positive relationship with CWD volume, although it relates to a tapering curve given the negative CHM_{max}^2 coefficient.

3.5.5. Issues and Limitations

As discussed previously, the main sources for underprediction of CWD volume (i.e. false negatives in the vCWD raster image) in the presented models are occlusions caused by superimposed vegetation. ML data aided in diminishing the effect of occlusion, however due to low point density in ML point clouds the benefits of these datasets was limited. It is likely that more powerful ML sensors will be available in future which would enable denser ground sampling and smaller gaps, potentially even causing dense ML point clouds to eliminate the need for image analysis altogether.

Aside from the issue of gaps in the ML data due to diminished returns at ground level, the NIR ML band also displayed a noticeable banding issue caused by variations of return intensities on each laser scan line. This effect caused some noise to be translated to our aNDVI and aNBR layers, which probably reduced the accuracy of our results presented here. There have been studies on possible solutions for banding problems (Yan and Shaker, 2017). However, since the vegetation indices were sampled at plot level, while averaging the values of all pixels within each plot, we considered that the effect of banding was attenuated for the

purposes of answering the questions posed in our study and we decided to not perform any noise attenuation procedure on our datasets. We suggest that banding issues should be addressed in order to increase accuracies in future studies.

The main sources for overprediction of CWD volume (i.e. false positives in the vCWD raster image), observed on plots below the regression line in Figure 3.3 seem to be: a small quantity of occluded CWD being interpreted as a large quantity of CWD, which may be attributed to the noisy nature of the ML data; and tall neighboring trees with a lower than average CWD quantity, which highlights one disadvantage of using the CHM_{max} variable as an indicator for CWD volume. The presence of the canopy closure (CC) and height of tallest tree (CHM_{max}) variables in all candidate models might be indicating that the ML data is not providing enough information about the occluded portions of the study area, and that the height of the tallest tree within each plot as well as the percentage of occluded area are supplementing that lack of information and improving the CWD volume estimates. If the ML datasets were more comprehensive and consistent, the value of CC and CHM_{max} variables would likely diminish.

Aside from the sources of overprediction described above, upon close examination of the final maps presented in Figure 3.4 and Figure 3.5 we found additional sources of localized error: clear-cut edges, isolated snags and wet mud surfaces. Some shadowed edges between clear-cuts and natural forest seem to have caused overprediction of CWD, probably given that our sampling design avoided and therefore did not account for these transitions between forest and disturbances. Some isolated snags, especially on clear-cuts, caused CWD overprediction; even though in some studies snags are defined as a type of CWD in here it acts as a source of error. Additionally, extensive wet mud surfaces located on wetlands, which usually surround water bodies, are seen as highly reflective bumpy areas with low NDVI, which caused the RF classifier to overpredict CWD. These three additional sources of error present situations which were not accounted for in the training data, which reinforce the importance of having a representative sample for your application area.

Finally, we believe that our map of seismic line volume (Figure 3.5) should only be used as a reference for field operators and we recognize that it is likely to have lower accuracy than our map for the overall forest (Figure 3.6). Volume values for line segments were derived from the raster of volume in the overall area (as specified in subsection 3.3.7.2), therefore cells positioned in an arbitrarily placed grid may be at the transition between disturbance and forest. For a better estimate of volume on seismic lines, future models should be constrained by the spatial extent of seismic lines, excluding the surrounding forest. GIS procedures could be applied to generate irregular 100m^2 cells within the boundaries of seismic lines and CWD volume models could be applied to such cells for a more reliable prediction.

3.5.6. Future Work

We used data collected over the summer (leaf-on) to generate all intermediate products presented in this document. We believe the incorporation of spring (leaf-off) datasets as an additional resource for CWD volume estimation should increase the accuracy of predictive models especially on areas with occluded CWD. We note that upon inspection, most plots well above the regression lines on Figure 3.3a and Figure 3.3c represented piles of CWD occluded by tall grass on seismic lines. On leaf-off data the CWD on these same plots should be much more distinct, since the live vegetation is less dense that time of year. Additionally, it is possible that incorporating the ML datasets into the GEOBIA workflow may increase the accuracy of the vCWD layer. Finally, it is unclear if ensemble models could perform better than single models within this context given most linear models presented here as candidate models were quite similar.

We encourage future researchers to investigate these options, to explore the utility of other explanatory variables (e.g., time since disturbance, tree-species composition, etc.), and to test the development of remotely sensed models of CWD in other forest ecosystems. Additionally, the possibility of creating accurate high-resolution (10 m GSD) CWD maps over

extensive study areas may be beneficial to improve a variety of ecological models including wildlife habitat and seismic line use models.

3.6. Conclusions

A method for creating accurate and extensive maps of CWD volume on boreal forests was presented in this study as a novel solution using multispectral LiDAR (ML) for volume estimation of both visible and occluded CWD. Visible CWD was mapped using geographical object-based image analysis, and occluded CWD was modeled using infra-canopy normalized burn ratio. The best zero-adjusted gamma models (ZAGA) using ML data and without ML were selected with small-sample Akaike's information criterion (AICc). Many of the variables we predicted would control CWD quantities and occlusion were selected as predictor variables in the best models, including visible CWD area, height of tallest alive trees, canopy closure, visible water area, wetland probability, passive NDVI and active NBR. The ZAGA models performed very well when tested with the reference data, both in cross-validation tests with the training samples (0.623 R^2, 0.224 RMSE using ML data; 0.514 R^2, 0.254 RMSE without ML) as well as in verification tests using independent samples from a spatially separated from the training area (0.721 R^2, 0.198 RMSE using ML data; 0.628 R^2, 0.203 RMSE without ML). The best model using ML performed better than the best model lacking ML variables. Our final CWD volume maps provide accurate, extensive and high-resolution (10m GSD) estimates for our study area and provide the foundation for a variety of management activities, including seismic line restoration and fire-hazard assessment.

CWD used to protect regeneration efforts on seismic lines are usually applied based on the natural range observed in the environment (Vinge and Pyper, 2012). This natural range can be accurately mapped using the method presented here. Field operators can use extensive maps of CWD volume as guides to select areas for CWD treatment as well as for improved navigation in seismic lines. Conversely, large accumulations of CWD which can configure a

fire hazard (Partners in Protection (Canada), 2003) can be detected in these map products and addressed to prevent wildfires.

The methods presented here could be applied to any forested environment to generate extensive CWD volume maps which may be used for forest management as well as ecological research. Some methodological steps of our method may be improved and expanded, such as the inclusion of leaf-off data and the use of ensemble models. ML-derived vegetation indices proved to be useful in detecting CWD but could not be applied reliably to generate active NDVI due to attenuation losses in the green channel. More research is required in this context.

3.7. Appendix D: Illustrated Field Sampling Strategy

Twenty-seven sites were selected for CWD volume sampling in the study area based on accessibility, forest composition and seismic line treatment. Sites were selected centered around seismic lines and in each site four 100 m^2 sampling plots were laid out (Figure 3.8): two circular forest plots randomly placed within a buffer from 12 to 36 meters away from the line, and two disturbance plots placed systematically starting 15 meters away from the beginning of the line and spaced 75 meters apart. Forest plots had a 5.645 m radius and disturbance plots had the same width as the seismic line and variable length to obtain a 100 m^2 area (Figure 3.9). Plots were located using a real-time kinematics (RTK) unit, by locating the center point of forest plots and the start and end points of disturbance plots. Volume was sampled for each CWD piece by obtaining three diameter measurements and one length measurement (Figure 3.10) exclusively within the sampling plots, objects crossing the edge of the plots were measured as if they ended at the limits of the plot (Figure 3.11).

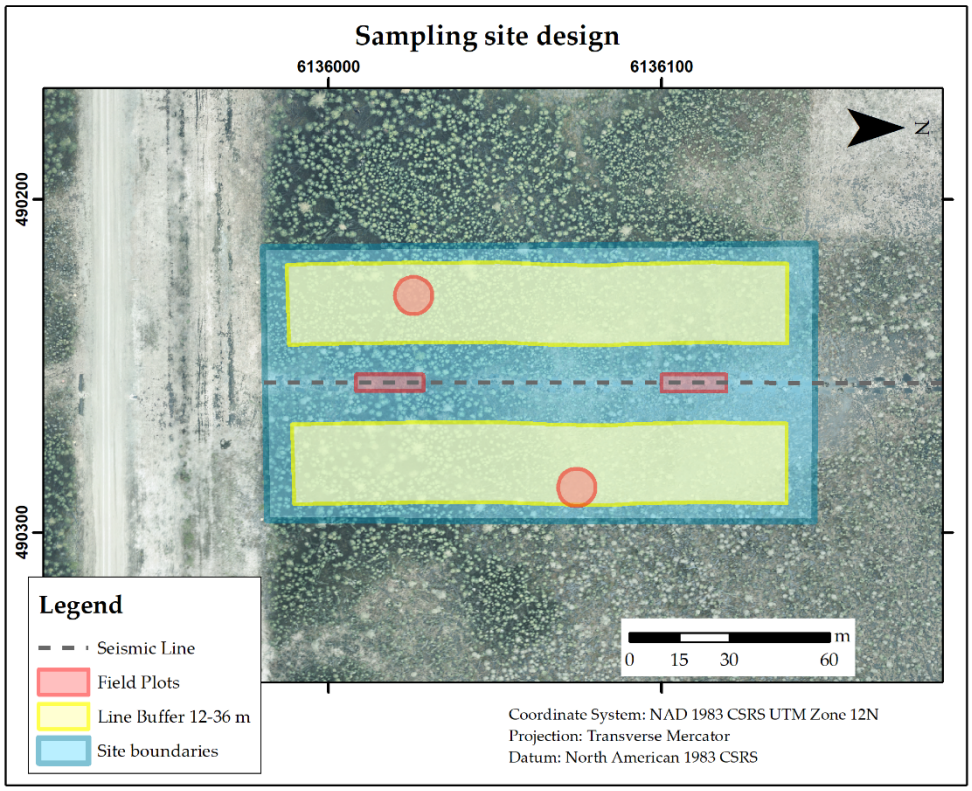

Figure 3.8. Examples of sampling areas for the collection of training and calibration CWD data. For each study site two (belt) disturbance plots are laid out on the seismic line and two (circle) forest plots are laid out off the seismic lines centered within a buffer from 12 to 36 meters away from the line.

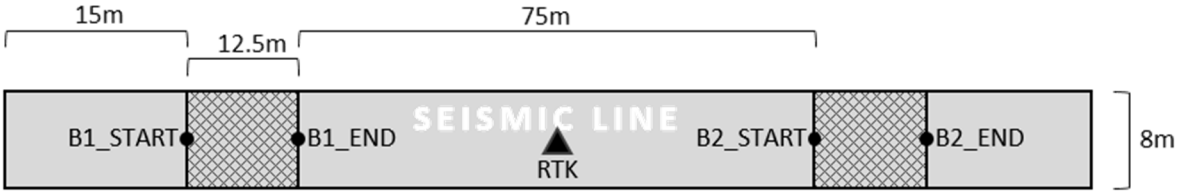

Figure 3.9. Belt plot design for disturbance sampling. The belts have 100 m^2 area and the same width as the seismic line, the first belt starts 15 meters away from the start of the line, the second belt starts 75 meters away from the end of the first belt. A real-time kinematics (RTK) base-station is located somewhere close to the site for good signal with a rover sensor which was used to collect the coordinates of the start and end points.

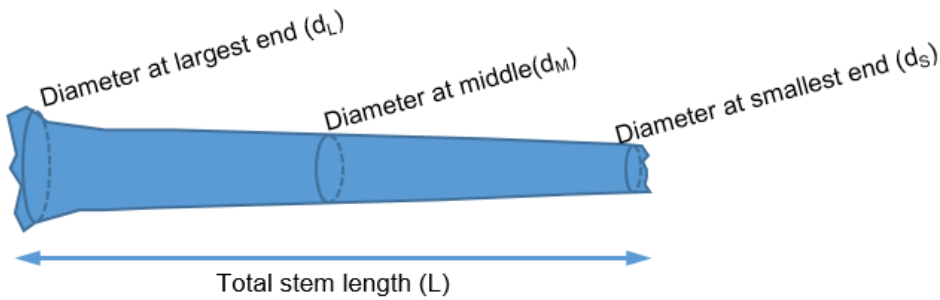

Figure 3.10. Measuring volume of fallen dead trees (logs).

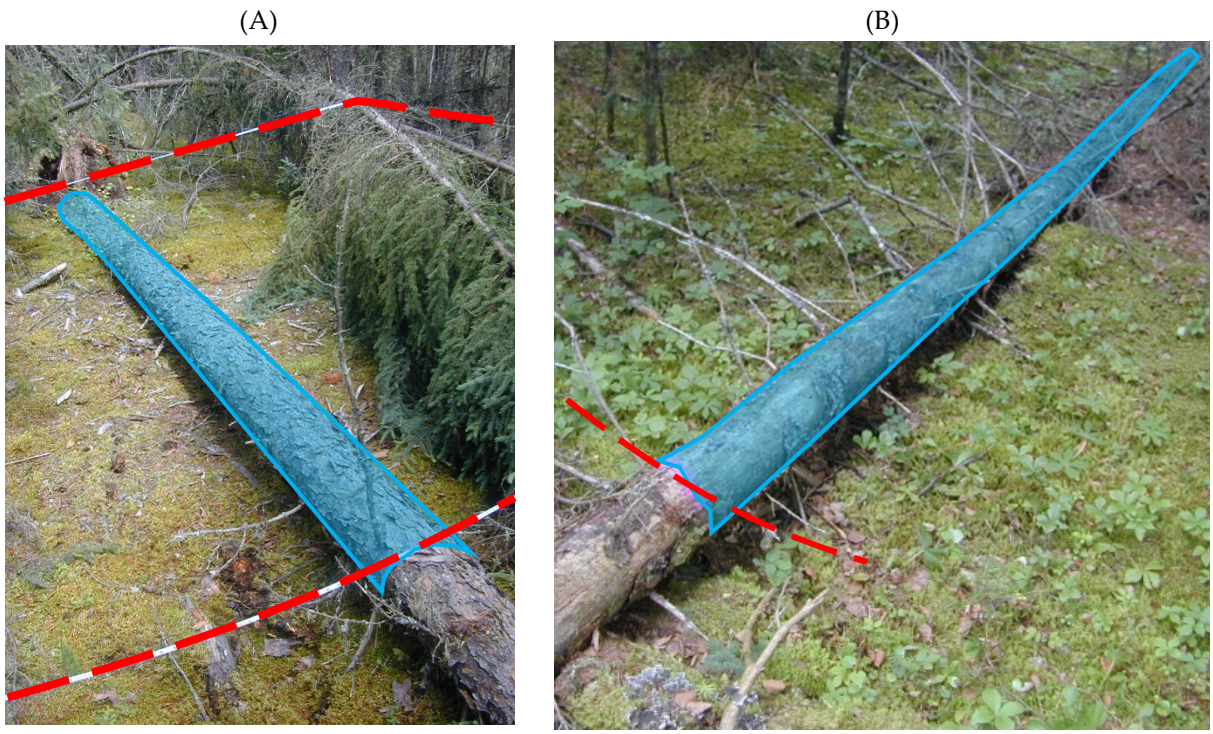

Figure 3.11. Measuring strategy for CWD partly outside the sampling area. Only the (blue) segment within the area is measured, as if it ended at the edge of the sampling area. The dashed red lines represent tape used in (A) disturbance plots or biodegradable paint used in (B) forest plots to mark the edges of the plots.

3.8. References

Alberta Parks. (2015). *Natural Regions and Subregions of Alberta*. Retrieved from http://albertaparks.ca/ albertaparksca/management-land-use/ current-parks-system.aspx

Axelsson, P. (2000). *DEM generation from laser scanner data using adaptive tin models*.

Baumann, M., Ozdogan, M., Wolter, P. T., Krylov, A., Vladimirova, N., & Radeloff, V. C. (2014). Landsat remote sensing of forest windfall disturbance. *Remote Sensing of Environment*, *143*, 171–179. https://doi.org/10.1016/j.rse.2013.12.020

Breiman, L. (2001). Random Forests. *Machine Learning*, *45*(1), 5–32. https://doi.org/10.1023/A:1010933404324

Breslow, N. E. (1996). Generalized linear models: Checking assumptions and strengthening conclusions. *Statistica Applicata*, *8*(1), 23–41.

Brown, J. K., Reinhardt, E. D., & Kramer, K. A. (2003). *Coarse woody debris: Managing benefits and fire hazard in the recovering forest*. https://doi.org/10.2737/RMRS-GTR-105

Budei, B. C., St-Onge, B., Hopkinson, C., & Audet, F.-A. (2018). Identifying the genus or species of individual trees using a three-wavelength airborne lidar system. *Remote Sensing of Environment*, *204*, 632–647. https://doi.org/10.1016/j.rse.2017.09.037

Burnham, K. P., & Anderson, D. R. (2002). *Model selection and multimodel inference: A practical information-theoretic approach* (2nd edition). New York: Springer.

Chasmer, L. E., Hopkinson, C. D., Petrone, R. M., & Sitar, M. (2017). Using Multitemporal and Multispectral Airborne Lidar to Assess Depth of Peat Loss and Correspondence With a New Active Normalized Burn Ratio for Wildfires. *Geophysical Research Letters*, *44*(23), 11,851-11,859. https://doi.org/10.1002/2017GL075488

Dabros, A., Pyper, M., & Castilla, G. (2018). Seismic lines in the boreal and arctic ecosystems of North America: Environmental impacts, challenges, and opportunities. *Environmental Reviews*, *26*(2), 214–229.

DeLancey, E. R., Kariyeva, J., Bried, J. T., & Hird, J. N. (2019). Large-scale probabilistic identification of boreal peatlands using Google Earth Engine, open-access satellite data, and machine learning. *PLOS ONE*, *14*(6), e0218165. https://doi.org/10.1371/journal.pone.0218165

Downing, D. J., & Pettapiece, W. (2006). *Natural regions and subregions of Alberta*. Natural Regions Committee.

Duan, F., Wan, Y., & Deng, L. (2017). A Novel Approach for Coarse-to-Fine Windthrown Tree Extraction Based on Unmanned Aerial Vehicle Images. *Remote Sensing*, *9*(4). https://doi.org/10.3390/rs9040306

ESRI. (2017). ArcGIS Desktop (Version 10.6.1). Redlands, California.

Government of Alberta. (2019). *Forest and vegetation inventories data*. Retrieved from https://www.alberta.ca/forest-and-vegetation-inventories-data.aspx

Guisan, A., Edwards Jr, T. C., & Hastie, T. (2002). Generalized linear and generalized additive models in studies of species distributions: Setting the scene. *Ecological Modelling*, *157*(2–3), 89–100.

Hagan, J. M., & Grove, S. L. (1999). Coarse Woody Debris: Humans and Nature Competing for Trees. *Journal of Forestry*, *97*(1), 6–11. https://doi.org/10.1093/jof/97.1.6

Harmon, M. E., Franklin, J. F., Swanson, F. J., Sollins, P., Gregory, S., Lattin, J., … others. (1986). Ecology of coarse woody debris in temperate ecosystems. In *Advances in ecological research* (Vol. 15, pp. 133–302). Elsevier.

Hay, G. J., & Castilla, G. (2008). Geographic Object-Based Image Analysis (GEOBIA): A new name for a new discipline. In T. Blaschke, S. Lang, & G. J. Hay (Eds.), *Object-Based Image Analysis: Spatial Concepts for Knowledge-Driven Remote Sensing Applications* (pp. 75–89). https://doi.org/10.1007/978-3-540-77058-9_4

Hird, J., DeLancey, E., McDermid, G., & Kariyeva, J. (2017). Google Earth Engine, Open-Access Satellite Data, and Machine Learning in Support of Large-Area Probabilistic Wetland Mapping. *Remote Sensing*, *9*(12), 1315. https://doi.org/10.3390/rs9121315

Hopkinson, C., Chasmer, L., Gynan, C., Mahoney, C., & Sitar, M. (2016). Multisensor and Multispectral LiDAR Characterization and Classification of a Forest Environment. *Canadian Journal of Remote Sensing*, *42*(5), 501–520. https://doi.org/10.1080/07038992.2016.1196584

Husch, B., Beers, T. W., & Kershaw, J. A. (2002). *Forest Mensuration*. Retrieved from https://books.google.ca/books?id=p0v3m8Pau-kC

Inoue, T., Nagai, S., Yamashita, S., Fadaei, H., Ishii, R., Okabe, K., … Suzuki, R. (2014). Unmanned Aerial Survey of Fallen Trees in a Deciduous Broadleaved Forest in Eastern Japan. *PLOS ONE*, *9*(10), e109881. https://doi.org/10.1371/journal.pone.0109881

Isenburg, M. (2019). *LAStools—Efficient tools for LiDAR processing*.

Kashani, A., Olsen, M., Parrish, C., & Wilson, N. (2015). A review of LiDAR radiometric processing: From ad hoc intensity correction to rigorous radiometric calibration. *Sensors, 15*(11), 28099-28128.

Lee, P. C., Crites, S., Nietfeld, M., Nguyen, H. V., & Stelfox, J. B. (1997). Characteristics and origins of deadwood material in aspen-dominated boreal forests. *Ecological Applications*, *7*(2), 691–701.

Lim, K., Treitz, P., Wulder, M., St-Onge, B., & Flood, M. (2003). LiDAR remote sensing of forest structure. *Progress in Physical Geography: Earth and Environment*, *27*(1), 88–106. https://doi.org/10.1191/0309133303pp360ra

Linder, P., Elfving, B., & Zackrisson, O. (1997). Stand structure and successional trends in virgin boreal forest reserves in Sweden. *Forest Ecology and Management*, *98*(1), 17–33. https://doi.org/10.1016/S0378-1127(97)00076-5

Lopes Queiroz, G., McDermid, J. G., Castilla, G., Linke, J., & Rahman, M. M. (2019). Mapping Coarse Woody Debris with Random Forest Classification of Centimetric Aerial Imagery. *Forests*, *10*(6). https://doi.org/10.3390/f10060471

Losada, S., McDermid, G., Cole, S., Lopes Queiroz, G., Rahman, M. M., & Linke, J. (2018, November). *Seismic Line Mapper*. Presented at the Lightning talk and poster presentations at the BERA fall research workshop, Edmonton, AB.

McWinn, J. W., & Crossley, D. A. (1996). *Biodiversity and Coarse Woody Debris in Southern Forests* (No. SE-94; p. 146p). Retrieved from U.S. Department of Agriculture, Forest Service, Southeastern Forest Experiment Station website: https://www.fs.usda.gov/treesearch/pubs/199

Mücke, W., Deák, B., Schroiff, A., Hollaus, M., & Pfeifer, N. (2013). Detection of fallen trees in forested areas using small footprint airborne laser scanning data. *Canadian Journal of Remote Sensing*, *39*(sup1), S32–S40. https://doi.org/10.5589/m13-013

Partners in Protection (Canada). (2003). *FireSmart: Protecting Your Community from Wildfire*. Partners in Protection.

Pedlar, J. H., Pearce, J. L., Venier, L. A., & McKenney, D. W. (2002). Coarse woody debris in relation to disturbance and forest type in boreal Canada. *Forest Ecology and Management*, *158*(1–3), 189–194.

Pix4D SA. (2019). *Pix4Dmapper*. Retrieved from https://www.pix4d.com/

R Core Team. (2018). *R: A language and environment for statistical computing*. Retrieved from https://www.R-project.org/

Richardson, J. J., & Moskal, M. L. (2016). An Integrated Approach for Monitoring Contemporary and Recruitable Large Woody Debris. *Remote Sensing*, *8*(9). https://doi.org/10.3390/rs8090778

Riffell, S., Verschuyl, J., Miller, D., & Wigley, T. B. (2011). Biofuel harvests, coarse woody debris, and biodiversity – A meta-analysis. *Forest Ecology and Management*, *261*(4), 878–887. https://doi.org/10.1016/j.foreco.2010.12.021

Rüetschi, M., Small, D., & Waser, T. L. (2019). Rapid Detection of Windthrows Using Sentinel-1 C-Band SAR Data. *Remote Sensing*, *11*(2). https://doi.org/10.3390/rs11020115

Sippola, A.-L., Siitonen, J., & Kallio, R. (1998). Amount and quality of coarse woody debris in natural and managed coniferous forests near the timberline in Finnish Lapland. *Scandinavian Journal of Forest Research*, *13*(1–4), 204–214.

Stasinopoulos, D., & Rigby, R. (2007). Generalized Additive Models for Location Scale and Shape (GAMLSS) in R. *Journal of Statistical Software, Articles*, *23*(7), 1–46. https://doi.org/10.18637/jss.v023.i07

Stereńczak, K., Kraszewski, B., Mielcarek, M., & Piasecka, Ż. (2017). Inventory of standing dead trees in the surroundings of communication routes – The contribution of remote sensing to potential risk assessments. *Forest Ecology and Management*, *402*, 76–91. https://doi.org/10.1016/j.foreco.2017.07.018

Sturtevant, B. R., Bissonette, J. A., Long, J. N., & Roberts, D. W. (1997). Coarse woody debris as a function of age, stand structure, and disturbance in boreal Newfoundland. *Ecological Applications*, *7*(2), 702–712.

Sumnall, M. J., Hill, R. A., & Hinsley, S. A. (2016). Comparison of small-footprint discrete return and full waveform airborne lidar data for estimating multiple forest variables. *Remote Sensing of Environment*, *173*, 214–223. https://doi.org/10.1016/j.rse.2015.07.027

Teledyne Optech. (2019). *LiDAR Mapping Suite*. Toronto, ON, Canada.

Trimble. (2018). ECognition Developer (Version 9.4) [Windows]. Munich, Germany: Trimble Germany GmbH.

Vinge, T., & Pyper, M. (2012). *Managing woody materials on industrial sites: Meeting economic, ecological, and forest health goals through a collaborative approach*. Department of Renewable Resources, University of Alberta, Edmonton, Alberta.

Yan, E., Wang, X., & Huang, J. (2006). Concept and Classification of Coarse Woody Debris in Forest Ecosystems. *Frontiers of Biology in China*, *1*(1), 76–84.

Yan, W. Y., & Shaker, A. (2017). *Correction of Overlapping Multispectral LIDAR Intensity Data: Polynomial Approximation of Range and Angle Effects*.

Yee, T. W., & Mitchell, N. D. (1991). Generalized additive models in plant ecology. *Journal of Vegetation Science*, *2*(5), 587–602.

Chapter Four: Conclusions

Coarse woody debris (CWD) directly and indirectly impacts many biological, chemical, physical, economic, and social aspects of forest ecosystems and forest management (Harmon et al., 1986; McWinn et al., 1996; Hagan and Grove, 1999; Brown et al., 2003; Riffell et al., 2011). CWD has an especially important role within the context of Alberta's boreal forest and its relationship with seismic lines (Vinge and Pyper, 2012). Undoubtedly there is interest in studying CWD spatially, mapping its occurrence and quantifying CWD over large application areas. With increasingly more accessible and detailed remote sensing data for forested environments, as well as more powerful algorithms and processing units, several studies have attempted to provide accurate solutions for remote sensing of CWD within this decade (Baumann et al., 2014; Polewski et al., 2015; Richardson and Moskal, 2016; Stereńczak et al., 2017; Duan et al., 2017; Panagiotidis et al., 2019; Rüetschi et al., 2019). However, there are still issues with detecting small CWD or objects partially occluded by canopy, and many of these studies apply their methods on small application areas or only on recently windthrown trees. Additionally, research on quantification of CWD volume over large study areas using remote sensing is limited (Sumnall et al., 2016). The research presented in this thesis aims to fill these literature gaps by providing sophisticated workflows capable of accurate mapping of logs and snags, as well as the quantification of CWD volumes over large study areas, demonstrated here within the context of a disturbed boreal forest in Alberta. The methods used to achieve these products include geographical object-based image analysis (GEOBIA) with machine learning classification to identify CWD objects on aerial data, as well as zero-adjusted CWD volume models selected via the akaike information criterion (AIC). The results of this research suggest that the presented workflows were successful in accurate detection and measurement of CWD both in natural and disturbed environments. Additionally, the models were capable of being transferred to a nearby application area without the need for additional training data. LiDAR data aided in improving the distinction between logs and snags,

and multispectral LiDAR aided in modeling occluded CWD volumes. These findings suggest that large-scale automated CWD quantification will become increasingly more feasible and accurate, as new technologies provide more accessible and detailed information of the visible forest surface as well as of the forest elements occluded beneath vegetation.

4.1. Research Objectives Summary

The overarching goal of this research was to provide accurate workflows for mapping and quantifying CWD over extensive forested areas, with special attention to Alberta's boreal environment. The main objectives were:

1. Evaluate the capability of GEOBIA via supervised classification of aerial photos and LiDAR to accurately classify both logs and snags in the boreal forest. To do so smaller objectives were pursued:
    a. Assess the accuracy and transferability of the best developed workflow in the study area.
    b. Evaluate the worth of LiDAR in addition to spectral predictor variables to increase classification accuracies.
    c. Gain insight into the minimum number of predictor variables and number of training samples required for accurate classification.
2. Select the best regression models for CWD volume estimation on the study area using image-analysis layers, multispectral LiDAR and other spectral indices. In addressing this objective two smaller goals were pursued:
    a. Test the accuracy and transferability of the best predictive model in the study area.
    b. Assess the value and impact of multispectral LiDAR data in improving the prediction of occluded CWD.

The research performed aiming to address each specific objective and sub-objective is summarized here:

- (Objective 1) A literature review was performed on current methods used to perform accurate remote sensing of CWD in forested environments, which was summarized in the introduction of Chapter 2. Based on this review, a GEOBIA workflow including machine learning classification was chosen as the most promising approach for accurate results in the study area. These methods were performed using high-resolution aerial photos and a high-density LiDAR point cloud.
- (Objective 1a) The accuracy of the GEOBIA workflow was assessed via cross-validation tests within a calibration area, where the classification models were fine-tuned and trained, as well as in a verification area which was a minimum of 4 km away from all training data. Results indicated that the method was very accurate when there is no distinction between logs and snags (93.4% completeness and 94.5% correctness), and accurate when logs (76.9% completeness and 87.0% correctness) and snags (95.5% completeness and 91.7% correctness) are mapped separately. Also, transferability was very good when there was no distinction of CWD classes (80.6% completeness and 92.3% correctness) but produced lower accuracies when separating logs (81.5% completeness, 75.8% correctness) and snags (65.7% completeness, 88.8% correctness).
- (Objective 1b) Accuracy tests were performed with random forest classifiers trained using spectral and spatial data, as well as height data: a canopy height model (CHM) and a digital surface model (DSM). Tests alternating the available height data, with both CHM and DSM, only CHM or DSM, and none of the height data, revealed that height information was valuable to increase the distinction between logs and snags (~6% better distinction; significant at α 0.05). CHM was

more valuable than DSM for this purpose (~1.5% better distinction; significant at α 0.05), and there was a small but statistically significant drop in accuracy of overall CWD (no class distinction) when not using any height data as opposed to using the least valuable height variables (~2.2% more accurate; significant at α 0.05).

- (Objective 1c) Training dataset size was incrementally reduced by independently and randomly removing samples from the reference data while assessing the accuracy of predictions on each iteration. This test revealed that good classification accuracy (~90%) could be achieved for both logs and snags with as few as 1000 training samples obtained using the presented sampling strategy, and even less samples were required when there is no distinction between logs and snags, with more than 90% completeness and correctness achieved using as few as 512 samples.
- (Objective 2) Given the classification layers obtained via GEOBIA of the study area, additional potential predictive layers were selected for modeling CWD volume. A wetland-probability layer was obtained to account for differences in CWD distribution in upland and lowland portions of the study area. Multiple sub-products of the remote sensing data used in GEOBIA were used, including: Brightness, NDVI, CHM, DSM and canopy closure (CC). Additionally, multispectral LiDAR (ML) containing green, near-infrared and shortwave-infrared wavelength bands were used to generate active NDVI and normalized burn ratio (NBR) spectral indices. Conversely, field data acquired on both natural and disturbed sampling sites in the study area were used as ground-truth reference data to train and test the CWD volume regression models. Models were selected using Akaike's information criterion for small samples (AICc), and the best models with and without ML data were chosen for application in the study area based on their AICc.

- (Objectives 2a and 2b) The accuracy of the best regression models with and without ML data were tested with cross-validation within a calibration area, where the models were trained, as well as in a verification area which was a minimum of 4 km away from all training data. Results indicated that the method was accurate in the calibration area (0.623 R^2, 0.224 RMSE) and even when models were applied to the verification sites (0.721 R^2, 0.198 RMSE) without additional training. ML-inclusive models performed better than models without ML data, both in accuracies (~ 0.1 higher R^2 and ~0.018 lower RMSE) and to some extent in AIC ranking (~1.1 lower ΔAIC), indicating that ML improved CWD modeling in occluded areas.

In conclusion, the greater goals and sub-objectives of this thesis were successfully achieved through the development and application of novel CWD classification and regression models. GEOBIA with random forest classification was able to provide accurate map products, with results comparable to some of the best reported in the literature. Zero-adjusted models were able to provide accurate CWD volume maps of the study area and demonstrated that ML data is valuable to improve prediction of occluded CWD.

4.2. Research Contributions

This thesis presents several methodological and theoretical contributions in the fields of remote sensing and forest management. The study area represents a relatively complex boreal environment, with drastically different CWD distributions between uplands and lowlands, natural environment and human disturbances, mixedwood stands and pine or spruce dominated stands. Studies of remote sensing of CWD available in the literature seldom select study areas or CWD elements exhibiting such level of complexity. One of the main contributions of this research is the development of workflows capable of accurately detecting and measuring CWD in this kind of environment. Undoubtedly the same methods presented here could be applied to simpler study areas with an even higher level of success. As part of

this contribution, the importance of traditional LiDAR and multispectral LiDAR to CWD detection and measurement were important findings, especially given that multispectral LiDAR is seldom seen in applied studies of forest mensuration and is novel within the context of CWD. Methods described extensively in chapters 2 and 3 could also be adapted for application targeting forest elements other than CWD and could even be applied in different environments such as deserts or cities, assuming a new set of calibration and training data is introduced. The anticipated citations for the published chapters 2 and 3 are as follows:

Chapter 2: Lopes Queiroz, G., McDermid, J. G., Castilla, G., Linke, J., & Rahman, M. M. (2019). Mapping Coarse Woody Debris with Random Forest Classification of Centimetric Aerial Imagery. *Forests*, *10*(6). https://doi.org/10.3390/f10060471

Chapter 3: Lopes Queiroz, G., McDermid, J. G., Castilla, G., Linke, J., & Rahman, M. M., Hopkinson, C., Kariyeva, J. (2019). Estimating Coarse Woody Debris Volume Using Image Analysis and Multispectral LiDAR. [Manuscript in preparation]

The map products made available by this research, as well as the potential to apply the developed workflow in other boreal sites, has the potential to facilitate forest-management programs and monitoring efforts in Alberta. As of now forest restoration programs and field operators have difficulties planning and executing CWD treatment in boreal sites, partly because natural CWD occurrence is unpredictable and consequently the natural range within the landscape hard to estimate, and partly because the presence of CWD dramatically hinders navigation of field operators and machinery within seismic lines. Knowing the precise location and quantities of CWD within the entire network of seismic lines in a study area could accelerate and improve the effectiveness of restoration efforts in the boreal forest. This is especially important in Alberta given the delicate state of endangered caribou herds and their dependence on structural elements such as CWD which hinder the hunting efficacy of predators. Not only agencies working to restore the boreal environment disturbed by oil and gas development, but the ones which monitor their progress may be interested in more

detailed products such as the ones made available by this research. Considering the increasing concern towards habitat protection made evident with recently established guidelines for seismic line restoration, it is likely that in future years the government of Alberta may begin to monitor restoration efforts more closely. In such case detailed region-wide maps of CWD would certainly be of interest. Finally, these products may enhance the understanding of CWD dynamics and allow novel studies of the impact of CWD in the ecosystem and in forest management.

4.3. Recommendations for Future Research

The research presented in this thesis provided several contributions; meanwhile there are many avenues left for exploration in the improvement of the presented workflows and in the use of the enabled map products for ecology and forestry related studies. Some of the possible areas for future research in light of this work were identified and divided into two categories: I) remote sensing studies exploring possible improvements to the developed CWD models; II) biogeographical studies using region-wide CWD maps and CWD seismic line maps. These are briefly discussed below.

4.3.1. Future Remote Sensing of CWD Research

The results of classification and regression of CWD suggest that the main source for false negatives is the presence of superimposed vegetation, mainly observed as tall grass on seismic lines and canopy cover on undisturbed forest sites. Therefore, given this thesis used leaf-on data (i.e. data collected during summer) it is likely that leaf-off data (i.e. data collected during spring) would enable an enhanced view of CWD in these situations, considering low-lying vegetation and canopy are substantially less dense during spring. Undoubtedly there are trade-offs between using leaf-on and leaf-off data for CWD detection, given the latter provides NDVI layers with less contrast between alive and dead vegetation. Studies could compare the effectiveness of datasets from spring and summer to map and model CWD quantities, and

even attempt to combine both datasets to obtain more robust, potentially more accurate, predictions.

Multispectral LiDAR (ML) has improved the accuracy of CWD volume predictions in occluded areas. However, it could also have been incorporated in the GEOBIA workflow to potentially improve classification accuracy of visible CWD. This potential application is yet to be tested. Additionally, given the wet conditions prior to ML data acquisition over the study area, the green wavelength point cloud was lacking much information when compared to the other bands due to atmospheric attenuation losses. In theory, NDVI could be a better predictive variable than NBR for CWD quantities. This could be tested if a new ML dataset collected under more appropriate conditions was used in model selection.

The article presented in Chapter 2 mapped both logs and snags in the study area, but the article presented in Chapter 3 only modeled log volumes in the study area. It is likely that snag volumes could be modeled in a similar fashion, using similar datasets to the ones presented here. However, the accuracies for snag volume estimation using these methods are yet to be tested as is the influence of ML data for this purpose. Additionally, there are many other types of models which could be used for CWD volume estimation aside from the zero-adjusted model described in Chapter 3. Given a more comprehensive reference dataset, with a much larger sample size, it is likely that sophisticated machine learning models such as random forest would be able to improve prediction accuracies for CWD volume.

4.3.2. Future Ecology Research Using CWD Maps

The detailed region-wide map of CWD presented in Chapter 3 as well as the potential of generating such products in other application areas allows for a variety of future biogeography research to explore the influence of CWD on the environment. Maps could be produced in a study area before and after controlled fires to evaluate the impact of CWD quantities on fire severity and spread. Similarly, these maps along with wildlife location data for any given

organism could be used to evaluate the CWD use by that wildlife and to improve predictive location models for that species.

The detailed seismic line map of CWD presented in Chapter 3 and the potential of creating similar maps for other study areas allow for biogeography studies to further our understanding of CWD dynamics on seismic lines. Using these maps along with plant-growth data it would be possible to quantify the influence of CWD on seedling survival and growth rate, which is yet unknown and could drastically change the way restoration programs use CWD on seismic lines. By producing CWD seismic line maps on caribou range where wolf collar data is available and comparing these datasets, it would be possible to quantify the deterring effect of CWD on wolf selection and navigation in seismic lines. This knowledge could also dramatically change the way restoration programs use CWD in caribou range. Additionally, it could improve predictive models of seismic line use by wolves. Finally, using knowledge of how wolves use seismic lines for improved navigation and how CWD affects the hunting effectiveness of wolves, it would be possible to produce a tool or workflow which identifies the most critical areas in a seismic line network for CWD treatment aiming to reduce caribou predation rates.

Potential future improvements and applications for the developed workflows and maps described here are some of the possible future research identified by the author. Given the work of this thesis was conducted within the context of Alberta's boreal forests most of the imagined future research listed here is focused in this environment and its most pressing issues. It is possible that the work presented here could spawn research within other contexts.

4.4. Bibliography

Agisoft. (2016). AgiSoft PhotoScan (Version 1.2.4.2399). St. Petersburg, Russia: Agisoft LLC.

Alberta Parks. (2015). *Natural Regions and Subregions of Alberta*. Retrieved from http://albertaparks.ca/ albertaparksca/management-land-use/ current-parks-system.aspx

Axelsson, P. (2000). *DEM generation from laser scanner data using adaptive tin models*.

Baumann, M., Ozdogan, M., Wolter, P. T., Krylov, A., Vladimirova, N., & Radeloff, V. C. (2014). Landsat remote sensing of forest windfall disturbance. *Remote Sensing of Environment*, *143*, 171–179. https://doi.org/10.1016/j.rse.2013.12.020

Blanchard, S. D., Jakubowski, M. K., & Kelly, M. (2011). Object-based image analysis of downed logs in disturbed forested landscapes using lidar. *Remote Sensing*, *3*(11), 2420–2439.

Blaschke, T., Hay, G. J., Kelly, M., Lang, S., Hofmann, P., Addink, E., … others. (2014). Geographic object-based image analysis–towards a new paradigm. *ISPRS Journal of Photogrammetry and Remote Sensing*, *87*, 180–191.

Brandt, J., Flannigan, M., Maynard, D., Thompson, I., & Volney, W. (2013). An introduction to Canada's boreal zone: Ecosystem processes, health, sustainability, and environmental issues. *Environmental Reviews*, *21*(4), 207–226.

Breiman, L. (2001). Random Forests. *Machine Learning*, *45*(1), 5–32. https://doi.org/10.1023/A:1010933404324

Breslow, N. E. (1996). Generalized linear models: Checking assumptions and strengthening conclusions. *Statistica Applicata*, *8*(1), 23–41.

Brown, J. K., Reinhardt, E. D., & Kramer, K. A. (2003). *Coarse woody debris: Managing benefits and fire hazard in the recovering forest*. https://doi.org/10.2737/RMRS-GTR-105

Budei, B. C., St-Onge, B., Hopkinson, C., & Audet, F.-A. (2018). Identifying the genus or species of individual trees using a three-wavelength airborne lidar system. *Remote Sensing of Environment*, *204*, 632–647. https://doi.org/10.1016/j.rse.2017.09.037

Burnett, C., & Blaschke, T. (2003). A multi-scale segmentation/object relationship modelling methodology for landscape analysis. *Ecological Modelling*, *168*(3), 233–249.

Burnham, K. P., & Anderson, D. R. (2002). *Model selection and multimodel inference: A practical information-theoretic approach* (2nd edition). New York: Springer.

Bütler, R., & Schlaepfer, R. (2004). Spruce snag quantification by coupling colour infrared aerial photos and a GIS. *Forest Ecology and Management*, *195*(3), 325–339. https://doi.org/10.1016/j.foreco.2004.02.042

Chasmer, L. E., Hopkinson, C. D., Petrone, R. M., & Sitar, M. (2017). Using Multitemporal and Multispectral Airborne Lidar to Assess Depth of Peat Loss and Correspondence With a New Active Normalized Burn Ratio for Wildfires. *Geophysical Research Letters*, *44*(23), 11,851-11,859. https://doi.org/10.1002/2017GL075488

Dabros, A., Pyper, M., & Castilla, G. (2018). Seismic lines in the boreal and arctic ecosystems of North America: Environmental impacts, challenges, and opportunities. *Environmental Reviews*, *26*(2), 214–229.

Davis, B. (2017). *Refinement of a Drone-Based Method for Estimating Coarse Woody Debris and Biomass Residue Following Forest Harvest* (Master of Science). University of Georgia, Athens, Georgia.

DeLancey, E. R., Kariyeva, J., Bried, J. T., & Hird, J. N. (2019). Large-scale probabilistic identification of boreal peatlands using Google Earth Engine, open-access satellite data, and machine learning. *PLOS ONE*, *14*(6), e0218165. https://doi.org/10.1371/journal.pone.0218165

Dickie, M. M. (2015). *The use of anthropogenic linear features by wolves in northeastern Alberta* (Master's Thesis). University of Alberta, Department of Biological Sciences, Edmonton, Canada.

Duan, F., Wan, Y., & Deng, L. (2017). A Novel Approach for Coarse-to-Fine Windthrown Tree Extraction Based on Unmanned Aerial Vehicle Images. *Remote Sensing*, *9*(4). https://doi.org/10.3390/rs9040306

Environment Canada. (2012). *Recovery strategy for the woodland caribou (Rangifer tarandus caribou), Boreal population, in Canada* (No. 9; p. 138). Ottawa, Canada: Environment Canada.

Escuin, S., Navarro, R., & Fernández, P. (2008). Fire severity assessment by using NBR (Normalized Burn Ratio) and NDVI (Normalized Difference Vegetation Index) derived from LANDSAT TM/ETM images. *International Journal of Remote Sensing*, *29*(4), 1053–1073. https://doi.org/10.1080/01431160701281072

ESRI. (2017). ArcGIS Desktop (Version 10.6.1). Redlands, California.

Fisher, P. (1997). The pixel: A snare and a delusion. *International Journal of Remote Sensing*, *18*(3), 679–685.

Fisher, J. T., & Burton, A. C. (2018). Wildlife winners and losers in an oil sands landscape. *Frontiers in Ecology and the Environment*, *16*(6), 323–328.

Government of Alberta. (2017). *Provincial Restoration and Establishment Framework for Legacy Seismic Lines in Alberta*. Prepared for Alberta Environment and Parks, Land and Environment Planning Branch, Edmonton, Alberta. 9, 70.

Government of Alberta. (2019). *Forest and vegetation inventories data*. Retrieved from https://www.alberta.ca/forest-and-vegetation-inventories-data.aspx

Guisan, A., Edwards Jr, T. C., & Hastie, T. (2002). Generalized linear and generalized additive models in studies of species distributions: Setting the scene. *Ecological Modelling*, *157*(2–3), 89–100.

Hagan, J. M., & Grove, S. L. (1999). Coarse Woody Debris: Humans and Nature Competing for Trees. *Journal of Forestry*, *97*(1), 6–11. https://doi.org/10.1093/jof/97.1.6

Harmon, M. E., Franklin, J. F., Swanson, F. J., Sollins, P., Gregory, S., Lattin, J., … others. (1986). Ecology of coarse woody debris in temperate ecosystems. In *Advances in ecological research* (Vol. 15, pp. 133–302). Elsevier.

Hay, G. J., & Castilla, G. (2008). Geographic Object-Based Image Analysis (GEOBIA): A new name for a new discipline. In T. Blaschke, S. Lang, & G. J. Hay (Eds.), *Object-Based Image Analysis: Spatial Concepts for Knowledge-Driven Remote Sensing Applications* (pp. 75–89). https://doi.org/10.1007/978-3-540-77058-9_4

Hebblewhite, M. (2017). Billion dollar boreal woodland caribou and the biodiversity impacts of the global oil and gas industry. *Biological Conservation*, *206*, 102–111. https://doi.org/10.1016/j.biocon.2016.12.014

Hird, J., DeLancey, E., McDermid, G., & Kariyeva, J. (2017). Google Earth Engine, Open-Access Satellite Data, and Machine Learning in Support of Large-Area Probabilistic Wetland Mapping. *Remote Sensing*, *9*(12), 1315. https://doi.org/10.3390/rs9121315

Hopkinson, C., Chasmer, L., Gynan, C., Mahoney, C., & Sitar, M. (2016). Multisensor and Multispectral LiDAR Characterization and Classification of a Forest Environment. *Canadian Journal of Remote Sensing*, *42*(5), 501–520. https://doi.org/10.1080/07038992.2016.1196584

Husch, B., Beers, T. W., & Kershaw, J. A. (2002). *Forest Mensuration*. Retrieved from https://books.google.ca/books?id=p0v3m8Pau-kC

Inoue, T., Nagai, S., Yamashita, S., Fadaei, H., Ishii, R., Okabe, K., … Suzuki, R. (2014). Unmanned Aerial Survey of Fallen Trees in a Deciduous Broadleaved Forest in Eastern Japan. *PLOS ONE*, *9*(10), e109881. https://doi.org/10.1371/journal.pone.0109881

Isenburg, M. (2019). *LAStools—Efficient tools for LiDAR processing*.

Jensen, J. R. (2015). *Introductory digital image processing: A remote sensing perspective*. Prentice Hall Press.

Jonsson, B. G., & Kruys, N. (2001). Ecology of Coarse Woody Debris in Boreal Forests: Future Research Directions. *Ecological Bulletins*, (49), 279–281. Retrieved from JSTOR.

Kashani, A., Olsen, M., Parrish, C., & Wilson, N. (2015). A review of LiDAR radiometric processing: From ad hoc intensity correction to rigorous radiometric

calibration. *Sensors, 15*(11), 28099-28128.King, R. (2002). Land cover mapping principles: A return to interpretation fundamentals. *International Journal of Remote Sensing*, *23*(18), 3525–3545.

Kirkland, J. (2015). Bioenergy from forests: The power potential of woody biomass. *Science Findings 174. Portland, OR: US Department of Agriculture, Forest Service, Pacific Northwest Research Station. 6 p.*, *174*.

Korzukhin, M. D., Ter-Mikaelian, M. T., & Wagner, R. G. (1996). Process versus empirical models: Which approach for forest ecosystem management? *Canadian Journal of Forest Research*, *26*(5), 879–887.

Lee, P., & Boutin, S. (2006). Persistence and developmental transition of wide seismic lines in the western Boreal Plains of Canada. *Journal of Environmental Management*, *78*(3), 240–250. https://doi.org/10.1016/j.jenvman.2005.03.016

Lee, P. C., Crites, S., Nietfeld, M., Nguyen, H. V., & Stelfox, J. B. (1997). Characteristics and origins of deadwood material in aspen-dominated boreal forests. *Ecological Applications*, *7*(2), 691–701.

Liaw, A., & Wiener, M. (2018). Breiman and Cutler's Random Forests for Classification and Regression (Version 4.6-14) [R]. Retrieved from https://cran.r-project.org/web/packages/randomForest/randomForest.pdf

Lim, K., Treitz, P., Wulder, M., St-Onge, B., & Flood, M. (2003). LiDAR remote sensing of forest structure. *Progress in Physical Geography: Earth and Environment*, *27*(1), 88–106. https://doi.org/10.1191/0309133303pp360ra

Lindberg, E., Hollaus, M., Mücke, W., Fransson, J. E., & Pfeifer, N. (2013). Detection of lying tree stems from airborne laser scanning data using a line template matching algorithm. *ISPRS Annals of Photogrammetry, Remote Sensing and Spatial Information Sciences*, *5*, 169–174.

Linder, P., Elfving, B., & Zackrisson, O. (1997a). Stand structure and successional trends in virgin boreal forest reserves in Sweden. *Forest Ecology and Management*, *98*(1), 17–33.

Linder, P., Elfving, B., & Zackrisson, O. (1997b). Stand structure and successional trends in virgin boreal forest reserves in Sweden. *Forest Ecology and Management*, *98*(1), 17–33. https://doi.org/10.1016/S0378-1127(97)00076-5

Lopes Queiroz, G., McDermid, J. G., Castilla, G., Linke, J., & Rahman, M. M. (2019). Mapping Coarse Woody Debris with Random Forest Classification of Centimetric Aerial Imagery. *Forests*, *10*(6). https://doi.org/10.3390/f10060471

Losada, S., McDermid, G., Cole, S., Lopes Queiroz, G., Rahman, M. M., & Linke, J. (2018, November). *Seismic Line Mapper*. Presented at the Lightning talk and poster presentations at the BERA fall research workshop, Edmonton, AB.

Macias Fauria, M., & Johnson, E. (2007). Climate and wildfires in the North American boreal forest. *Philosophical Transactions of the Royal Society B: Biological Sciences*, *363*(1501), 2315–2327.

Marcus, W. A., Marston, R. A., Colvard Jr, C. R., & Gray, R. D. (2002). Mapping the spatial and temporal distributions of woody debris in streams of the Greater Yellowstone Ecosystem, USA. *Geomorphology*, *44*(3–4), 323–335.

McWinn, J. W., & Crossley, D. A. (1996). *Biodiversity and Coarse Woody Debris in Southern Forests* (No. SE-94; p. 146p). Retrieved from U.S. Department of Agriculture, Forest Service, Southeastern Forest Experiment Station website: https://www.fs.usda.gov/treesearch/pubs/199

Mücke, W., Deák, B., Schroiff, A., Hollaus, M., & Pfeifer, N. (2013). Detection of fallen trees in forested areas using small footprint airborne laser scanning data. *Canadian Journal of Remote Sensing*, *39*(sup1), S32–S40. https://doi.org/10.5589/m13-013

Natural Regions Committee. (2006). Natural regions and subregions of Alberta. *Compiled by DJ Downing and WW Pettapiece. Government of Alberta. Pub*.

Panagiotidis, D., Abdollahnejad, A., & Surový, P. (2019). Detection of fallen logs from high-resolution UAV Images. *New Zealand Journal of Forestry Science*, *49*.

Partners in Protection (Canada). (2003). *FireSmart: Protecting Your Community from Wildfire*. Partners in Protection.

Pasher, J., & King, D. J. (2009). Mapping dead wood distribution in a temperate hardwood forest using high resolution airborne imagery. *Forest Ecology and Management*, *258*(7), 1536–1548.

Pedlar, J. H., Pearce, J. L., Venier, L. A., & McKenney, D. W. (2002). Coarse woody debris in relation to disturbance and forest type in boreal Canada. *Forest Ecology and Management*, *158*(1), 189–194. https://doi.org/10.1016/S0378-1127(00)00711-8

Percy, K. E. (2012). *Alberta oil sands: Energy, industry and the environment* (Vol. 11). Newnes.

Pix4D SA. (2019). *Pix4Dmapper*. Retrieved from https://www.pix4d.com/

Polewski, P., Yao, W., Heurich, M., Krzystek, P., & Stilla, U. (2015). Detection of fallen trees in ALS point clouds using a Normalized Cut approach trained by simulation. *ISPRS Journal of Photogrammetry and Remote Sensing*, *105*, 252–271. https://doi.org/10.1016/j.isprsjprs.2015.01.010

R Core Team. (2018). *R: A language and environment for statistical computing*. Retrieved from https://www.R-project.org/

Richardson, J. J., & Moskal, M. L. (2016). An Integrated Approach for Monitoring Contemporary and Recruitable Large Woody Debris. *Remote Sensing*, *8*(9). https://doi.org/10.3390/rs8090778

Riffell, S., Verschuyl, J., Miller, D., & Wigley, T. B. (2011). Biofuel harvests, coarse woody debris, and biodiversity – A meta-analysis. *Forest Ecology and Management*, *261*(4), 878–887. https://doi.org/10.1016/j.foreco.2010.12.021

Rowe, J. S., & Scotter, G. W. (1973). Fire in the boreal forest. *Quaternary Research*, *3*(3), 444–464. https://doi.org/10.1016/0033-5894(73)90008-2

Rüetschi, M., Small, D., & Waser, T. L. (2019). Rapid Detection of Windthrows Using Sentinel-1 C-Band SAR Data. *Remote Sensing*, *11*(2). https://doi.org/10.3390/rs11020115

Schneider, R., & Dyer, S. (2006). *Death by a thousand cuts: Impacts of in situ oil sands development on Alberta's boreal forest*. Pembina Institute Calgary, AB, Canada.

Selvarajan, S. (2011). *Fusion of LiDAR and aerial imagery for the estimation of downed tree volume using support vector machines classification and region based object fitting*. University of Florida.

Sippola, A.-L., Siitonen, J., & Kallio, R. (1998). Amount and quality of coarse woody debris in natural and managed coniferous forests near the timberline in Finnish Lapland. *Scandinavian Journal of Forest Research*, *13*(1–4), 204–214.

Stasinopoulos, D., & Rigby, R. (2007). Generalized Additive Models for Location Scale and Shape (GAMLSS) in R. *Journal of Statistical Software, Articles*, *23*(7), 1–46. https://doi.org/10.18637/jss.v023.i07

Stereńczak, K., Kraszewski, B., Mielcarek, M., & Piasecka, Ż. (2017). Inventory of standing dead trees in the surroundings of communication routes – The contribution of remote sensing to potential risk assessments. *Forest Ecology and Management*, *402*, 76–91. https://doi.org/10.1016/j.foreco.2017.07.018

Sturtevant, B. R., Bissonette, J. A., Long, J. N., & Roberts, D. W. (1997). Coarse woody debris as a function of age, stand structure, and disturbance in boreal Newfoundland. *Ecological Applications*, *7*(2), 702–712.

Sumnall, M. J., Hill, R. A., & Hinsley, S. A. (2016). Comparison of small-footprint discrete return and full waveform airborne lidar data for estimating multiple forest variables. *Remote Sensing of Environment*, *173*, 214–223. https://doi.org/10.1016/j.rse.2015.07.027

Teledyne Optech. (2019). *LiDAR Mapping Suite*. Toronto, ON, Canada.

Timoney, K., & Lee, P. (2001). Environmental management in resource-rich Alberta, Canada: First world jurisdiction, third world analogue? *Journal of Environmental Management*, *63*(4), 387–405.

Trimble. (2016, July 27). *ECognition Developer 9.2 Reference Book*. Retrieved from http://www.ecognition.com/free-trial

Trimble. (2018). ECognition Developer (Version 9.4) [Windows]. Munich, Germany: Trimble Germany GmbH.

Ucitel, D., Christian, D. P., & Graham, J. M. (2003). Vole Use of Coarse Woody Debris and Implications for Habitat and Fuel Management. *The Journal of Wildlife Management*, *67*(1), 65–72. https://doi.org/10.2307/3803062

Vinge, T., & Pyper, M. (2012). *Managing woody materials on industrial sites: Meeting economic, ecological, and forest health goals through a collaborative approach*. Department of Renewable Resources, University of Alberta, Edmonton, Alberta.

Westoby, M. J., Brasington, J., Glasser, N. F., Hambrey, M. J., & Reynolds, J. M. (2012). 'Structure-from-Motion' photogrammetry: A low-cost, effective tool for geoscience applications. *Geomorphology*, *179*, 300–314. https://doi.org/10.1016/j.geomorph.2012.08.021

Yan, E., Wang, X., & Huang, J. (2006). Concept and Classification of Coarse Woody Debris in Forest Ecosystems. *Frontiers of Biology in China*, *1*(1), 76–84.

Yan, W. Y., & Shaker, A. (2017). *Correction of Overlapping Multispectral LIDAR Intensity Data: Polynomial Approximation of Range and Angle Effects*.

Yee, T. W., & Mitchell, N. D. (1991). Generalized additive models in plant ecology. *Journal of Vegetation Science*, *2*(5), 587–602.

Appendix: Copyright Permissions

This appendix provides the copyright permissions from coauthors of Chapter 2 and anticipated coauthors of Chapter 3 to share the manuscripts in this thesis.

From: Gustavo Lopes Queiroz <[redacted]>
Sent: Wednesday, September 18, 2019 3:26 PM
To: Greg McDermid <[redacted]>; Julia Linke <[redacted]>; Castilla, Guillermo (NRCan/RNCan) <[redacted]>; Hopkinson, Christopher <[redacted]>; Jahan Kariyeva <[redacted]>
Subject: URGENT: Copyright permission to publish thesis

According to the rules for thesis submission at Faculty of Graduate Studies at UofC, I need the permission from coauthors of my manuscripts to publish material that is in preparation in order to share that material in my thesis.

Please simply answer "in accordance" if you agree to give me permission to share the material in my thesis (The published MDPI paper https://www.mdpi.com/1999-4907/10/6/471/htm and the manuscript following that work using multispectral LiDAR)

Thank you,
Gus

PS.: I need this permission before Friday if possible.

From: Castilla, Guillermo (NRCan/RNCan) <[redacted]>
Sent: Wednesday, September 18, 2019 3:35 PM
To: Gustavo Lopes Queiroz <[redacted]>

Hi Gus,

Of course, you have my permission to use our manuscript below in your ~~Ph.D~~ thesis

Best of success

Guillermo

From: Julia Linke <[redacted]>
Sent: Wednesday, September 18, 2019 4:19 PM
To: Gustavo Lopes Queiroz <[redacted]>

In accordance

_____

Julia Linke, PhD
Science Coordinator
- NSERC CRD Boreal Ecosystem Recovery and Assessment Project
- ABBY-NET
University of Calgary
Phone: [redacted]
E-mail: [redacted]

_____

From: Jahan Kariyeva <[redacted]>
Sent: Wednesday, September 18, 2019 4:20 PM
To: Gustavo Lopes Queiroz <[redacted]>

Hi Gustavo:

Yes, in accordance.

Thanks,
Jahan

From: Greg McDermid <[redacted]>
Sent: Wednesday, September 18, 2019 4:20 PM
To: Gustavo Lopes Queiroz <[redacted]>

In accordance.

Greg
--
Greg McDermid
Professor, Graduate Program Director
Department of Geography
University of Calgary

Applied Geospatial Research Group
www.AppliedGRG.ca

From: Hopkinson, Christopher <[redacted]>
Sent: Wednesday, September 18, 2019 4:31 PM
To: Gustavo Lopes Queiroz <[redacted]>
Cc: Greg McDermid <[redacted]>

Hi Gustavo,
I have no problem whatsoever with you sharing any outputs from your thesis. I would be wary about any commitment to share raw data given potential ongoing uses but I don't think that is required here.
All the best and chat tomorrow.
Chris

From: Mustafizur Rahman <[redacted]>
Sent: Wednesday, September 18, 2019 4:45 PM
To: Gustavo Lopes Queiroz <[redacted]>; Greg McDermid <[redacted]>; Julia Linke <[redacted]>; Castilla, Guillermo (NRCan/RNCan) <[redacted]>; Hopkinson, Christopher <[redacted]>; Jahan Kariyeva <[redacted]>

I agree.
Cheers
Mustafiz

From: Gustavo Lopes Queiroz <[redacted]>
Sent: Wednesday, September 18, 2019 4:54 PM
To: Mustafizur Rahman <[redacted]>; Greg McDermid <[redacted]>; Julia Linke <[redacted]>; Castilla, Guillermo (NRCan/RNCan) <[redacted]>; Hopkinson, Christopher <[redacted]>; Jahan Kariyeva <[redacted]>

Thank you everyone for your permissions.

Chris, no raw data will be shared, just the manuscript which presents results derived from the Multispectral LiDAR data.

Cheers,
Gus